July 2008

Preparing, Characterizing, On-Line Digital Image Processing of Residence Time Distribution and Modeling of Mechanical Properties of Nanocomposite Foams

Siew Yoong Lee
University of Nebraska - Lincoln, siew18@gmail.com

PREPARING, CHARACTERIZING, ON-LINE DIGITAL IMAGE PROCESSING OF RESIDENCE TIME DISTRIBUTION AND MODELING OF MECHANICAL PROPERTIES OF NANOCOMPOSITE FOAMS

by

Siew Yoong Lee

A DISSERTATION

Presented to the Faculty of

The Graduate College at the University of Nebraska

in Partial Fulfillment of Requirements

for the Degree of Doctor of Philosophy

Major: Interdepartmental Area of Engineering
(Agricultural and Biological Systems Engineering)

Under the Supervision of

Professor Milford A. Hanna

Lincoln, Nebraska

August 2008

PREPARING, CHARACTERIZING, ON-LINE DIGITAL IMAGING OF RESIDENCE TIME DISTRIBUTION AND MODELING OF MECHANICAL PROPERTIES OF NANOCOMPOSITE FOAMS

Siew Yoong Lee, Ph. D.

University of Nebraska, 2008

Advisor: Milford A. Hanna

The objectives of this research were to prepare, characterize and to study the effects of organoclay and extrusion variables on the physical, mechanical, structural, thermal and functional properties of tapioca starch (TS)/poly(lactic acid) (PLA) nanocomposite foams. On-line digital imaging processing was used to determine residence time distribution (RTD). Adaptive neuro-fuzzy inference system (ANFIS) was used to model the mechanical properties of nanocomposite foams.

Four different organoclays (Cloisite 10A, 25A, 93A, 15A) were used to produce nanocomposite foams by melt-intercalation. The properties were characterized using X-ray diffraction, scanning electron microscopy, differential scanning calorimetric, and Instron universal testing machine. The properties were influenced significantly with the addition of different organoclays. TS/PLA/Cloisite 30B nanocomposite foams, with four clay contents of 1, 3, 5, 7 wt%, were prepared by a melt-intercalation method. Among the four nanocomposites, 3 wt% clay content produced significantly different properties.

Screw speed, screw configuration, die nozzle diameter and moisture content were varied to determine their effects on organoclay intercalation. These extrusion variables had significant effects on the properties of TS/PLA /Cloisite 10A nanocomposite foams due to the intercalation of organoclay.

Multiple inputs single output (MISO) models were developed to predict mechanical properties of nanocomposite foams. Four individual ANFIS models were developed. All models preformed well with R^2 values > 0.71 and had very low root mean squared errors (RMSE). Effects of screw configurations and barrel temperatures on the RTD and MISO models were developed to predict mechanical properties. The influence of the extrusion variables had a significant effect on the mean residence time (MTR).

On-line digital image processing (DIP) technique was developed to measure the RTD as compared to the colorimeter method. R^2 showed a correlation of 0.88 of a* values from both methods. The influence of screw configuration and temperature on RTD were analyzed by the MRT and variance for both methods. Mixing screws and lower temperature resulted in higher MRT and variance for both methods.

ACKNOWLEDGEMENTS

The author is grateful to Dr. Milford A. Hanna for his guidance, support and supervision during my Ph. D. program. I am grateful to Dr. Hanna for being effective at reviewing the manuscripts and dissertation. I also would like to thank the other members of my supervisory committee, Dr. David D. Jones, Dr. Randy L. Wehling and Dr. Yiqi Yang, for their support and intellectual inputs throughout the program. I am grateful to Dr. Jones for his patience and valuable time in teaching me to use MATLAB and his assistance in writing the scripts on modeling. I also am indebted to Dr. Yang for his guidance and valuable time during the initial stage of my research in the nanocomposite field. His suggestions, especially in the characterization of nanocomposite foams, have helped me to persevere through difficult times. Thanks also are due to Dr. Kent Eskrige for his advice on statistical analyses and his contribution in my research. I am thankful to the Industrial Agricultural Products Center (IAPC) staff especially Robert Weber, Terry L. Bartels, Nancy J. Hepburn and the student workers who have helped with the experiments. I thank staff of the Biological Systems Engineering Department especially Gail Ogden, Garret F. Coffman, Scotts Minchow and Gary J. Deberg for their help related to research.

Special thanks are due to the Malaysian Agricultural Research and Development Institute, for providing the financial support. Finally, I am very grateful to my husband and daughters who have been patient and independent during my absence while I was spending long hours in the department and also during weekends.

THESIS FORMAT

This thesis was written as a series of six chapters suitable for publication in journals. Each chapter has its own abstract, introduction, materials and methods, results and discussion, conclusions and references.

The first chapter is an introduction, preceding the six chapters, describes the overall objective of the research. The second chapter presents the effect of types of organoclay on the properties of nanocomposite foams by melt-intercalation. The third chapter presents the effect of organoclay contents on the properties of nanocomposite foams. The fourth chapter presents the influence of extrusion variables on the properties of nanocomposite foams. The fifth chapter deals with modeling the mechanical properties as a function of input variables. The sixth chapter presents the influence of extrusion variables on the retention time distribution and models were developed using adaptive neuro-fuzzy inference system to predict mechanical properties. The seventh chapter describes the on-line digital image processing technique to measure the residence time distribution as compared to the colorimeter method. The eighth chapter, succeeding the six publication-format chapters, contains the combined recommendations for those chapters.

TABLE OF CONTENTS

LIST OF TABLES

CHAPTER V

CHAPTER VI

CHAPTER VII

LIST OF FIGURES

CHAPTER II

CHAPTER III

CHAPTER IV

CHAPTER V

CHAPTER VI

CHAPTER VII

CHAPTER I

INTRODUCTION

The large amount of plastics that are produced from petroleum resources, once used and discarded into the environment, ends up as nondegradable waste. For this reason, there is a need to develop biodegradable plastic materials, especially for short-term packaging that could degrade naturally.

Starch is known to be completely biodegradable in soil and water. It is inexpensive and readily available, but has severe limitations due to its solubility and poor water-resistance. Therefore it is often blended with other polymers to improve the properties. One of the most promising polymers is poly(lactic acid) (PLA) because it is produced from renewal sources. PLA is insoluble in water, has good moisture and grease resistance and good mechanical properties. However it is expensive. To reduce cost, starch is used in a higher proportion. Therefore, PLA and starch in the right combination, forms excellent packaging foams.

Nanocomposite foams can be produced by melt-intercalation using an extruder. Incorporation of a small quantity of nano-sized clay particles can improve the physical, thermal and functional properties. However, these improvements are dependent upon the types and percentages of clay and on the processing conditions (screw configurations, screw speeds, temperature, etc.). The design of screw configuration and the selection of temperature and screw rotating speed are critical in the processing of nanocomposites. Sufficiently long residence time, moderate shear intensity and high extrusion temperature are known to produce nanocomposites with improved functional properties.

Residence time distribution (RTD) relates to the optimal processing conditions, and is a result of the flow patterns inside an extruder. It describes the time distribution of a material that is inside the extruder. Effects of operating conditions on RTD which affects the properties of nanocomposites have been studied. An online digital imaging processing (DIP) technique was used to analyze RTD. The resulting RTD were compared to RTD obtained by a conventional colorimeter method.

In summary, the overall objectives of this research were to:

1. Investigate the influence of types of nanoclay on the intercalation and properties of tapioca starch/PLA nanocomposite foams;
2. Investigate the influence of clay contents on the intercalation and properties of tapioca starch/PLA nanocomposite foams;
3. Investigate the influence of extrusion variables on the intercalation and properties of tapioca starch/PLA nanocomposite foams;
4. Model selected properties of the nanocomposite foams by using adaptive neuro-fuzzy inference system (ANFIS);
5. Investigate the influence of extrusion variables on RTD and modeling of the mechanical properties of nanocomposite foams using ANFIS; and
6. Determine RTD by using on-line digital imaging processing.

CHAPTER II

PREPARATION AND CHARACTERIZATION OF TAPIOCA STARCH-POLY(LACTIC ACID) NANOCOMPOSITE FOAMS BY MELT INTERCALATION BASED ON CLAY TYPE

This research paper has been published as:

Siew Yoong Lee, Han Chen, Milford A. Hanna (2008). Preparation and characterization of tapioca starch-poly(lactic acid) nanocomposite foams by melt intercalation based on clay type. *Ind. Crops and Prod*., 28(1): 95-106.

Preparation and characterization of tapioca starch-poly(lactic acid) nanocomposite foams by melt intercalation based on clay type

Abstract:

Tapioca starch (TS), poly(lactic acid) (PLA), and four different organoclays (Cloisite 10A, Cloisite 25A, Cloisite 93A and Cloisite 15A) were used to produce nanocomposite foams by melt-intercalation. Structural, thermal, physical and mechanical properties were characterized using X-ray diffraction (XRD), scanning electron microscopy (SEM), differential scanning calorimetry (DSC), and an Instron universal testing machine, respectively. The first XRD peaks for all four nanocomposite foams, were observed to shift to lower angles, indicating that intercalation occurred. The extent of intercalation depended on the type of organoclay and was exhibited in the sequence of Cloisite 10A > 25A > 93A > 15A. Glass transition temperatures (T_g) and melting temperatures (T_m) of the foams were investigated by DSC. Radial expansion ratio (RER), unit density, BSI (bulk spring index), bulk compressibility, Young's modulus (E), water absorption index (WAI) and water solubility index (WSI) were influenced (p<0.05) significantly with the addition of different organoclays into the TS/PLA matrix.

Keywords: Nanocomposites; Organoclay; Properties; Extrusion; Foams

1. Introduction

There is a growing interest in developing biodegradable polymers to replace synthetic nondegradable materials. Poly(lactic acid) (polylactate or polylactide) (PLA) is a biodegradable polyester that can be used to alleviate the waste disposal problem. It is synthesized from L- and D-lactic acid, which are produced from the fermentation of sugar and (poly)saccharides such as sugar feedstocks and corn, wheat and other starch sources, either by ring-opening polymerization or by condensation polymerization (Stevens, 2002). PLA is insoluble in water and has good moisture and grease resistance. Its mechanical properties can be modified by varying its molecular weight and its crystallinity. PLA is used widely as a biodegradable and renewable plastic for uses in service ware, grocery, waste-composting bags, mulch films, controlled release matrices for fertilizers, pesticides and herbicides (Fang and Hanna, 1999). However, PLA is expensive due to the complicated synthesis.

Starch is a natural polymer, inexpensive and readily available resource, and is often used as a filler for the replacement of petroleum-derived synthetic polymers to decrease environmental pollution. However, starch has severe limitations because of its solubility and poor water-resistance, making starch products very sensitive to the relative humidity at which they are stored and used (Simmons and Thomas, 1995). Starch-polyester blends are being produced with the objective of maintaining the excellent physical properties of the polyesters while reducing cost. A process was developed at the University of Nebraska-Lincoln to produce starch-based plastic foam with 70% starch combined with a variety of ingredients and plastics (Chinnaswamy and Hanna, 1993). Fang and Hanna (2000a) found that addition of PLA to regular and waxy corn starches

improved the physical and mechanical properties of the foams. Recently, formation of nanocomposites with the aim to improve functional properties has become popular. One of the most promising nanocomposites is formed from organic polymer and inorganic clay minerals consisting of layered silicates.

Polymer nanocomposites are a class of reinforced polymers containing small quantities (1-5 wt%) of nanometric-sized clay particles. Smectite – type clays, such as hectorite, synthetic mica, and montmorillonite were employed as fillers to enhance the properties of the composites. The functional properties of the nanocomposites were improved markedly compared to those of the unfilled polymer or conventional composites. These improvements included high moduli (Lim and Park, 2000; Nam et al., 2001); increased tensile strength (Dennis et al., 2001) and thermal stability (Chang et al., 2003); decreased gas permeability (Yuen et al., 2006), flammability (Morgan, 2006) and water absorbance (Chiou et al., 2006); and increased biodegradability of biodegradable polymers (Ray et al., 2003).

Of the four methods (solution intercalation, in situ polymerization, melt intercalation, and template synthesis) which have been used to synthesize nanocomposites, melt intercalation is the most appealing approach because of its versatility, compatibility with polymer processing equipment, and because it is an environmentally friendly process that requires no solvent and is suitable for industrial uses (Choi et al., 2003; Li and Ha, 2003). In melt intercalation, the clay and polymer are added together above the melting temperature of the polymer; they may be held at this temperature for a period of time, put under shear, or other conditions to encourage intercalation and exfoliation of the clay (Dean and Yu, 2005).

Generally, polymer/layered silicate composites are divided into three main types: tactoid, intercalated, and exfoliated nanocomposites. In a tactoid, the polymer is unable to intercalate between the silicate sheets and the properties of the composites stay in the same range as the traditional microcomposites. Intercalated nanocomposites occur when a small amount of polymer moves into the gallery spacing between the silicate platelets. When the silicate layers are completely and uniformly dispersed in a continuous polymer matrix, an exfoliated or delaminated structure is formed (Pollet et al., 2002). The intercalated and exfoliated nanocomposites currently are of primary interest because their properties are significantly improved, even at low clay concentrations. However, the formation of intercalated or exfoliated nanocomposites depends on the type of organoclay (Choi et al., 2003; Ammala et al., 2007) the clay content (Artzi et al., 2002; Nobel and Picken, 2007) and the processing conditions (Dennis et al., 2001; Tanoue et al., 2006).

The objectives of this study were to prepare TS/PLA/clay nanocomposite foams using four different clays via melt-intercalation and to investigate the influence of the type of clay on structural, morphological, thermal, physical and mechanical properties of the foams.

2. Materials and Methods

2.1. Materials

Semicrystalline poly(lactic acid) (PLA) resin of MW_n 85,000 was produced by Cargill, Inc. (Minneapolis, MN). It contained ~93% L-lactide, 2% D-lactide and 5% mesolactide. It was in the form of 2 – 4 mm spheres. The thermal properties measured by

DSC showed a glass transition temperature of 70˚C and a melting point of 174˚C. The true density of PLA resin was 1.22 g/cm ^{3}. PLA usually is used as an amorphous material in molded products because of its low rate of crystallization, though it is a semi-crystalline polymer. Commercially available tapioca starch was purchased from Starch Tech. Inc. (Golden Valley, MN). Tapioca starch was agglomerated into spherical granules of 2-4 mm diameter to facilitate feeding into the extruder. The moisture content of the tapioca starch was adjusted to 18%, dry basis, with distilled water prior to extrusion. Tapioca starch and 10% PLA (10% w/w PLA/starch) were blended with 0.5% sodium bicarbonate, 0.5% citric acid and 3% clay in a Hobart mixer (Model C-100, Horbart Corp., Troy, OH) and stored in plastic jars prior to extrusion. PLA content of 10% was selected based on preliminary experiments. Fang and Hanna (2000b) found that at 10% PLA content, the foams possessed the highest spring index and intermediate compressibility and Young's modulus values. They concluded that for practical applications, the bulk mechanical properties were more meaningful. Sodium bicarbonate and citric acid were added to degrade the biodegradable polymer into chains of between 1,000 and 100,000 Daltons or approximately 500 to 50,000 monosaccharide groups to promote expansion (Chinnaswamy and Hanna, 1993). Four commercial clays, namely Cloisite 10A, Cloisite 15A, Cloisite 25A and Cloisite 93A, were purchased from Southern Clay Products Inc (Gonzalez, TX) and used as nanofillers, hereafter referred to as 10A, 15A, 25A and 93A, respectively. They were organically-modified montmorillonite (MMT) also known as organoclays. The ammonium cations of the organoclays were dimethyl benzyl hydrogenated-tallow quaternary ammonium for the Cloisite 10A, dimethyl dihydrogenated-tallow quaternary ammonium for the Cloisite 15A, dimethyl hydrogenated-tallow 2-etylhexyl quaternary ammonium for the Cloisite 25A and

methyl dehydrogenated-tallow quaternary ammonium for the Cloisite 93A. The characteristics of the clays used in this work are summarized in Table 1. Table 2 gives the five different formulations used in this research work.

2.2. Extrusion

A twin-screw extruder (Model DR-2027-K13, C. W. Brabender, Inc., S. Hackensack, NJ, USA) with corotating mixing screws (Model CTSE-V, C. W. Brabender, Inc., S. Hackensack, NJ, USA) was used to conduct extrusions. The conical screws had diameters decreasing from 43 mm to 28 mm along their length of 365 mm from the feed end to the exit end. On each screw, there was a mixing section, in which small portions of the screw flights were cut away. The mixing section enhanced the mixing action and also increased the residence time of the sample in the barrel. A 150-rev/min screw speed was used for all extrusions. The temperature at the feeding section was maintained at 50°C, the second barrel section at 120°C, the third barrel section at 150°C and die section at 170°C. A 3 mm diameter die nozzle was used to produce continuous cylindrical rope-like extrudates which were cut by a rotary cutter. The extruder was controlled by a Plasti-Corder (Type FE 2000, C. W. Brabender, Inc. S. Hackensack, NJ). Data including screw rotating speeds, barrel temperature profiles, pressure profiles and torque readings were recorded for subsequent analyses. Extrusion conditions selected were based on preliminary studies and previous experiments.

2.3. X-ray diffraction

The x-ray patterns of the samples were obtained using a Rigaku D/Max– B X-ray diffractometer (Tokyo, Japan) with Cu-Kα radiation (λ = 1.544 Å) at a voltage of 40 kV and 30 mA. Samples were scanned in the range of diffraction angle 2θ = 2-10° with a scan speed of 1°/min at room temperature.

2.4. Scanning electron microscopy (SEM)

The morphologies of TS/PLA and TS/PLA nanocomposite foams were observed under a SEM (Hitachi S-3000N, Tokyo, Japan). Before testing, the samples were mounted on SEM stubs with double-sided adhesive tape and then coated with platinum under vacuum to make the sample conductive.

2.5. *Differential scanning calorimetry (DSC)*

DSC measurement was performed with a Mettler DSC (Columbus, OH, USA). About 10 mg of the dried, ground samples were placed in an aluminum sample pan. The samples were heated from 25 to 200 °C at a heating rate of 10 ° C/min in a nitrogen atmosphere. The sample was kept at 200°C for 1 min for the elimination of the previous heat history and was subsequently cooled to 25°C at 10°C/min. The sample was then heated again to 200°C at 10°C/min. The glass transition temperature (T_g) of the foams was taken as the inflection point of the increment of specific heat capacity. The values of melting temperature (T_m), for the first heating and second heating process were obtained for the analysis. The melting temperature was determined as the temperature at the

maximum value of the endothermic melting peak of the heating scans. The transition enthalpy was determined from the areas under the melting peaks.

2.6. Radial expansion ratio (RER)

Radial expansion ratios of the extruded foams were calculated by dividing the mean cross-sectional areas of the foams by the cross-sectional area of the die nozzle. Each calculated value was a mean of 20 observations.

2.7. Unit density

Unit densities of the extrudates were determined using a glass bead displacement method originally developed for determining the volume of cookies (Hwang and Hawakawa, 1980) with modifications (Bhatnagar and Hanna, 1991). Glass beads of 0.1 mm diameter were used as the displacement medium. A mean value was obtained by averaging five replicates.

2.8. Bulk spring index (BSI)

BSI measurements were made using an Instron universal testing machine (Model 5566, Instron Engineering Corp., Canton, MA). A cylindrical aluminium container with a volume of 365 cm^3 (6.93 cm in diameter and 9.68 cm in depth) was used to confine the bulk samples (Fang and Hanna, 2000b). The forces required to initially compress the samples to 80% of their original volumes and the forces required to recompress the same samples 1 min after releasing the initial load were recorded. BSI was calculated by

dividing the recompression force by the initial compression force and has an ideal value of 1. A mean value was obtained by averaging five replicates.

2.9. Bulk compressibility

Bulk compressibility was calculated using the same data collected in the BSI test. It was calculated by dividing the peak force required to compress (deform) the sample by 80% [to 20% of their original dimension (diameter)] by the initial axial cross-sectional area of the foams (Fang and Hanna, 2000b). A mean value was obtained by averaging five replicates.

2.10. Young's Modulus (E)

The Young's Modulus (E) of foams was determined using the least-square regression method from the slopes of the strain-stress curves. The strain-stress curves were generated from the Instron testing machine data for the compressibility and spring index determinations (Fang and Hanna 2000b). All calculations had r^2 values greater than 0.95.

2.11. Water absorption index (WAI) and water solubility index (WSI)

WAI and WSI of the foams were measured by a procedure similar to AACC Method 56-20 (AACC 1983). To determine WAI and WSI, the foams were ground to pass through a #80 sieve. The samples (about 1 g) were dispersed in 30 ml of distilled water in pre-weighed centrifuge tubes. The centrifuge tubes were placed in a shaking water bath at 30°C for 30 min, and then centrifuged at 5000 x g for 10 min. The

supernatants were decanted carefully into pre-weighed aluminum dishes, dried at 103°C for 12 h, cooled and weighed. The remaining sediment with tube was weighed. WAI and WSI were calculated as,

$$WAI = \frac{\text{Weight of tube with sediment - Weight of tube}}{\text{Weight of sample (d.b.)}}$$

$$WSI = \frac{\text{Weight of dish with solids - Weight of dish}}{\text{Weight of sample (d.b.)}} \text{ x } 100\%$$

2.12. Statistical analyses

All results reported are means of two or more replications. The radial expansion ratio, unit density, bulk spring index and bulk compressibility data were analyzed using general linear models (GLM) in SAS analysis program (SAS Institute Inc., Cary, NC). Duncan's multiple range tests were conducted to check for significant ($p<0.05$) differences between treatment groups.

3. Results and discussions

3.1. Structural properties of TS/PLA/clay nanocomposite foams

Wide-angle x-ray diffraction (WAXD) is a classical method for determining the gallery height (d-spacing distance) in clay particles (Di et al., 2003). The d-spacing can be determined from the diffraction peak in the XRD patterns, and can be expressed by Bragg's equation ($\lambda = 2d_{001}\sin\theta$), where d_{001} is the interplanar distance of the (001) diffraction face, θ is the diffraction position, and λ is the wavelength (Choi et al., 2003).

During melt intercalation, the insertion of polymer into the organoclay galleries forces the platelets apart and increases the d-spacing, resulting in a shift of the diffraction peak to lower angles.

In all four nanocomposite foams, the first diffraction peaks were observed to shift to lower angles compared to those of the original organoclays, indicating that intercalation of TS/PLA polymer into the organoclay layers occurred (Table 3). The peak of the organoclay 10A ($2\theta = 4.66^{\circ}$) shifted to 2.58° for the TS/PLA/10A nanocomposite foam (Table 3). The d_{001}-spacing of TS/PLA/10A nanocomposite foam was 34.24 Å, a 15.28 Å increase compared to that of the original organoclay 10A (18.96 Å) and exhibited the greatest extent of enlargement compared to the other nanocomposite foams. This increase of d_{001}-spacing caused the clay to swell by 43.00% which was attributed to the miscibility of the polymers (Ishida et al., 2000). However, Park et al. (2002) found that there was little or no intercalation between thermoplastic starch and organoclay 10A hybrid. They explained that organoclay 10A was too hydrophobic and did not match with the polarity of thermoplastic starch, therefore discouraging intercalation. The degree of enlargement of the d_{001}-spacings decreased in the case of the nanocomposite foams with organoclay 25A (9.79 Å), organoclay 93A (8.64 Å), and organoclay 15A (3.46 Å), suggesting a decreasing interaction between TS/PLA and these organoclays (Table 3). The degrees of swell for the TS/PLA/25A, TS/PLA/93A, and TS/PLA/15A nanocomposite foams were 33.5%, 27.0%, and 10.9%, respectively. It is believed that the greater the d_{001}-spacings, the greater the interaction of polymer molecular chain with clay layered silicate (Choi et al., 2003). The interactions between polymer and nanoclays

depend on the compatibility of the surface polarities of polymer and clay (Park et al., 2003).

In Figure 1, the WAXD patterns of the organoclay 10A and TS/PLA/10A nanocomposite foam were compared. The organoclay 10A had one peak at the diffraction angle of 2θ = 4.66º. The spectra of the TS/PLA/10A nanocomposite foam had two peaks. The first diffraction peak (001) *d*-spacing occurred at 2θ = 2.58˚. The first diffraction peak (001) *d*-spacing was observed to shift to a lower angle compared to that of organoclay, indicating that intercalation of TS/PLA polymer into the organoclay layers occurred. This result was attributed to the compatibility between the clay modifier and the TS/PLA matrix which were both hydrophobic (Pérez et al., 2006). The first diffraction peak (001) *d*-spacing for the intercalated nanocomposite was narrow, indicating a strong intercalated behavior and a high stacking order of the successive clay layers in the nanocomposites. Similar occurrence also was observed by Kumar et al. (2003) and Ranade et al. (2002). The second diffraction peak occurred at 2θ = 5.16˚, appeared smaller and weaker and was due to the second registry (002) *d*-spacing of the organoclay (Ray et al., 2002; Pluta, 2004). The presence of a smaller peak indicated that a small fraction of the clay was still present as agglomerated sheets which contributed to a tactoid structure. A similar occurrence was observed by Kalambur and Rizvi (2005).

Figure 2 shows the diffraction spectra of organoclay 25A and its nanocomposite foam. The organoclay 25A had one peak at the diffraction angle 2θ of 4.54º. The WAXD diffractogram for TS/PLA/25A nanocomposite foam showed two peaks at the diffraction angles of 2θ = 3.02º and 6.04º. Pluta et al. (2003) observed two diffraction peaks from the intercalation of the polymer chains into the clay interlayers.

The peak (2θ = 3.78º) of organoclay 93A shifted to a lower angle (2.76º) as compared to the TS/PLA/93A nanocomposite foam (Figure 3) suggesting intercalation occurred. However, the interaction between TS/PLA and the nonpolar group of the modifier in organoclay 93A was not strong (Di et al., 2005). Inspite of intercalation of TS/PLA into the silicate layers of organoclay 93A, the degree of intercalation was less.

WAXD patterns of the organoclay 15A and TS/PLA/15A nanocomposite foam are shown in Figure 4. The organoclay 15A had two peaks at the diffraction angles of 2θ = 3.12º and 7.02º. The spectra of the TS/PLA/15A nanocomposite foam had two peaks. The first diffraction peak did not shift much to 2θ = 2.78˚ and had a lower peak intensity suggesting less intercalation (Dennis et al., 2001). The second diffraction peak appeared as a weak shoulder at 2θ = 7.36˚, indicating the presence of clay as agglomerated sheets (Kalambur and Rizvi, 2005).

The morphologies of the foams were observed by SEM and representative images of TS/PLA, TS/PLA/10A, TS/PLA/25A, TS/PLA/93A and TS/PLA/15A nanocomposite foams are presented in Figures 5 – 9, respectively. The TS/PLA foam, without organoclay filler exhibited very large cell structure. The nanocomposite foams had a higher cell density and exhibited cell structures of smaller and more uniform cells with noticeably decreased cell size. This indicated that the dispersed organoclay particles acted as nucleating sites for cell formation (Fujimoto et al., 2003). The surface chemistry of clay nanoparticles had an effect on the nucleating mechanism, thus producing smaller cells and increased cell density due to the high nucleation efficiency (Lee et al., 2005).

3.2. Thermal properties of TS/PLA /clay nanocomposite foams

Glass transition temperature (T_g) and melting temperatures (T_m) of the first and second heating of TS/PLA and its nanocomposite foams were investigated by DSC. DSC plots for the first heating scan and second heating scan are presented in Figures 10 and11, respectively. In the DSC cooling process, none of the foams showed any crystallization peaks. Di et al. (2003) explained, in addition to nucleation effect, that organoclay can act as a retardant to crystallization if there is a strong interaction between the polymer matrix and organoclay. The data for all measurements are given in Table 4. As can be seen, the TS/PLA foam had a T_g of 63.4 °C. The TS/PLA/10A and TS/PLA/93A nanocomposite foams had the same T_g of 63.8°C which were similar to the T_g of TS/PLA foam. This could have been due to organoclays 10A and 93A having strong interactions between the surface of the platelets and the functional groups on the main polymer chains which caused reductions in the mobility of the molecules. The T_g of TS/PLA/25A and TS/PLA/15A nanocomposite foams were lower than the T_g of TS/PLA foam at 60.8°C and 62.4°C, respectively. The decrease in T_g with the addition of organoclays 25A and 15A could have been due to their plasticizing effects on the TS/PLA chains. Ranade et al. (2004) reported similar results in their work.

Figure 10 shows typical DSC thermographs of the first heating scans with the distinct endothermic peaks (T_m) of the foams. TS/PLA foam had a T_m of 171.5 °C as shown in Table 4. T_m of the TS/PLA/10A, TS/PLA/93A and TS/PLA/15A nanocomposite foams were 164.2 °C, 157.4 °C and 169.1 °C, respectively, were lower than the T_m of the TS/PLA foam. TS/PLA/25A nanocomposite foam had the same T_m as the TS/PLA foam. The organoclay resulted in strong interactions between the polymer

matrix and the organoclay depressed crystallization. Therefore, T_m was reduced due to this phenomenon. It is worth noting that T_m did not decrease linearly with decreasing degree of swell (Table 3) based on the type of organoclay, which may have been caused by the random, but not uniform, dispersion of organoclay in the nanocomposites. Similar observations were reported by Zhang and Yan (2003).

Figure 11 shows the DSC thermographs of the second heating scans of the foams. Table 4 shows the T_m and ΔH of the TS/PLA foam of 165 °C. T_m of all the nanocomposite foams were lower than the TS/PLA foam.

3.3. Physical and mechanical properties of TS/PLA /clay nanocomposite foams

Radial expansion ratio (RER) and unit density are important physical properties of foams. High RER and low unit density are desirable attributes for foams because of reduced material cost. RER values of the foams were significantly different ($p<0.05$) from each other (Table 5). TS/PLA foam had a RER of 26.8 and the RER of the nanocomposites foams ranged between 46.4 (TS/PLA/93A) to 15.2 (TS/PLA/25A). These results indicated that the addition of organoclay had an effect on the RER of the foams, especially with organoclay 93A which had a positive effect on the RER. In the case of organoclay 93A, the presence of H instead of CH3 (Table 1) had the advantage of enhancing nucleation, thereby forming a highly expanded nanocomposite. TS/PLA foam had a unit density of 43.4 kg/m^3. Unit density of TS/PLA/93A nanocomposite foam was significantly lower (23.0 kg/m3) than the unit density of TS/PLA foam. However, the unit densities of the TS/PLA/10A, TS/PLA/25A and TS/PLA/15A nanocomposite foams

were significantly ($p<0.05$) higher than both the TS/PLA foam and TS/PLA/93A nanocomposite foams.

Bulk spring index (BSI) and bulk compressibility are important mechanical properties of foams. BSI and bulk compressibility are interrelated properties. BSI relates to resiliency, and refers to the ability of a material to recover its original shape after it has been deformed. A greater BSI indicates a greater degree of rebound of a material after being compressed. Bulk compressibility describes the cushioning ability of a material, and is related to its relative softness or hardness. High BSI and low bulk compressibility are desirable for loose-fill packaging material (Bhatnagar and Hanna, 1995) The BSI and bulk compressibility of the foams are presented in Table 5. The highest BSI was obtained for TS/PLA/25A nanocomposite foam (0.960) and the lowest BSI was obtained for TS/PLA/93A nanocomposite foam (0.944). BSI was influenced ($p<0.05$) significantly with the addition of different organoclays into the TS/PLA matrix. The bulk compressibilities of the foams were significantly different ($p<0.05$) from each other. The lowest bulk compressibility of 0.989 MPa was obtained from the TS/PLA/93A nanocomposite foam which had the softest foam. This significantly low value could have been due to the organoclay 93A being compatible with the TS/PLA molecules, allowing it to interact readily with the matrix to form strong interactions between them (Pluta et al., 2002). The strong interactions increased the strength of the cell walls, making the nanocomposite foams more rigid and resulting in low bulk compressibility.

Young's modulus (E) measures the stiffness or elasticity of a material. The stress-strain curves of the foams are presented in Figure 12. All curves had similar trends with a smooth increasing rate of stress as strain increased and exhibited a smooth elastic

deformation range. These foams should perform better when higher deformations are encountered. TS/PLA/10A nanocomposite foam was the strongest followed by TS/PLA/25A and TS/PLA/15A nanocomposite foams as compared to the TS/PLA foam. This could have been due to the compatibility of the organoclay with the TS/PLA molecules forming a continuous network throughout the matrix which reinforced the foam making them more resilient. However, the TS/PLA/93A nanocomposite foam had a lower strength than the TS/PLA foam which could have been due to the soft texture of the foam with thin cell walls which collapsed during deformation.

Young's modulus (E) of the foams were significantly affected ($p<0.05$) by type of organoclay, as shown in Table 5. The largest increase in E (96%) was obtained from TS/PLA/10A nanocomposite foam as compared to the TS/PLA foam, followed by the TS/PLA/25A (14%) and TS/PLA/15A (6%) nanocomposite foams. TS/PLA/93A nanocomposite foam had a significantly lower E because of its softer texture.

3.4. Physico-chemical properties of TS/PLA /clay nanocomposite foams

WAI measures the volume occupied by the starch after swelling in excess water, which correlates with the degree of cook (Masson and Hoseney, 1986) and WSI can be used as an indication of the degree of molecular damage (Colonna et al., 1989). The data for WAI and WSI are shown in Table 6. WAI and WSI of the foams were affected significantly ($p<0.05$) by type of organoclay. TS/PLA/10A, TS/PLA/25A and TS/PLA/15A nanocomposite foams had significantly higher WAI values as compared to the TS/PLA and TS/PLA/93A foams. Similarly, in the reverse trend, TS/PLA/10A, TS/PLA/25A and TS/PLA/15A nanocomposite foams had significantly lower WSI values

as compared to the TS/PLA and TS/PLA/93A foams. This indicated that organoclays 10A, 25A and 15A had compatible interactions with the TS/PLA molecules, resulting in increased WAI and decreased WSI.

4. Conclusions

From the WAXD study, the first diffraction peaks for all four nanocomposite foams, were observed to shift to lower angles compared to those of the original organoclays, indicating that the intercalation of TS/PLA polymer into the organoclay layers occurred. The d_{001}-spacing of TS/PLA/10A nanocomposite foam was 34.24 Å, a 15.28 Å increase compared to that of the original organoclay 10A (18.96 Å) and exhibited the greatest extent of enlargement compared to the other nanocomposite foams. The degree of enlargement of the d_{001}-spacings decreased in the case of the nanocomposite foams with organoclay 25A (9.79 Å), organoclay 93A (8.64 Å), and organoclay 15A (3.46 Å), suggesting a decreasing interaction between TS/PLA and these organoclays. The morphological study showed that the four nanocomposites had higher cell densities and exhibited smaller and more uniform cells with noticeably decreased cell size.

From the DSC study, the TS/PLA/10A and TS/PLA/93A nanocomposite foams had the same T_g of 63.8°C which was quite similar to the T_g of TS/PLA foam. The T_g of TS/PLA/25A and TS/PLA/15A nanocomposite foams were lower than the T_g of TS/PLA foam at 60.8°C and 62.4°C, respectively. From the DSC thermographs of the first heating scans, T_m of the TS/PLA/10A, TS/PLA/93A and TS/PLA/15A nanocomposite

foams were 164.2 °C, 157.4 °C and 169.1 °C, respectively, were lower than the T_m of the TS/PLA foam. TS/PLA/25A nanocomposite foam had the same T_m of the TS/PLA foam. From the second heating scans, T_m of all the nanocomposite foams were lower than the TS/PLA foam.

RER values of the foams were significantly different ($p<0.05$) from each other. TS/PLA foam had a RER of 26.8 and the RER of the nanocomposites foams ranged between 46.4 (TS/PLA/93A) to 15.2 (TS/PLA/25A). These results indicated that the addition of organoclay had an effect on the RER of the foams, especially with organoclay 93A which had a positive effect on the RER. TS/PLA foam had a unit density of 43.4 kg/m3. Unit density of TS/PLA/93A nanocomposite foam was significantly lower (23.0 kg/m3) than the unit density of TS/PLA foam. However the unit densities of the TS/PLA/10A, TS/PLA/25A and TS/PLA/15A nanocomposite foams were significantly ($p<0.05$) higher than both the TS/PLA foam and TS/PLA/93A nanocomposite foams.

The highest BSI was obtained from TS/PLA/25A nanocomposite foam (0.960) and the lowest BSI was obtained from TS/PLA/93A nanocomposite foam (0.944). BSI was influenced ($p<0.05$) significantly with the addition of different organoclays into the TS/PLA matrix. The bulk compressibilities of the foams were significantly different ($p<0.05$) from each other. The lowest bulk compressibility of 0.989 MPa was obtained for the TS/PLA/93A nanocomposite foam which was the softest foam.

Young's modulus (E) of the foams were significantly affected ($p<0.05$) by type of organoclay. The largest increase in E (96%) was obtained from TS/PLA/10A nanocomposite foam as compared to the TS/PLA foam, followed by the TS/PLA/25A

(14%) and TS/PLA/15A (6%) nanocomposite foams. TS/PLA/93A nanocomposite foam had a significantly lower E because of its softer texture.

WAI and WSI of the foams were affected significantly ($p<0.05$) by type of organoclay. TS/PLA/10A, TS/PLA/25A and TS/PLA/15A nanocomposite foams had significantly higher WAI values and in the reverse trend, had significantly lower WSI values as compared to the TS/PLA and TS/PLA/93A foams.

References

AACC Method 56-20, 1983. Hydration capacity of pregelatinized cereal products. American Association of Cereal Chemists Approved Methods, 8th edn. Am. Assoc. Cereal Chem., St. Paul, MN.

Ammala, A., Hill, A.J., Lawrence, K.A., Tran, T., 2007. Poly(*m*-xylene adipamide)-kaolinite and poly(m-xylene adipamide)-montmorillonite nanocomposites. J. Appl. Polym. Sci. 104, 1377-1381.

Artzi, N., Nir, Y., Narkis, M., Siegmann. A., 2002. Melt blending of ethylene-vinyl alcohol copolymer/clay nanocomposites: effect of the clay type and processing conditions. J. Polym. Sci.: Part B: Polym. Physics. 40, 1741-1753.

Bhatnagar, S., Hanna, M.A., 1991. Effect of lipids on physico-chemical properties of extruded corn starch. ASAE Paper No. 916541. St. Joseph, Mich.: ASAE

Bhatnagar, S., Hanna, M.A., 1995. Physical, mechanical and thermal properties of starch-based plastic foams. Trans. ASAE 38, 567-571.

Chang, J-H., Jang, T.-G., Ihn, K. J., Lee, W. K., Sur, G.S., 2003. Poly (vinyl alcohol) nanocomposites with different clays: pristine clays and clays. J. Appl. Polym. Sci. 90, 3208-3214.

Chinnaswamy, R., Hanna, M.A., 1993. Biodegradable polymers. U.S. Patent 5 496 895.

Chiou, B-S., Yee, E., Wood, D., Shey, J., Glenn, G., Orts, W., 2006. Effects of processing conditions on nanoclay dispersion in starch-clay nanocomposites. Cereal Chem. 83(3), 300-305.

Choi, W.M., Kim, T.W., Park, O.O., Chang, Y.K., Lee, J.W., 2003. Preparation and characterization of poly (hydroxybutyrate-co-hydroxyvalerate)-clay nanocomposite. J. Appl. Polym. Sci. 90, 525-529.

Colonna, P.; Tayeb, J.; Mercier, C. 1989. Extrusion cooking of starch and starchy products. In: Mercier, C.; Linko, P.; Harper, J. M. (Eds.), Extrusion Cooking. Am. Assoc. Cereal Chem., St. Paul, MN.

Dean, K.; Yu, L. 2005. Biodegradable Protein-Nanoparticle Composites. In: Smith, R. (Ed.), Biodegradable Polymers for Industrial Applications. CRC Press, Boca Raton, FL., pp. 289-309.

Dennis, H.R., Chang, D., Kim, S., White, J.L., Cho, J.W., Paul, D.R., 2001. effect of melt processing conditions on the extent of exfoliation in clay-based nanocomposites. Polym., 42, 9513-9522.

Di, Y., Iannace, S., Miao, E.D., Nicolais, L., 2003. Nanocomposites by melt intercalation based on polycaprolactone and organoclay. J. Polym. Sci.: Part B: Polym. Phys. 41, 670-678.

Di, Y., Iannace, S., Miao, E.D., Nicolais, L., 2005. Poly(lactic acid)/clay nanocomposites: thermal, rheological properties and foam processing. J. Polym. Sci.: Part B: Polym. Phys. 43, 689-698.

Fang, Q., Hanna, M.A., 1999. Rheological properties of amorphous and semicrystalline poly (lactic acid) polymers. Ind. Crops and Prod.10, 47-53.

Fang, Q., Hanna, M.A., 2000a. Functional properties of poly (lactic acid) starch-based loose-fill packaging foams. Cereal Chem. 77(6), 779-783.

Fang, Q., Hanna, M.A. 2000b. Mechanical properties of starch-based foams as affected by ingredient formulation and foam physical properties. Trans. ASAE 43, 1715-1723.

Fujimoto, Y., Ray, S., Okamoto, M., Ogami, A., Yamada, K., Ueda, K., 2003. Well-controlled biodegradable nanocomposite foams: from microcellular to nanocellular. Macromol. Rapid Commun. 24, 457-461.

Hwang, M.P., Hayakawa, K., 1980. Bulk densities of cookies undergoing commercial baking process. J. Food Sci. 45(5), 1400-1402, 1407.

Ishida, H., Campbell, S., Blackwell, J., 2000. General approach to nanocomposite preparation. Chem. Mater., 12, 1260-1267.

Kalambur, S., Rizvi, S.S.H., 2005. Biodegradable and functionally superior starch-polyester nanocomposites from reactive extrusion. J. Appl. Polym. Sci., 96, 1072-1082.

Kumar, S., Jog, J.P., Natarajan, U., 2003. Preparation and characterization of poly(methyl methacrylate)-clay nanocomposites via melt intercalation: the effects of organoclay on the structure and thermal properties. J. Appl. Polym. Sci. 89, 1186-1194.

Lee, L.J., Zeng, C., Cao, X., Han, X., Shen, J., Xu, G., 2005. Polymer nanocomposite foams. Composites Sci. and Tech. 65, 2344-2363.

Li, X.C., Ha, C-S., 2003. Nanostructure of Eva/clay nanocomposites: effects of kinds of clay and grafting of maleic anhydride onto Eva. J. Appl. Polym. Sci. 87, 1901-1909.

Lim, Y.T., Park, O.O., 2000. Rheological evidence for the microstructure of intercalated polymer/layered silicate nanocomposites. Macromol. Rapid Commun. 21, 231-235.

Masson, W.R., Hoseney, R.C. 1986. Factors affecting the viscosity of extrusion-cooked wheat starch. Cereal Chem. 63, 436-441.

Morgan, A.B., 2006. Flame retarded polymer layered silicate nanocomposites: a review of commercial and open literature systems. Polym. Adv. Technol. 17, 206-217.

Nam, P.H., Maiti, P., Okamoto, M., Kotaka, T., Hasegawa, N., Usuki, A., 2001. A hierarchical structure and properties of intercalated polypropylene/clay nanocomposites. Polym. 42, 9633-9640.

Nobel, M.L., Picken, S.J., 2007. Acrylic-based nanocomposite resins for coating applications. J. Appl. Polym. Sci. 104, 2146-2156.

Park, H-M., Li, X., Jin, C- Z., Park, C-Y., Cho, W-J.; Ha, C-S., 2002. Preparation and properties of biodegradable thermoplastic starch/clay hybrids. Macromol. Mater. Eng. 287, 553-558.

Park, H-M., Lee, W.K., Park, C.-Y., Cho, W.-J., Ha, C.-S., 2003. Environmentally friendly polymer hybrids: Part 1 mechanical, thermal, and barrier properties of the thermoplastic starch/clay nanocomposites. J. Mater. Sci. 38, 909-915.

Pérez, C.J., Alvarez, V.A., Mondragón, I., Vázquez, A., 2006. Mechanical properties of layered silicate/starch polycaprolactone blend nanocomposites. Polym. Int. 56, 686-693.

Pluta, M., Galeski, A., Alexandre, M., Paul, M.-A., Dubois,P., 2002. Polylactide/montnorillonite nanocomposites and microcomposites prepared by

melt blending: structure and some physical properties. J. Appl. Polym. Sci. 86, 1497-1506.

Pluta, M., Galeski, A., Alexandre, P. Degée., Henrist, A.R., Dubios, Ph., 2003. New nanocomposite materials based on plasticized poly(L-lactide) and organo-modified montmorillonites: thermal and morphological study. Polymer 44, 443-450.

Pluta, M., 2004. Morphology and properties of polylactide modified by thermal treatment, filling with layered silicates and plasticization. Polym. 45, 8239-8251.

Pollet, E., Paul, M-A., Dubois, Ph., 2002. New Aliphatic Polyester Layered-Silicate Nanocomposites. In: Chiellini, E., Solaro, R., (Eds.), Biodegradable Polymers and Plastics. Kluwer Academic/Plenum Publishers, New York, pp. 327-350.

Ranade, A., D'Souza, N., Gnade, B., Thellen., Orroth, C., Froio, D., Lucciarini, J., Ratto, J.A., 2004. Effect of Coupling Agent on the Dispersion of PETG Montmorillonite Nanocomposite films. In: Ovid'ko, I., Pande, C.S., Krishnamoorti, R., Lavernia, E., Skandan, G., (Eds.), Mat. Res. Soc. Symp. Proc. – Mechanical Properties of Nanostructured Materials and Nanocomposites Materials Research Society: Warrendale, Pennsylvania, Vol. 791, 283-288.

Ray, S.S., Yamada, K., Okamoto, M., Fujimoto, Y., Ogami, A. Ueda, K., 2002. New polylactide/layered silicate nanocomposites. 1. preparation, characterization and properties. Macromol. 35, 3104-3110.

Ray, S.S., Okamoto, K., Okamoto, M., 2003. Structure – property relationship in biodegradable poly (butylene succinate)/layered silicate nanocomposites. Macromol. 36, 2355-2367.

Simmons, S., Thomas, E.L., 1995. Structural characteristics of biodegradable thermoplastic starch/poly (ethylene-vinyl alcohol) blends. J. Appl. Polym. Sci. 58, 2259- 2285.

Stevens, E.S., 2002. The Reemergence of Bioplastics. In: Green Plastics – An Introduction to the New Science of Biodegradable Plastics. Princeton University Press, Princeton, pp. 104-134.

Tanoue, S., Hasook, A., Itoh, T., Yanou, M., Iemoto, Y., Unryu, T., 2006. Effect of screw rotation speed on the properties of polystyrene/clay nanocomposites prepared by a twin-screw extruder. J. Appl. Polym. Sci. 101, 1165-1173.

Yuen, J-H., Bang, G-S., Park, B.J., Ham, S.K., Chang, J-H., 2006. Poly (vinyl alcohol) nanocomposite films: thermo optical properties, morphology, and gas permeability. J. Appl. Polym. Sci. 101, 591-596.

Zhang, G., Yan, D., 2003. Crystallization kinetics and melting behavior of nylon 10,10 in nylon 10,10-montmorillonite nanocomposites. J. Appl. Polym. Sci. 88, 2181-2188.

Table 1
Characteristics of the four clays. T = tallow (~65% C18, ~30% C16, ~5% C14), HT = hydrogenated tallow, anion = chloride

Clay	Ammonium cations	Modifier concentration (meq/100g)	Basal spacing (001) (Å)
10A	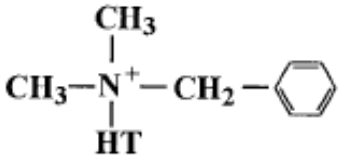	125	19.2
25A	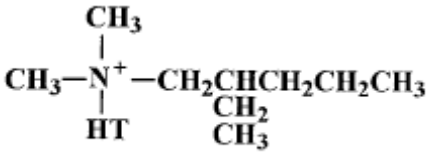	95	18.6
93A	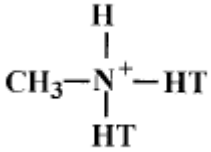	90	23.6
15A	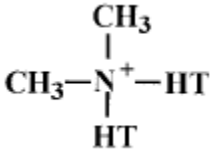	125	31.5

Table 2

Tapioca starch-PLA (TS/PLA)-organoclay formulations

Samples	Organoclay (3%)
TS/PLA	-
TS/PLA/10A	10A
TS/PLA/25A	25A
TS/PLA/93A	93A
TS/PLA/15A	15A

Table 3
Diffraction peaks, d_{001}-spacings and $\Delta\, d_{001}$-spacings of 10A, 15A, 25A and 93A and their nanocomposite foams with tapioca starch-PLA (TS/PLA)

Samples	Diffraction peak (2θ, degree)	d_{001}-spacings (Å)	$\Delta\, d_{001}$-spacings (Å)	Degree of swell (%)
10A	4.66	18.96		
TS/PLA/10A	2.58	34.24	15.28	43.00
25A	4.54	19.46		
TS/PLA/25A	3.02	29.25	9.79	33.46
93A	3.78	23.37		
TS/PLA/93A	2.76	32.01	8.64	26.99
15A	3.12	28.32		
TS/PLA/15A	2.78	31.78	3.46	10.89

Table 4
Thermal properties of tapioca starch-PLA (TS/PLA) and TS/PLA/clay nanocomposite foams

Samples	Thermal property		
	First heating		Second heating
	T_g (º C)	T_m (º C)	T_m (º C)
TS/PLA	63.4	171.5	165.0
TS/PLA/10A	63.8	164.2	163.4
TS/PLA/25A	60.8	171.6	161.4
TS/PLA/93A	63.8	157.4	163.9
TS/PLA/15A	62.4	169.1	163.9

Table 5
Physical and mechanical properties of tapioca starch-PLA (TS/PLA) and TS/PLA/clay nanocomposite foams

Samples	Physical property		Mechanical property		
	Radial expansion ratio	Unit density (kg/m^3)	Bulk spring index	Bulk compressibility (MPa)	Young's modulus (kPa)
TS/PLA	26.8±0.870b	43.4±4.60b	0.955±0.009ab	8.78±2.98c	135.2±18.2b
TS/PLA/10A	21.4±2.06c	61.7±11.9a	0.951±0.007ab	16.6±1.36a	263.7±15.7a
TS/PLA/25A	15.2±0.651e	53.4±2.60a	0.960±0.004a	12.8±1.03b	154.2±13.7b
TS/PLA/93A	46.4±1.80a	23.0±0.80c	0.944±0.015b	0.989±0.025d	49.97±5.32c
TS/PLA/15A	17.4±0.584d	57.6±5.30a	0.955±0.005ab	8.05±0.426c	143.2±6.73b

[a-c] means with same letter within a column indicate no significant (P>0.05) difference by Duncan multiple range test

Table 6
Physico-chemical properties of tapioca starch-PLA (TS/PLA) and TS/PLA/clay nanocomposite foams

Samples	Physico-chemical property	
	WAI (g/g)	WSI (%)
TS/PLA	1.96±0.11c	76.3±2.88a
TS/PLA/10A	7.07±0.16a	46.3±0.58b
TS/PLA/25A	6.60±0.29b	51.3±7.23b
TS/PLA/93A	1.98±0.22c	77.7±0.58a
TS/PLA/15A	7.14±0.24a	47.0±1.00b

[a-c] means with same letter within a column indicate no significant (P>0.05) difference by Duncan multiple range test

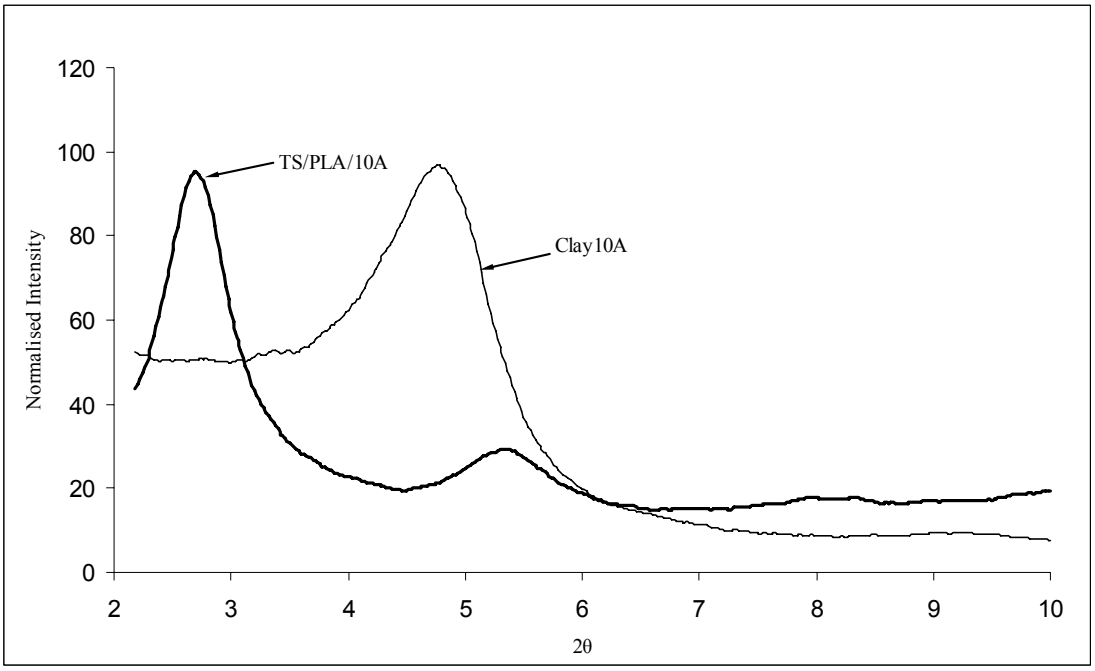

Fig. 1. X-ray patterns of 10A and its nanocomposite foam with tapioca starch and PLA (TS/PLA).

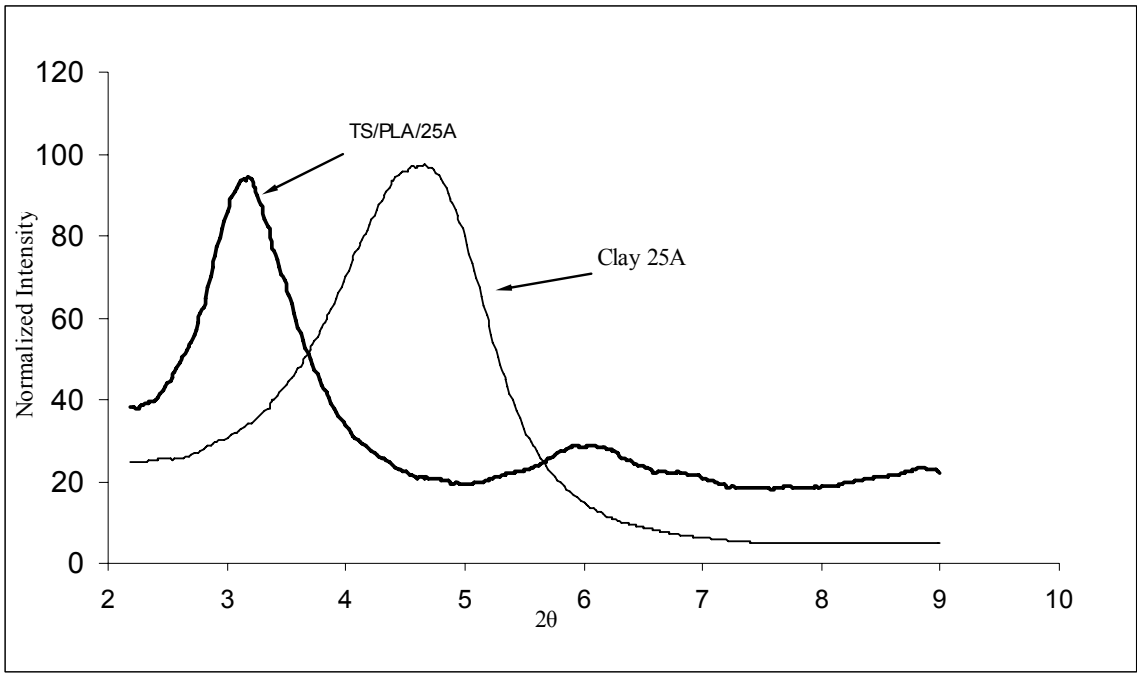

Fig. 2. X-ray patterns of 25A and its nanocomposite foam with tapioca starch and PLA (TS/PLA).

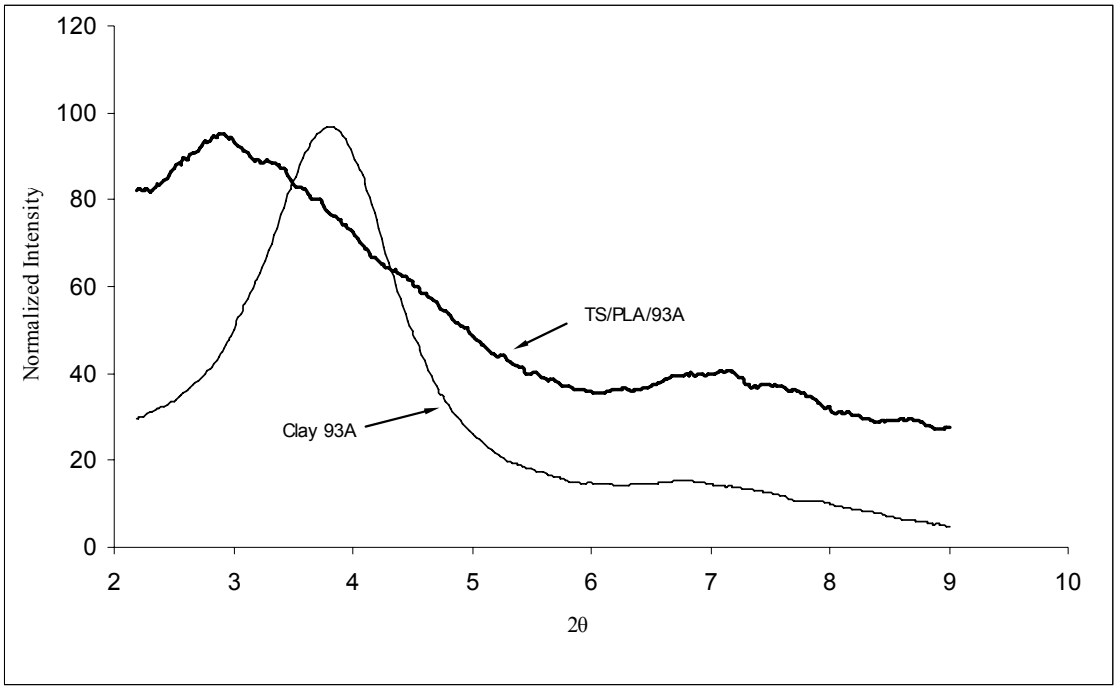

Fig. 3. X-ray patterns of 93A and its nanocomposite foam with tapioca starch and PLA (TS/PLA).

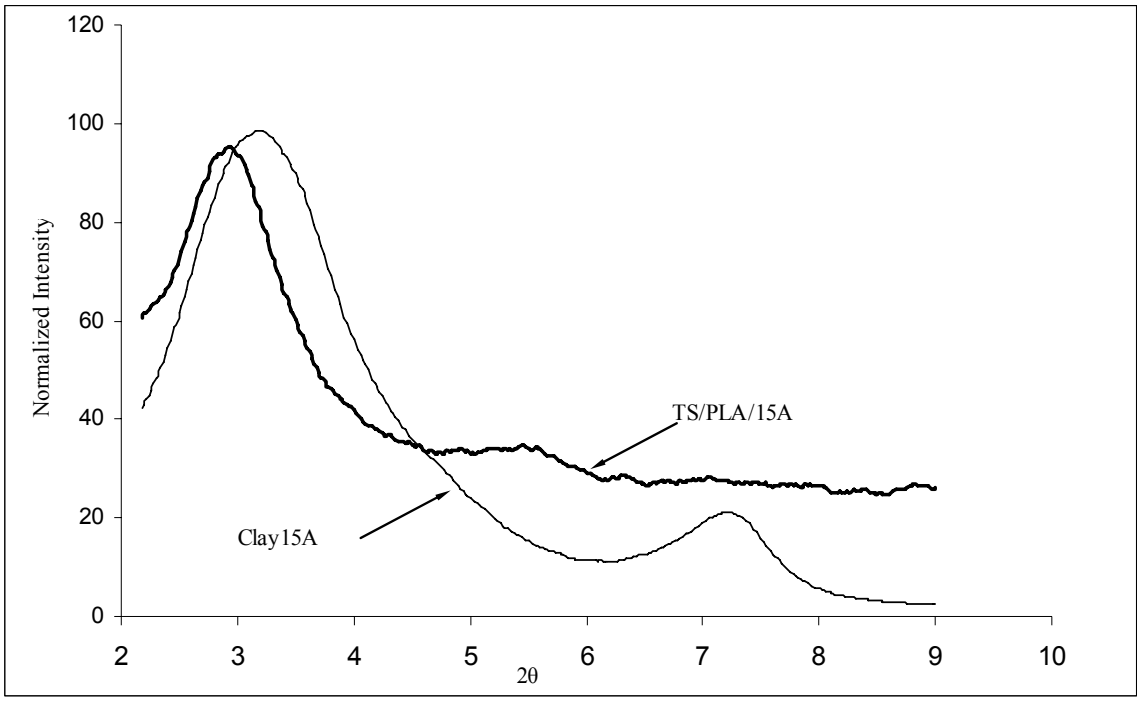

Fig. 4. X-ray patterns of 15A and its nanocomposite foam with tapioca starch and PLA (TS/PLA).

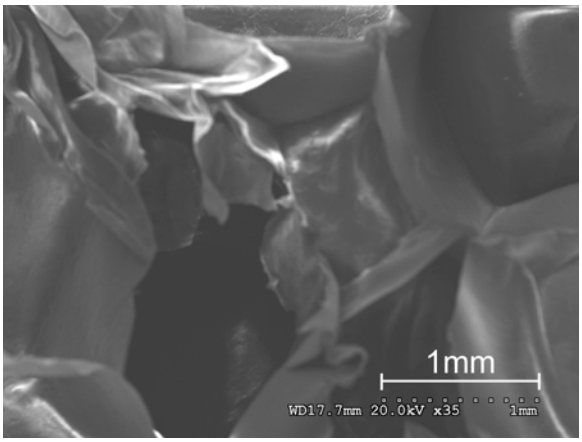

Fig. 5. Scanning electron micrograph of tapioca starch and PLA (TS/PLA) composite foam (magnification 35x).

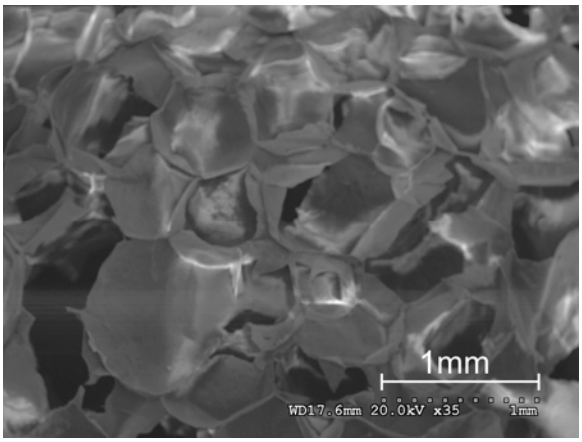

Fig. 6. Scanning electron micrograph of TS/PLA/Cloisite 10A nanocomposite foam (magnification 35x).

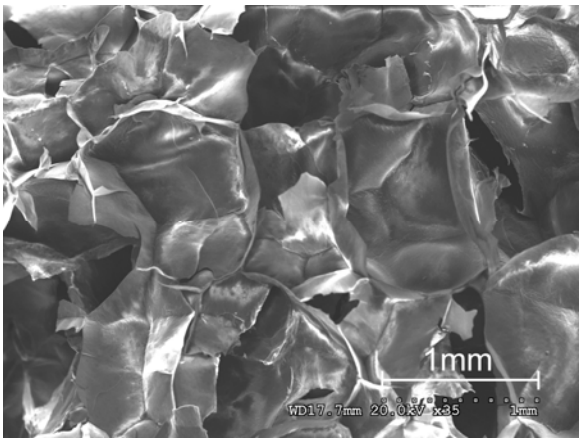

Fig. 7. Scanning electron micrograph of TS/PLA/Cloisite 25A nanocomposite foam (magnification 35x).

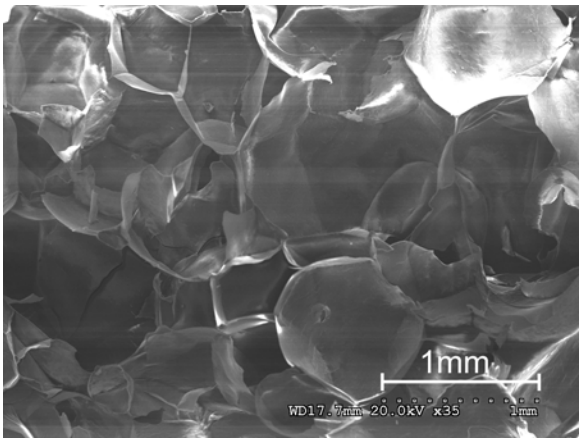

Fig. 8. Scanning electron micrograph of TS/PLA/Cloisite 93A nanocomposite foam (magnification 35x).

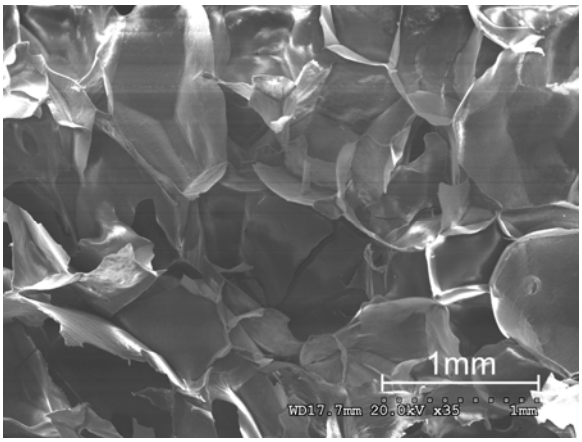

Fig. 9. Scanning electron micrograph of TS/PLA/Cloisite 15A nanocomposite foam (magnification 35x).

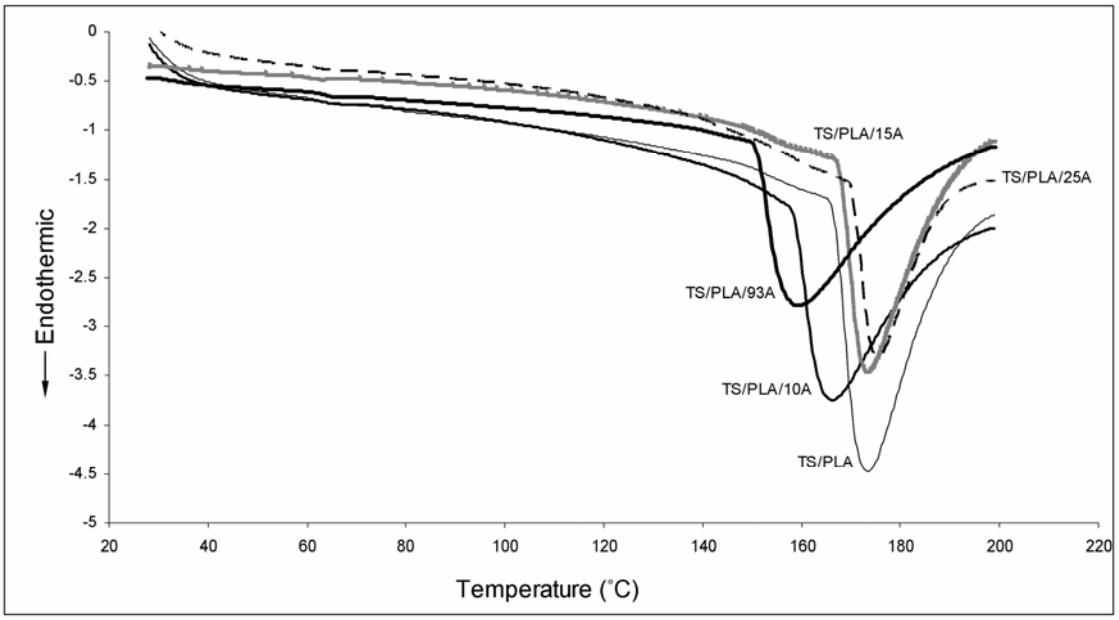

Fig. 10. DSC thermographs (first heating scans) of tapioca starch and PLA (TS/PLA) and TS/PLA/clay nanocomposite foams.

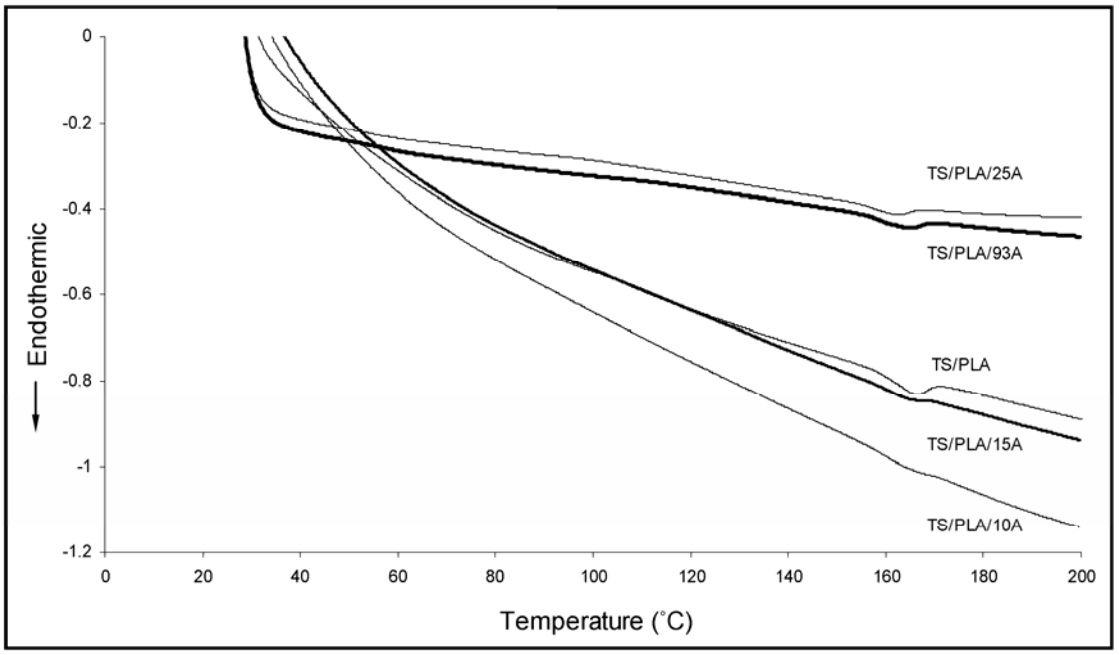

Fig. 11. DSC thermographs (second heating scans) of tapioca starch and PLA (TS/PLA) and TS/PLA/clay nanocomposite foams.

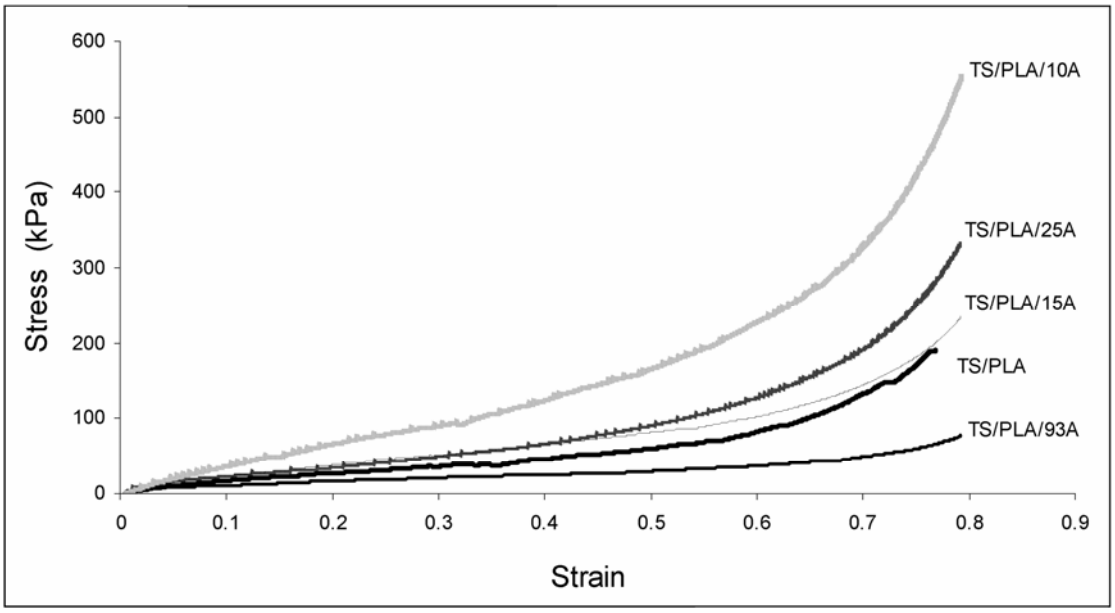

Fig. 12. Stress and strain curves of tapioca starch, PLA (TS/PLA) and clay nanocomposite foams.

CHAPTER III

TAPIOCA STARCH-POLY(LACTIC ACID)-CLOISITE 30B NANOCOMPOSITE FOAMS

This research paper has been published as:

Siew Yoong Lee, Milford A. Hanna (2008). Tapioca Starch-Poly(Lactic Acid)-Cloisite 30B Nanocomposite Foams. *Polymer Composites* (In press).

Tapioca Starch-Poly(Lactic Acid)-Cloisite 30B Nanocomposite Foams

ABSTRACT

Tapioca starch (TS), poly(lactic acid) (PLA), and Cloisite 30B nanocomposite foams, with four clay contents of 1, 3, 5, 7 wt%, were prepared by a melt-intercalation method. Selected structural, thermal, physical and mechanical properties were characterized using X-ray diffraction (XRD), scanning electron microscopy (SEM), differential scanning calorimetry (DSC), thermogravimetry analyses (TGA), and an Instron universal testing machine, respectively. XRD results indicated that intercalation of TS/PLA into the nanoclay layers occurred in all four nanocomposite foams. At the same time, tactoid structures were observed in all nanocomposite foams but to a lesser extend with 1 and 3 wt% clay contents. Effect of clay content on melting temperature (T_m), onset degradation temperature, radial expansion ratio (RER), unit density, bulk compressibility and bulk spring index (BSI) of the nanocomposites were investigated. Among the four nanocomposites, 3 wt% clay content produced significantly different (p<0.05) properties.

INTRODUCTION

Poly(lactic acid) (polylactate or polylactide) (PLA) is a polyester, and is synthesized from L- and D-lactic acid, which are produced from the fermentation of sugar and (poly)saccharides such as sugar feedstocks and corn, wheat and other starch sources. The lactic acid is converted to PLA either by ring-opening polymerization or by condensation polymerization. PLA is insoluble in water and has good moisture and grease resistance. Its mechanical properties can be modified by varying its molecular weight and its crystallinity [1]. PLA is used widely as a biodegradable and renewable plastic for uses in service ware, grocery, waste-composting bags, mulch films, controlled release matrices for fertilizers, pesticides and herbicides [2].

Starch is an inexpensive and readily available resource, and is often used as a filler for the replacement of petroleum-derived synthetic polymers to decrease environmental pollution. However, starch has severe limitations because of its solubility and poor water-resistance, making starch products very sensitive to the relative humidity at which they are stored and used [3]. Starch-polyester blends are being produced with the objective of maintaining the excellent physical properties of the polyesters while reducing cost. A process was developed at the University of Nebraska-Lincoln to produce starch-based plastic foam with 70% starch combined with a variety of ingredients and plastics [4]. Fang and Hanna [5] found that addition of PLA to regular and waxy corn starches improved the physical and mechanical properties of the foams. Recently, formation of nanocomposites with the aim of improving functional properties has become popular.

Polymer nanocomposites are a class of reinforced polymers containing small quantities (1-5 wt%) of nanometric-sized clay particles. The functional properties of the nanocomposites were improved markedly compared to those of the unfilled polymer or conventional composites. These improvements included high moduli [6,7]; increased tensile strength [8] and thermal stability [9]; decreased gas permeability [10], flammability [11] and water absorbance [12]; and increased biodegradability of biodegradable polymers [13]. Alexandre and Dubois [14] found that very low clay loading, typically 5 wt%, or lower increased moduli, strength and heat resistance, and decreased gas permeability and flammability of nanocomposites. Park et al [15] found that incorporating nanoclay resulted in material with higher tensile strength, reduced water vapor transmission and improved thermal stability.

Of the four methods (solution intercalation, in situ polymerization, melt intercalation, and template synthesis) which have been used to synthesize nanocomposites, melt intercalation is the most appealing approach because of its versatility, compatibility with polymer processing equipment, and because it is an environmentally friendly process that requires no solvent and is suitable for industrial uses [16,17]. This technique involves annealing, statically or under shear, a mixture of the polymer and silicates above the softening point of the polymer [18]. During annealing, the polymer chains diffuse from the bulk polymer melt into the galleries between the silicate layers.

Generally, polymer/layered silicate composites are divided into three main types: tactoid, intercalated, and exfoliated nanocomposites. In a tactoid, the polymer is unable to intercalate between the silicate sheets and the properties of the composites stay in the

same range as the traditional microcomposites. Intercalated nanocomposites occur when a small amount of polymer moves into the gallery spacing between the silicate platelets. When the silicate layers are completely and uniformly dispersed in a continuous polymer matrix, an exfoliated or delaminated structure is formed [19]. The intercalated and exfoliated nanocomposites currently are of primary interest because their properties are significantly improved, even at low clay concentrations. However, the formation of intercalated or exfoliated nanocomposites depends on the type of organoclay [20], the clay content [21,22] and the processing conditions [23].

The objectives of this study were to prepare tapioca starch/PLA/Cloisite 30B nanocomposite foams of different clay contents via melt-intercalation and to investigate the influence of clay content on selected structural, morphological, thermal, physical and mechanical properties of the foams.

EXPERIMENTAL PROCEDURES

Materials

Semicrystalline poly(lactic acid) (PLA) resin of MW_n 85,000 was produced by Cargill, Inc. (Minneapolis, MN). It contained ~93% L-lactide, 2% D-lactide and 5% mesolactide. Tapioca starch (17% amylose and 83% amylo-pectin) was purchased from CongAgra Foods (Omaha, NE), agglomerated into spherical granules of 2-4 mm diameter to facilitate feeding into the extruder, and adjusted to 18% moisture content, dry basis, prior to extrusion. Tapioca starch and 10% PLA were blended with 0.5% sodium bicarbonate, 0.5% citric acid and clay in a Hobart mixer (Model C-100, Horbart Corp.,

Troy, OH) and stored in plastic jars prior to extrusion. PLA content of 10% was selected based on preliminary experiments. Fang and Hanna [24] reported that at 10% PLA content, the foams possessed the highest spring index and intermediate compressibility and Young's modulus values. Sodium bicarbonate and citric acid were added to degrade the biodegradable polymer into chains of between 1,000 and 100,000 Daltons or approximately 500 to 50,000 monosaccharide groups to promote expansion [4]. Organically modified montmorillonite under the trade name of Cloisite 30B (methyl-tallow-bis-2-hydroxyethyl ammonium)(MT2EtOH) was obtained from Southern Clay Products Inc. (Gonzalez, TX). The particle size range of the nanoclay was 2-13 ηm. PLA and the nanoclay were dried in the oven at 70ºC for at least 24 h. Table 1 gives the six different formulations used.

Extrusion

A twin-screw extruder (Model DR-2027-K13, C. W. Brabender, Inc., S. Hackensack, NJ, USA) with corotating mixing screws (Model CTSE-V, C. W. Brabender, Inc., S. Hackensack, NJ, USA) was used to conduct extrusions. The conical screws had diameters decreasing from 43 mm to 28 mm along their length of 365 mm from the feed end to the exit end. On each screw, there was a mixing section, in which small portions of the screw flights were cut away. The mixing section enhanced mixing and also increased the residence time of the sample in the barrel. A 150-rev/min screw speed was used for all extrusions. The temperature at the feeding section was maintained at 50°C, the second barrel section at 120°C, the third barrel section at 150°C and die section at 170°C. A 3 mm diameter die nozzle was used to produce a continuous

cylindrical rope-like extrudates which were cut by a rotary cutter. Data including screw rotating speeds, barrel temperature profiles, pressure profiles and torque readings were recorded for subsequent analyses. Extrusion conditions selected were based on preliminary studies and previous experiments.

Extrudate property evaluations

X-ray patterns of the samples were obtained using a Rigaku D/Max– B X-ray diffractometer (Tokyo, Japan) with Cu-Kα radiation (λ = 1.544 Å) at a voltage of 40 kV and 30 mA. Samples were scanned in the range of diffraction angle 2θ = 2 - 10° with a scan speed of 1°/min at room temperature.

The morphologies of TS/PLA and TS/PLA nanocomposite foams were observed under a scanning electron microscope(SEM) (Hitachi S-3000N, Tokyo, Japan). Before testing, the samples were mounted on SEM stubs with double-sided adhesive tape and then coated with platinum under vacuum to make the sample conductive.

Differential scanning calorimetry (DSC) measurements were performed with a Mettler DSC (Columbus, OH, USA). About 10 mg of dried, ground samples were placed in aluminum sample pans. The samples were heated from 25 to 200 °C at a heating rate of 10 ° C/min in a nitrogen atmosphere. The melting temperature was determined as the temperature at the maximum value of melting peak.

Thermogravimetry analyses (TGA) were performed with a Perkin-Elmer TGA7 analyzer calibrated with nickel. Samples of 3-6 mg were placed in the balance system and heated from 50 to 600 °C at a heating rate of 20 °C/min in a nitrogen atmosphere. Onset temperature and weight loss were calculated using the TGA7 software.

Radial expansion ratio (RER) of the extruded foams were calculated by dividing the mean cross-sectional areas of the extrudates by the cross-sectional area of the die nozzle. Each calculated value was a mean of 20 observations.

Unit densities of the extrudates were determined using a glass bead displacement method originally developed for determining the volume of cookies [25] with modifications [26]. Glass beads of 0.1 mm diameter were used as the displacement medium. A mean value was obtained by averaging five replicates.

Bulk spring index (BSI) measurements were made using an Instron universal testing machine (Model 5566, Instron Engineering Corp., Canton, MA). A cylindrical aluminium container with a volume of 365 cm^3 (6.93 cm in diameter and 9.68 cm in depth) was used to confine the bulk samples. The forces required to initially compress the samples to 80% of their original volumes and the forces required to recompress the same samples 1 min after releasing the initial load were recorded. BSI was calculated by dividing the recompression force by the initial compression force and has an ideal value of 1. A mean value was obtained by averaging five replicates.

Bulk compressibility was calculated using the same data collected in the BSI test. It was calculated by dividing the peak force required to compress the sample to 80% of its initial volume. A mean value was obtained by averaging five replicates.

Statistical analyses

All results reported are means of two or more replications. The data from radial expansion ratio, unit density, bulk spring index and bulk compressibility measurement were analyzed using the general linear models (GLM) in SAS analysis program (SAS

Institute Inc., Cary, NC). Duncan's multiple range tests were conducted to check for significant ($p<0.05$) differences between treatment groups.

RESULTS AND DISCUSSION

A preliminary study using three types of clay (Cloisite 30B, Na^+ and 20A) at 3 wt% was conducted to determine the suitability of the type of clay with TS/PLA matrix. It was found that among the three types of clay, Cloisite 30B exhibited the greatest extent of enlargement confirming that the interactions between TS/PLA and nanoclays were compatible. In this study, four different relative contents of Cloisite 30B at 1, 3, 5 and 7 wt% were added to the TS/PLA matrices in order to study the most suitable clay content and its implication on the influence of the interlayer cations on the structural, morphological, thermal, physical and mechanical properties of the nanocomposite foams at a constant level of PLA.

Structural properties of TS/PLA/Cloisite 30B nanocomposites

Wide-angle x-ray diffraction (WAXD) is a classical method for determining the gallery height (*d*-spacing distance) in clay particles [27]. The *d*-spacing can be determined from the diffraction peak in the XRD patterns, and be expressed by Bragg's equation ($\lambda = 2d_{001}\sin\theta$), where d_{001} is the interplanar distance of the (001) diffraction face, θ is the diffraction position, and λ is the wavelength [16]. During melt intercalation, the insertion of polymer into the organoclay galleries forces the platelets apart and increases the *d*-spacing, resulting in a shift of the diffraction peak to lower angles.

Figure 1 shows the diffraction spectra of pristine Cloisite 30B clay and 1, 3, 5, 7 wt% clay nanocomposites. The diffractograms for the four nanocomposite foams showed two peaks. In all four nanocomposites, the first diffraction peaks were observed to shift to lower angles compared to that of pristine nanoclay, indicating that intercalation of TS/PLA polymer into the nanoclay layers occurred. The pristine Cloisite 30B clay had one peak at 4.81º. Paul et al. [28] also observed the presence of two peaks for poly(ethyleneglycol)-plasticized PLA/Cloisite 30B. They concluded that the small diffraction peak was due to the poly(ethyleneglycol)-plasticized PLA.

There were two peaks, a larger peak at 2θ = 2.46 - 2.72 º and a smaller peak at 2θ = 5.18- 5.88˚. The larger peaks for 1, 3, 5, 7 wt% clay had high intensities at 2θ = 2.46˚, 2.48˚, 2.68˚, and 2.72˚, respectively, indicative of intercalation. Intercalation was greater with the lower filler contents of 1 and 3 wt% clay, as shown by the sharp ascent of the diffraction profile baselines at very low angles. The higher clay contents of 5 and 7 wt% tended to have the same diffraction profiles at low angles indicating that they had similar intercalation properties. The smaller peaks for 1, 3, 5, 7 wt% clay had lower intensities at 2θ = 5.88˚, 5.18˚, 5.48˚, and 5.28˚, respectively. The smaller peaks for 1 and 3 wt% clay appeared as shoulders compared to more distinct peaks for the 5 and 7 wt% clays. The presence of smaller peaks indicated that a small fraction of the clay was still present as agglomerated sheets which contributed to a tactoid structure. A similar phenomenom was observed by Kalambur and Rizvi [29]. The tactoid structure was observed for all nanocomposite foams to a lesser extend at the 1 and 3 wt% clay contents.

The peak of the pristine Cloisite 30B clay (2θ = 4.81º) shifted to 2.26º for the 1 wt% clay nanoclay (Table 2). The d_{001}-spacing of 1 wt% clay nanocomposite was 35.91Å, a 17.52 Å increase compared to that of the original Cloisite 30B (18.39 Å). The d_{001}-spacing of 3 wt% clay nanocomposite was 35.62Å, a 17.23 Å increase compared to that of the neat clay. Both exhibited large displacements, indicating intercalation. The d_{001}-spacings of 5 and 7 wt% clay nanocomposites were 32.96Å and 32.48Å, respectively. They produced increases in d_{001}-spacings of 14.57Å and 14.09Å, respectively, compared to that of the neat clay. These data show that the nanocomposite was intercalated to a greater extent at lower clay contents (1 and 3 wt%) than at higher clay contents (5 and 7 wt%). It is believed that the greater the d_{001}-spacings, the greater the interaction of polymer molecular chain with clay layered silicate [16]. The interactions between polymer and nanoclays depend on the compatibility of the surface polarities of polymer and organoclay [30]. Polar-type intercalations also are critical for the formation of intercalated or exfoliated nanocomposites via polymer melt intercalation [31]. The strong interaction or miscibility between TS/PLA and Closite 30B, originated from the strong hydrogen bonding between the hydroxyl group of TS/PLA and the hydroxyl group in the gallery of Closite 30B. These results were consistent with the work of Xu et al. [32] in preparation of starch acetate nanocomposites using Closite 30B. Strong polar-type interactions, especially hydrogen bonding, are critical for the formation of intercalated and exfoliated hybrids [31]. Furthermore, the compatibility and optimum interactions between the polymer matrix and the silicate layer surface itself are crucial to the formation of intercalated and exfoliated nanocomposites [8].

Typical SEM micrographs of TS/PLA foam (Figure 2), 3 (Figure 3) and 7 (Figure 4) wt% clay nanocomposites are presented. The TS/PLA foam exhibited large cell size of ~1.35 mm, with a cell population of 0.804 cells/cm^2. The nanocomposites showed smaller and more compact cells. This indicated that the dispersed organoclay particles acted as nucleating sites for cell formation [33]. The cell sizes for 3 and 7 wt% clay nanocomposites were 0.421 and 0.309 mm, respectively, indicating that increasing clay content decreased the cell size. However, increasing the clay content increased the cell population. The cell populations for 3 and 7 wt% clay nanocomposites were 4.12 and 7.04 cells/cm^2, respectively. The nanoparticles provided an effective way to increase cell population and reduce cell size due to the high nucleation efficiency [34,35].

Thermal properties of TS/PLA / Cloisite 30B nanocomposites

Melting temperature (T_m) of TS/PLA and its nanocomposite foams were investigated by DSC as shown in Table 3. Tapioca starch foam had a T_m of 162.4 °C. T_m of PLA measured by DSC was 173.9 °C. TS/PLA foam had a T_m of 166.8 °C. At 1 wt% clay concentration, the T_m was 164.7 °C as shown in Figure 5. There was a sharp decrease in T_m of 3 wt% nanocomposite (152.0 °C). The T_m of 5 and 7 wt% clay nanocomposite foams were 163.8 °C and 169.8 °C, respectively. It was observed that 1, 5 and 7 wt% clay nanocomposites had T_m at a higher temperature range of 163.8 - 169.8 °C as compared to 3 wt% clay nanocomposites at 152.0 °C. The decrease in T_m with addition of Cloisite 30B into TS/PLA matrix was attributed to the compatibility of this organoclay with the starch and PLA mixture, which suppressed the crystallization [27]. Additionally, the silicate acted as a nucleating agent, causing the viscosity of the matrix

to drop, decreasing the T_m [36]. Artzi et al. [21] observed the same occurrence of decreased T_m with increasing clay content. The influence of nanoclay on the reduction of crystallization and melting behavior became distinct when the concentration of clay was around 3 wt % due to the intercalated nanostructure [28, 37, 38].

Changes in the thermal stability of TS/PLA and its nanocomposite foams with addition of different clay contents, were examined by TGA and are summarized in Table 3. The weight-loss curves of TS/PLA and its nanocomposite foams, as a function of temperature, are shown in Figure 6. The initial degradation of TS foam began at 343.9 °C with a weight loss of 89.2%. The onset degradation of TS/PLA foam was higher at 352.2 °C with a weight loss of 89.9%. This was due to the addition of PLA. Further heating to 600 °C resulted in carbonization and ash formation [39]. In general, the thermal stabilities of the nanocomposite foams were enhanced as compared to the TS/PLA foams. This was reflected by the fact that the onset temperature of thermal degradation increased with the incorporation of Cloisite 30B into TS/PLA matrix. For the nanocomposites containing 1, 3, 5, and 7 wt% of Cloisite 30B, the increases in the onset temperatures were 2, 1, 3, and 5 °C respectively, as compared to the TS/PLA foams. The weight loss values were 89.4, 91.1, 90.3, and 91.7% for the nanocomposite foams with clay loadings of 1, 3, 5, and 7 wt%, respectively.

The increase in thermal stability of the nanocomposites was a result of the interactions of TS/PLA molecules and clay. This interaction restricted the thermal motion of TS/PLA molecules, thus increasing the thermal stability. The presence of clay acted as insulators, thus inhibiting the passage of volatile degradation products and enhanced the thermal stability of the nanocomposites [40].

Physical and mechanical properties of TS/PLA / Cloisite 30B nanocomposites

Physical and mechanical properties of the foams are related strongly to the structure of inter-molecular matrices. These inter-molecular matrices resulted from the compatibility of polarities of tapioca starch, PLA and water which resulted in improved interfacial adhesion between starch and PLA [41]. It was expected that the foams with strong and well-developed inter-molecular matrices would have good high physical and mechanical properties. RER and unit density are important physical properties of foams. RER and unit density are inversely proportionally to each other. High RER and low unit density are desirable attributes for foams because of reduced material cost. Density is important because it affects the thermal properties of foams. RER values of the nanocomposites were significantly different ($p<0.05$) from each other (Table 4). Pure tapioca starch foam had the lowest RER of 12.0. The highest RER of TS/PLA foam was 21.1. This large increase in RER, with addition of PLA, was due to the effect of the PLA. The adhesion force between starches and PLA may have been caused by polar interactions between the two phases, and because hydrogen bonding forces existed between the carbonyl group on PLA and the hydroxyl groups on starch [42]. Among the four nanocomposite foams, the 3 wt% clay content gave the biggest RER of 20.5. The RER's of the 1 and 7 wt% clay nanocomposites were not significantly different at 17.2 and 17.8. The 5 wt% clay nanocomposite had a RER of 15.6. These results indicated that the addition of PLA and clay had an effect on RER of tapioca starch foam.

Pure tapioca starch foam had a unit density of 74 kg/m^3. Addition of PLA had a significant effect on the unit density of TS/PLA foam at 42 kg/m^3. It also was observed that the addition of different clay contents had significant effects on the unit density of

the nanocomposite foams. The 1, 5 and 7 wt% clay nanocomposites had unit densities which were not significantly different from each other at 54 kg/m^3, 57 kg/m^3 and 49 kg/m^3, respectively. The 3 wt% clay nanocomposite had the lowest unit density of 45 kg/m^3.

BSI and bulk compressibility are interrelated mechanical properties. BSI relates to resiliency, and refers to the ability of a material to recover its original shape after it has been deformed. A larger BSI indicates a greater degree of rebound of a material after being compressed. Bulk compressibility describes the cushioning ability of a material, and is related to its relative softness or hardness. High BSI and low compressibility are desirable for loose-fill packaging material [43]. Pure tapioca starch foam had a BSI of 0.964 and was significantly different from the BSI of TS/PLA foam (0.959). BSI was influenced (p<0.05) significantly with the addition of different clay contents into the TS/PLA matrix. The 1 wt% nanocomposite had the highest BSI of 0.958. The 3 and 5 wt% clay nanocomposites had BSI which were not significantly different from each other at 0.950 and 0.952, respectively. The highest clay content produced the lowest BSI of 0.947. This indicated that a small amount of nanoparticles can act as reinforcing filler to improve the mechanical properties due to the strong interaction between TS/PLA and Closite 30B. Borse and Kamal [44], used different nanoclays and different clay loadings in their work and found that Closite 30B showed modulus enhancement and improved tensile strength in the nanocomposites.

Pure tapioca starch foam had an exceptionally high bulk compressibility of 57.6 MPa. The bulk compressibility decreased drastically, to 7.19 MPa, with the addition of PLA. This could have been due to the PLA readily reacting with the starch matrix to

form strong interactions between them [45]. Addition of different clay contents to the nanocomposites reduced the bulk compressibility significantly. The lowest clay content (1 wt%) produced a bulk compressibility of 8.75 MPa while the highest loading of clay (7 wt%) produced a bulk compressibility of 4.99 MPa. The lowest bulk compressibility of 4.99 MPa was obtained with 3 wt% clay.

CONCLUSIONS

The purpose of this study was to investigate TS/PLA nanocomposites with the focus on the changes of the properties due to nanoclay content. From the WAXD study, all four TS/PLA/Closite 30B nanocomposites produced intercalated structures. At the same time, a tactoid structure was observed for all nanocomposites, to a lesser extent with the 1 and 3 wt% clay contents. The greatest increase in the d_{001}-spacings of Closite 30B were produced by low clay loadings of 1 and 3 wt%. The higher clay loadings at 5 and 7 wt% produced smaller increases in the d_{001}-spacings. The morphological study showed that the cell sizes for 3 and 7 wt% nanocomposites were 0.421 and 0.309 mm, respectively, indicating that increasing clay content decreased the cell size and increased the cell population. The cell populations for 3 and 7 wt% clay nanocomposites were 4.12 and 7.04 cell/cm^2, respectively.

In terms of thermal properties, the 1, 5 and 7 wt% clay nanocomposites had T_m in the range of 163.8 - 169.8 °C as compared to the 3 wt% clay nanocomposite at 152.0 °C. The thermal stabilities of the nanocomposite foams were enhanced as compared to the TS/PLA foams. For the nanocomposites containing 1, 3, 5, and 7 wt% of Cloisite 30B,

the increases in the onset temperatures were 2, 1, 3, and 5 °C, respectively, as compared to the TS/PLA foams.

The addition of 3 wt% clay produced the highest RER of 20.5, the lowest unit density of 45 kg/m^3 and the lowest bulk compressibility of 4.99 MPa which were desirable qualities in packaging foams. However, the highest bulk spring index of 0.958 was obtained with the addition of 1 wt% clay. Among the four nanocomposites, 3 wt% clay content produced significantly different (p<0.05) properties.

REFERENCES

1. E.S. Stevens, *Green Plastics – An Introduction to the New Science of Biodegradable Plastics*, Princeton University Press: Princeton, NJ. (2002).

2. Q. Fang, and M.A. Hanna, *Ind. Crops and Prod.*, **10**, 47 (1999).

3. S. Simmons, and E.L. Thomas, *J. Appl. Polym. Sci*., **58**, 2259 (1995).

4. R. Chinnaswamy, and M.A. Hanna, U.S. Patent, 496,895 (1993).

5. Q. Fang, and M.A. Hanna, *Trans. ASAE*, **43**, 1715 (2000).

6. Y.T. Lim, and O.O. Park, *Macromol. Rapid Commun*., **21**, 231 (2000).

7. P.H. Nam, P. Maiti, M. Okamoto, T. Kotaka, N. Hasegawa, and A. Usuki, *Polymer*, **42**, 9633 (2001).

8. H.R. Dennis, D.L. Hunter, D. Chang, S. Kim, , J.L. White, J.W. Cho, and D.R. Paul, *Polymer*, **42**, 9513 (2001).

9. J-H. Chang, T-G. Jang, K.J. Ihn, W-K. Lee, and G.S. Sur, *J. Appl. Polym. Sci.*, **90**, 3208 (2003).

10. J-H. Yuen, G-S. Bang, B.J. Park, S.K. Ham, and J-H. Chang, *J. Appl. Polym. Sci*., **101**, (2006).

11. A.B. Morgan, *Polym. Adv. Technol*., **17**, 206 (2006).

12. B-S. Chiou, E. Yee, D. Wood, J. Shey, G. Glenn, and W. Orts, *Cereal Chem.*, **83**, 300 (2006).

13. S.S. Ray, K. Yamada, M. Okamoto, and K. Ueda, *Polymer*, **44**, 867 (2003).

14. M. Alexandre, P. Dubois, *Mater. Sci. Eng*., **28**, 1 (2000).

15. H-M. Park, X. Li, C.Z. Jin, C.Y. Park, W.J. Cho, and C.-S. Ha, *Macromol. Mater. Eng.*, **287**, 553 (2002).

16. W.M. Choi, T.W. Kim, O.O. Park, Y.K. Chang, and J.W. Lee, 2003. *J. Appl. Polym.* Sci., **90**: 525 (2003).

17. X.C. Li, and C-S. Ha, *J. Appl. Polym. Sci*., **87**, 1901 (2003).

18. R.A. Vaia, and E.P. Giannelis, *Macromolecules*, **30**, 7990 (1997).

19. E. Pollet, M-A. Paul, and Ph. Dubois, *Biodegradable polymers and plastics*, Kluwer Academic/Plenum Publishers, New York (2002).

20. A. Ammala, A.J. Hill, K.A. Lawrence, and T. Tran, *J. Appl. Polym. Sci.*, **104**, 1377 (2007).

21. N. Artzi, Y. Nir, M. Narkis, and A. Siegmann, *J. Polym. Sci. Part B: Polym. Phys.*, **40**, 1741 (2002).

22. M.L. Nobel, and S.J. Picken, *J. Appl. Polym. Sci*., **104**, 2146 (2007).

23. S. Tanoue, A. Hasook, T. Itoh, M. Yanou, Y. Iemoto, and T. Unryu, *J. Appl. Polym. Sci*., **101**, 1165 (2006).

24. Q. Fang, and M.A. Hanna, *Cereal Chem*., **77**, 779 (2000).

25. M.P. Hwang, and K. Hayakawa. *J. Food Sci*., **45**, 1400 (1980).

26. S. Bhatnagar, and M.A. Hanna, ASAE Paper No., 916541 (1991).

27. Y. Di, S. Iannace, E.D. Maio, and L. Nicolais, *J. Polym. Sci. Part B: Polym. Phys.*, **43**, (2005).

28. M-A. Paul, M. Alexandra, Ph. Degee, C. Henrist, A. Rulmont, and Ph. Dubois, *Polymer*, **44**, 443 (2003).

29. S. Kalambur, and Syed.S.H. Rizvi, *J. Appl. Polym. Sci*., **96**, 1072 (2005).

30. H-M. Park, W-K. Lee, C-Y. Park, W-J. Cho, and C-S. Ha, *J. Mater. Sci*., **38**, 909 (2003).

31. R.A. Vaia, and E.P. Giannelis, *Macromolecules*, **30**, 8000 (1997).

32. Y.X. Xu, J. Zhou, and M.A. Hanna, *Cereal Chem*., **82**: 105 (2005).

33. Y. Fujimoto, S.S. Ray, M. Okamoto, A. Ogami, K. Yamada, and K. Ueda, *Macromol. Rapid Commun*., **24**, 457 (2003).

34. R.S. Lee, H.-M. Park, H. Lim, T. Kang, X.C. Li, W-.J. Cho, and C.-S. Ha, *J. Polym*., **43**, 2495 (2002).

35. V.K. Rangari, T.A. Hassan, Y.X. Zhou, H. Mahfuz, S. Jeelani, and B.C. Prorok, *J. Appl. Polym. Sci.*, **103**, 308 (2007).

36. K.H. Wang, M.H. Choi, C.M. Koo, M. Xu, I.J. Chung, M.C. Jang, S.W. Choi, and H.H. Song, *J. Polym. Sci*., **40**, 1454 (2002).

37. X. Hu, and A.J. Lesser, *J. Polym. Sci. Part B: Polym. Phys*., **41**, 2275 (2003).

38. M. Pulta, *Polymer*, **45**, 8239 (2004).

39. S. Thiebaud, J. Aburto, I. Alric, E. Borredon, D. Bikiaris, J. Prinos, C. Panayiotou, *J. Appl. Polym. Sci*., **65**, 705 (1997).

40. Y. Wang, F-B. Chen, and K-C. Wu, *J. Appl. Polym. Sci.*, **97**, 1667 (2005).

41. J.W. Park, S.S. Im, S.H. Kim, and Y.H. Kim, *Polym. Eng. Sci*., **40**, 2539 (2000).

42. T. Ke, and X. Sun, *Cereal Chem*., **77**, 761 (2000).

43. S. Bhatnagar, and M.A. Hanna, *Trans. ASAE* **38**, 567 (1995).

44. N.K. Borse, and M.R. Kamal, *Polym. Eng. Sci*., **46**, 1094 (2006).

45. M. Pluta, A. Galeski, M. Alexandre, M.-A. Paul, and P. Dubios, *J. Appl. Polym. Sci*. **86**, 1497 (2002).

TABLE 1. Clay contents used in the synthesis of tapioca starch-PLA (TS/PLA) nanoccomposite foams.

Materials	Cloisite 30B (wt%)
TS	-
TS/PLA	-
TS/PLA+30B1	1
TS/PLA+30B3	3
TS/PLA+30B5	5
TS/PLA+30B7	7

TABLE 2. Diffraction peaks, d_{001}-spacings and $\Delta\, d_{001}$-spacings of Cloisite 30B and its nanoccomposite foams with tapioca starch (TS/PLA) at different clay contents.

Materials	Diffraction peak (2θ, degree)	d_{001}-spacings (Å)	$\Delta\, d_{001}$-spacings (Å)
30B	4.81	18.39	-
TS/PLA+30B1	2.46	35.91	17.52
TS/PLA+30B3	2.48	35.62	17.23
TS/PLA+30B5	2.68	32.96	14.57
TS/PLA+30B7	2.72	32.48	14.09

TABLE 3. Thermal properties of tapioca starch (TS), tapioca starch-PLA (TS/PLA) and its nanoccomposite foams with different clay contents.

	Thermal Property		
Materials	T_m (º C)	Onset Degradation Temperature (º C)	Weight Loss (%)
TS	162.4	343.9	89.2
TS/PLA	166.8	352.2	89.9
TS/PLA+30B1	164.7	354.0	89.4
TS/PLA+30B3	152.0	353.2	91.1
TS/PLA+30B5	163.8	355.0	90.3
TS/PLA+30B7	169.8	356.8	91.7

TABLE 4. Physical and mechanical properties of tapioca starch (TS), tapioca starch-PLA (TS/PLA) and its nanoccomposite foams with different clay contents.

	Physical Property		Mechanical Property	
Materials	Radial Expansion Ratio	Unit Density (kg/m^3)	Bulk Spring index	Bulk Compressibility (MPa)
TS	12.0±0.863e	74±0.011a	0.964±0.005a	57.6±12.88a
TS/PLA	21.1±1.231a	42±0.006c	0.959±0.005b	7.19±0.419b
TS/PLA+30B1	17.2±1.088c	54±0.003bc	0.958±0.002b	8.75±0.481b
TS/PLA+30B3	20.5±0.681b	45±0.005c	0.950±0.001cd	4.99±0.391b
TS/PLA+30B5	15.6±1.209d	57±0.015b	0.952±0.005c	5.90±0.537b
TS/PLA+30B7	17.8±0.888c	49±0.003bc	0.947±0.004d	6.13±0.504b

[a-c] means with same letter within a column indicate no significant (P>0.05) difference by Duncan multiple range test

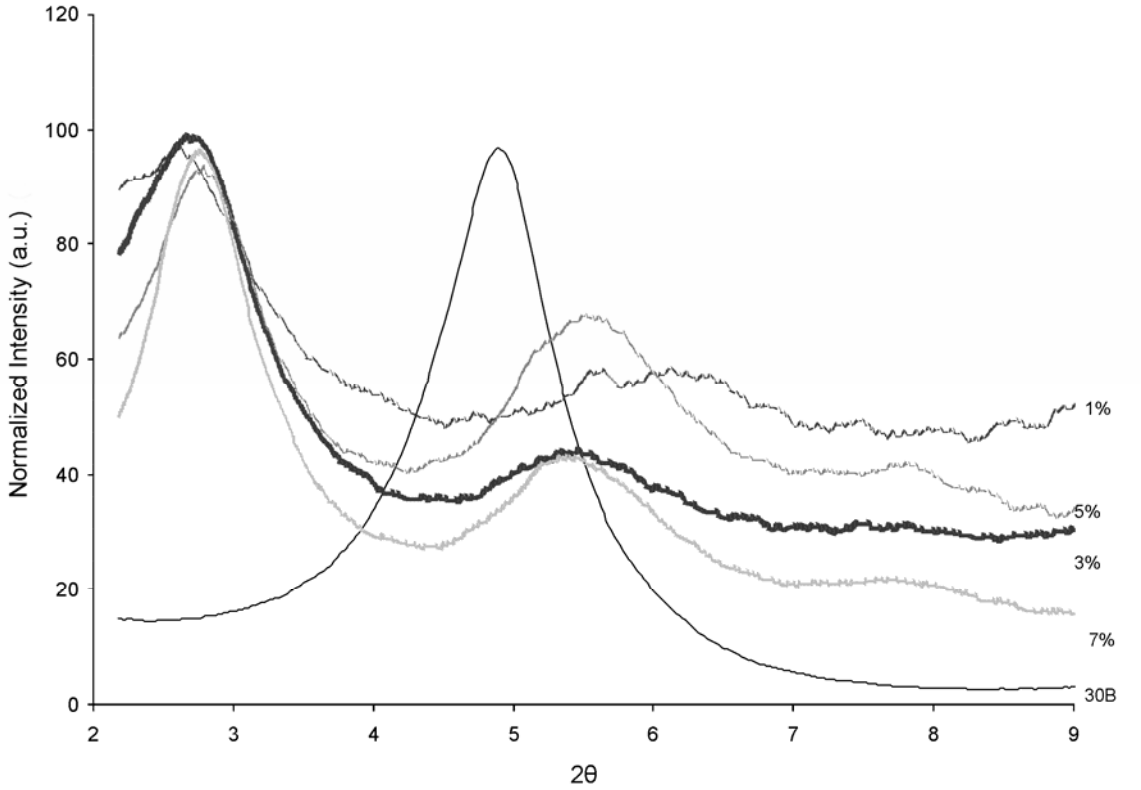

FIG. 1. X-ray patterns of Cloisite 30B and its nanoccomposite foams with tapioca starch and PLA (TS/PLA) at different clay contents; 1 wt%, 3 wt%, 5 wt%, 7 wt%.

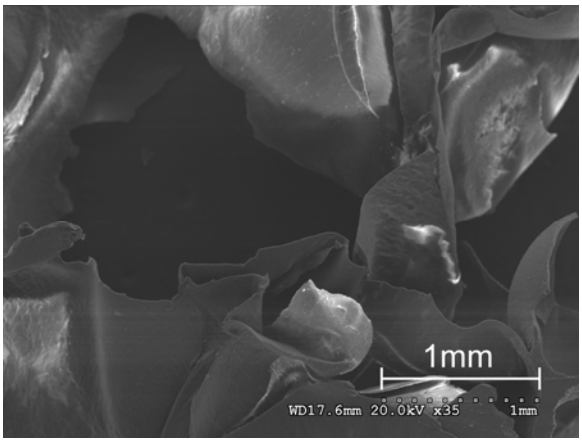

FIG. 2. Scanning electron micrograph of tapioca starch and PLA (TS/PLA) composite foam (magnification 30x).

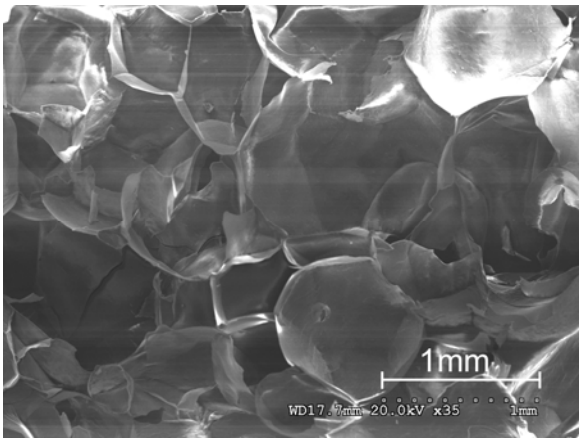

FIG. 3. Scanning electron micrograph of TS/PLA/Cloisite 30B nanoccomposite foam with 3 wt% clay (magnification 30x).

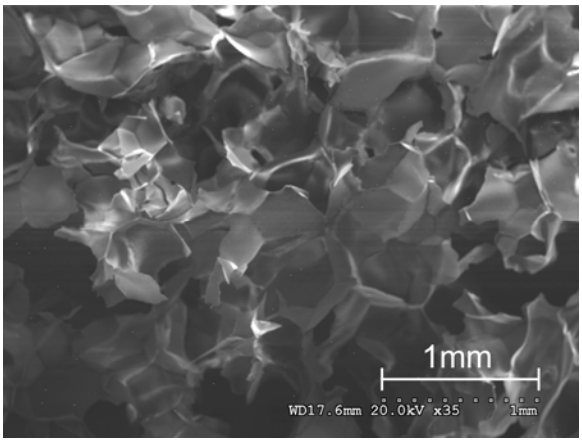

FIG. 4. Scanning electron micrograph of TS/PLA/Cloisite 30B nanoccomposite foam with 7 wt% clay (magnification 30x).

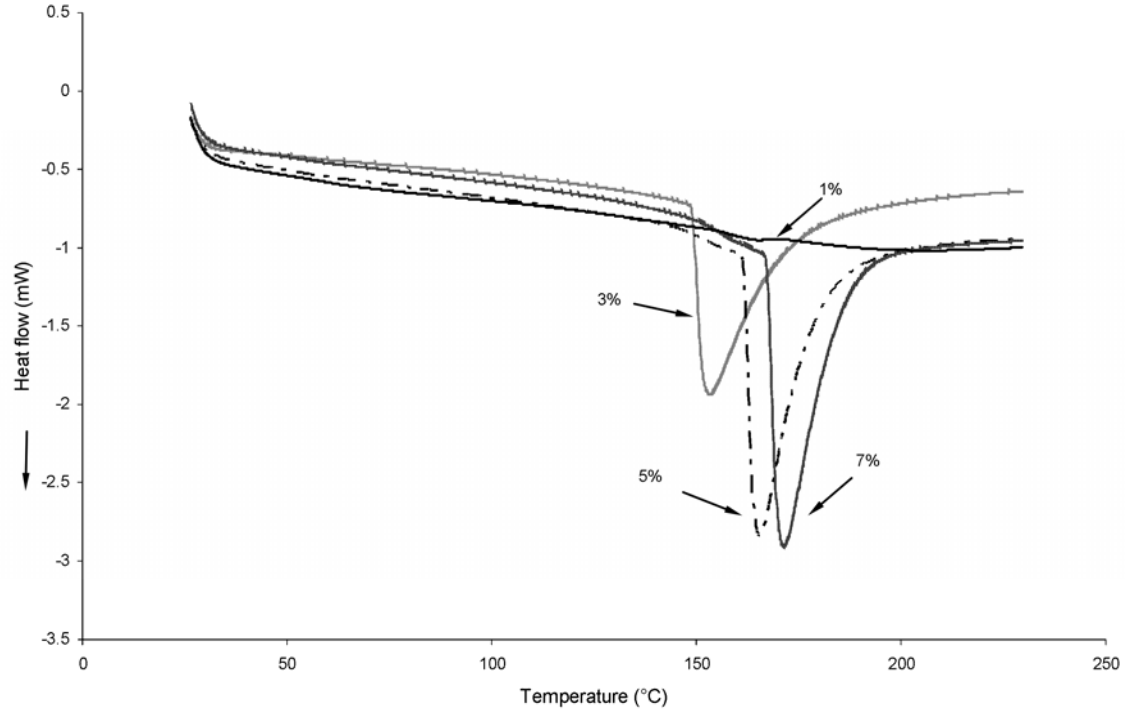

FIG. 5. DSC thermographs of tapioca starch-PLA/Cloisite 30B nanoccomposite foams with different Cloisite 30B contents; 1 wt%, 3 wt%, 5 wt%, 7 wt%.

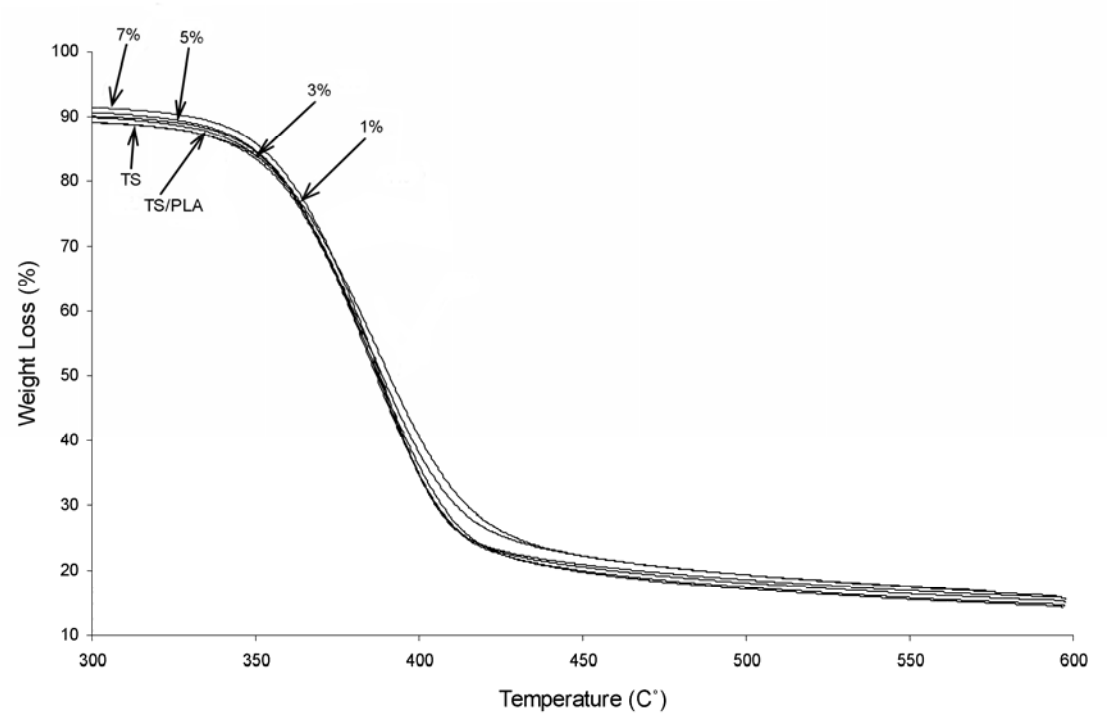

FIG. 6. TGA curves of tapioca starch (TS), tapioca starch-PLA (TS/PLA) and its nanoccomposite foams with different Cloisite 30B contents; 1 wt%, 3 wt%, 5 wt%, 7 wt%.

CHAPTER IV

EFFECTS OF EXTRUSION VARIABLES ON ORGANOCLAY INTERCALATION AND PROPERTIES OF TAPIOCA STARCH-POLY(LACTIC ACID) NANOCOMPOSITE FOAMS

This research paper has been published as:

Siew Yoong Lee, Kent M. Eskridge, Milford A. Hanna (2008). Effects of Extrusion Variables on Organoclay Intercalation and Properties of Tapioca Starch-Poly(Lactic Acid) Nanocomposite Foams. *Intern. Polym. Process*. (In press).

Effects of Extrusion Variables on Organoclay Intercalation and Properties of Tapioca Starch-Poly(Lactic Acid) Nanocomposite Foams

Abstract

Tapioca starch (TS) and poly(lactic acid) (PLA), in 90:10 weight ratio were blended with 3 % Cloisite 10A were prepared by a twin screw extruder. Screw speed, screw configuration, die nozzle diameter and moisture content were varied to determine their effects on organoclay intercalation. Selected structural, thermal, physical and mechanical properties were characterized by X-ray diffraction, scanning electron microscopy, and differential scanning calorimetry, and Instron universal testing machine, respectively. The first (X-ray) diffraction peak was observed to shift to a lower angle compared to that of pristine Cloisite 10A. The first diffraction peaks for the nanocomposites were narrow, indicating a strong intercalated behavior. These results were observed for all extrusion variables using mixing and compression screws, screw speeds of 100, 135 and 175 rpm; moisture contents of 14, 17 and 20%, and die nozzle diameters of 3 and 4 mm. These extrusion variables had significant effects on the structural, thermal, physical and mechanical properties and glass transition temperature and melting temperature of TS/PLA /Cloisite 10A nanocomposite foams due to the intercalation of organoclay.

Keywords: Screw configuration, screw speed, nozzle diameter, moisture content, Cloisite 10A

1 Introduction

Poly(lactic acid) (polylactate or polylactide) (PLA) is a polyester, and is synthesized from L- or D-lactic acid, which is produced from the fermentation of sugar and polysaccharides from corn, wheat and other starches, either by ring-opening or condensation polymerization. Because it is biodegradable, it can be employed in the preparation of bioplastic, loose-fill packaging, compost bags, food packaging, and disposable tableware. Its mechanical properties can be modified by varying its molecular weight and its crystallinity (Stevens, 2002).

Starch is an inexpensive and readily available resource, and is often used as a filler for the replacement of petroleum-derived synthetic polymers to decrease environmental pollution. However, starch has severe limitations because of its solubility and poor water-resistance, making starch products very sensitive to the relative humidity at which they are stored and used (Simmons and Thomas, 1995). Starch-polyester blends are being produced with the objective of maintaining the excellent physical properties of the polyesters while reducing cost.

Recently, formation of nanocomposites, with the aim of improving functional properties, has becoming popular (Kalambur and Rizvi, 2005). Polymer nanocomposites are a class of reinforced polymers containing small quantities (1-5 wt%) of nano-sized clay particles. Smectite – type clays, such as hectorite, synthetic mica and montmorillonite, are employed as fillers to enhance the properties of composites. The functional properties of the nanocomposites were improved markedly compared to those of unfilled polymers or conventional composites. These improvements include higher moduli (Lim and Park, 2000; Nam et al., 2001), tensile strengths (Dennis et al., 2001),

thermal stabilities (Chang et al., 2003) and biodegradability (Ray et al., 2003). Other improvements include lower gas permeabilities (Yuen et al., 2006), flammabilities (Morgan 2006) and water absorbances (Chiou et al., 2006).

Intercalated nanocomposites occur when a small amount of polymer moves into the gallery spacing between the silicate platelets. When the silicate layers are completely and uniformly dispersed in a continuous polymer matrix, an exfoliated or delaminated structure is formed (Pollet et al., 2002). The intercalated and exfoliated nanocomposites are of primary interest because the properties of the composites are improved significantly. However, the extent of intercalation or exfoliation depends on the processing conditions.

Borse and Kamal (2006) reported that a twin screw extrusion process with a longer residence time and higher mixing efficiency, produced the highest degrees of exfoliation and the largest enhancement of mechanical properties of polyamide 6 (PA6)/clay nanocomposites. Dennis et al. (2001) reported that twin screw extrusion dispersed nanoclay better than single screw extruder extrusion and that a medium shear twin screw extruder and longer mean residence time improved the dispersion of polyamide 6 (PA6)/clay nanocomposites. Artzi et al. (2002) found longer residence time, successive extrusion passes, higher screw speed (40 compared to 20 rpm) and higher extrusion temperature (220 compared to 200 ºC) resulted in higher delamination and platelets dispersion in ethylene vinyl alcohol (EVOH) copolymer/clay nanocomposites. Chiou et al. (2006) reported that the highest moisture content (47%) produced exfoliated nanoclays, whereas temperature and screw speed had little effect on clay dispersion in wheat starch-clay nanocomposites. Tanoue et al. (2006) reported that 70 and 100 rpm

fully exfoliated clay platelets in PLA/poly(ethylene glycol) nanocomposites. Xiao et al. (2007) showed that the order of mixing influenced the morphological and thermal properties of poly(butylene terephthalate)/acrylonitrile-butadiene-styrene nanocomposites.

Therefore, the objectives of this study were to investigate the effects of extrusion variables (screw configuration, screw speed, nozzle diameter and moisture content) on the intercalation of organoclay and on the properties (structural, thermal, physical and mechanical) of tapioca starch/PLA/clay nanocomposite foams.

2 Materials and Methods

2.1 Materials

Semicrystalline PLA resin with MW_n of 85,000, was purchased from NatureWorks LLC. It contained ~93% L-lactide, 2% D-lactide and 5% mesolactide. The PLA came in the form of spherical granules of 3 to 5 mm in diameter. Commercially available tapioca starch (17% amylose and 83% amylopectin) was purchased from Starch Tech, Inc. (Golden Valley, MN). The tapioca starch was agglomerated into spherical granules, 2-4 mm in diameter, to facilitate feeding into the extruder. Moisture content of the tapioca starch was adjusted to 14, 17 and 20 % dry basis with distilled water prior to extrusion. Tapioca starch and PLA (90:10 weight ratio) were blended with 3 % Cloisite 10A in a Hobart mixer (Model C-100, Horbart Corp., Troy, OH) and stored in plastic jars prior extrusion. PLA content of 10% was selected based on previous research indicated that the compatibility of PLA and tapioca starch resulted in a strong interfacial adhesion between them (Lee et al., 2007). Fang and Hanna (2000) found that at 10% PLA content, the foams possessed the highest spring index and intermediate compressibility and

Young's modulus values. They concluded that for practical applications, the bulk mechanical properties were more meaningful. Organoclay under the trade name of Cloisite 10A was purchased from Southern Clay Co. (Gonzales, TX) and used as a nanofiller. Cloisite 10A was chosen because of its extent of intercalation with the TS/PLA matrix (Lee et al., 2008). The organoclay was organically-modified montmorillonite (MMT). The ammonium cations of Cloisite 10A were dimethyl benzyl hydrogenated-tallow quaternary ammonium. The particle size range of the organoclay was 2-13 μm. PLA and the organoclay were dried in the vacuum oven at 50ºC for at least 24 h.

2.2 Extrusion

A twin-screw extruder (model DR-2027-K13, C. W. Brabender, Inc., S. Hackensack, NJ, USA) with two types of corotating screws, namely compression and mixing screws (model CTSE-V, C. W. Brabender, Inc., S. Hackensack, NJ, USA) was used to conduct extrusions. The conical screws had diameters decreasing from 43 mm to 28 mm along their length of 365 mm from the feed end to the exit end. The compression screws were universally single flighted corotating intermeshing screws with interrupted flight mixing zones. The mixing screws had a mixing section, in which small portions of the screw flights were cut away as shown in Fig. 1. The mixing section enhanced the mixing action and also increased the residence time of the sample in the barrel. Screw speeds of 100, 135 and 175 rpm were used. The temperature at the feeding section was maintained at 50 °C while the second barrel section at 120°C and the third barrel section and die section were maintained at 150°C. Die nozzles of 3 and 4 mm diameters were used to produce continuous cylindrical rope-like extrudates with diameters ranging from 10 – 20 mm,

which were cut by a rotating cutter. Feed rate was maintained at 7.74 kg/h by a gravimetric feeder and the extruder was starve-fed. The extruder was controlled by a Plasti-Corder (Type FE 2000, C. W. Brabender, Inc. S. Hackensack, NJ). Data including screw rotating speeds, barrel temperature profiles, pressure profiles and torque were recorded by a computer for subsequent analyses. The extrusion conditions selected were based on preliminary studies and previous experiments.

2.3 X-ray diffraction

The x-ray patterns of the samples were obtained using a Rigaku D/Max– B X-ray diffractometer (Tokyo, Japan) with Cu-Kα radiation (λ = 1.544 Å) at a voltage of 40 KV and 30 mA. Samples were scanned in the range of diffraction angle 2θ = 1-10° with a scan speed of 1°/min at room temperature.

2.4 Scanning electron microscopy (SEM)

The morphologies of TS/PLA and TS/PLA clay nanocomposite were observed under a SEM (Hitachi S-3000N, Tokyo, Japan). Before testing, the samples were mounted on the SEM stubs with double-sided adhesive tapes and then coated with platinum under vacuum to make the sample conductive.

2.5 Differential scanning calorimetry (DSC)

DSC measurements were performed with a Mettler DSC (Columbus, OH, USA). About 10 mg of the dried, ground samples were placed in an aluminum sample pan. The samples were heated from 50 to 200 °C at a heating rate of 10 ° C/min in a nitrogen atmosphere. The samples were held at 200°C for 1 min to eliminate the previous heat history and subsequently cooled to 25°C at 10°C/min. The samples were then heated again to 200°C at 10°C/min. This second heating process was regarded as a melting scan

for the analysis. The melting temperature was determined as the temperature at the maximum value of the melting peak.

2.6 Radial expansion ratio (RER)

Radial expansion ratios of the extruded foams were calculated by dividing the mean cross-sectional area of the extrudate by the cross-sectional area of the die nozzle. Each calculated value was a mean of 20 observations.

2.7 Unit density

Unit densities of the extrudates were determined using a glass bead displacement method originally developed for determining the volume of cookies (Hwang and Hayakawa, 1980) with modifications (Bhatnagar and Hanna, 1991). Glass beads of 0.1 mm diameter were used as the displacement medium. The mean value was obtained by averaging five replicates.

2.8 Bulk spring index (BSI)

BSI measurements were made using an Instron universal testing machine (model 5566, Instron Engineering Corp., Canton, MA). A cylindrical aluminum container with a volume of 365 cm^3 (6.93 cm in diameter and 9.68 cm in depth) was used to confine the bulk samples (Fang and Hanna, 2000). The forces required to initially compress the samples to 80% of their original volumes and the forces required to recompress the same samples 1 min after releasing the initial load were recorded. BSI was calculated by dividing the recompression force by the initial compression force and has an ideal value of 1. The mean value was obtained by averaging five replicates.

2.9 Bulk compressibility

Bulk compressibility was calculated using the same data collected in the BSI test. It was calculated by dividing the peak force required to compress (deform) the sample by 80% [to 20% of their original dimension (diameter)] by the initial axial cross-sectional area of the foams (Fang and Hanna, 2000). A mean value was obtained by averaging five replicates.

2.10 Experimental design and statistical analyses

The experimental design was a split-plot with two screw configurations (compression and mixing screws) and two die nozzle diameters (3 and 4 mm) as the main plot factors, and with three moisture contents (14, 17 and 20%) and screw speeds (100, 135 and 175 rpm) as the split-plot factors. The main plot design was a completely randomized design with a 2 x 2 factorial treatment layout where each whole plot unit was replicated twice. The split-plot factors were arranged in a 3 x 3 factorial in ten split-plot units where the 10^{th} unit resulted since the 135 rpm and 17% moisture content was repeated to study the 'sample to sample' variation. All the results reported were means of two or more replications. The data from RER, unit density, BSI and bulk compressibility measurements were analyzed by the general linear models (GLM) in SAS analysis program (SAS Institute Inc., Cary, NC). Duncan's multiple range tests were conducted to check for significant ($p<0.05$) differences between treatment groups.

3 Results and Discussion

In our previous research, we found that the intercalation of TS/PLA polymer into the organoclay layers that occurred was attributed to the compatibility between the Cloisite 10A and the TS/PLA matrix which were both hydrophobic (Lee et al., 2008). In this study, X-ray diffraction showed the first diffraction peaks were observed to shift to the

same lower angles compared to those of pristine Cloisite 10A for all extrusion variables with different screw configurations, screw speeds, moisture contents and die nozzle diameters. These results showed that all of the extrusion variables were favorable conditions for intercalation showing similar trends leaving little to discuss. However, intercalation of the organoclay caused the extrusion variables to have significant effects at different extents on the structural, thermal, physical and mechanical properties of TS/PLA /Cloisite 10A nanocomposite foams.

3.1 Structural properties of TS/PLA /Cloisite 10A nanocomposites

Wide-angle X-ray diffraction (WAXD) is a classical method for determining the gallery height (*d*-spacing distance) in clay particles (Di et al., 2005). The *d*-spacing can be determined by the diffraction peak in the XRD patterns, and be expressed by Bragg's equation ($\lambda = 2d_{001}\sin\theta$), where d_{001} is the interplanar distance of (001) diffraction face, θ is the diffraction position and λ is the wavelength (Choi et al., 2003). During melt intercalation, the insertion of polymer into the clay galleries forces the platelets apart and increases the *d*-spacing, resulting in a shift of the diffraction peak to lower angles.

The effects of the mixing screws at 135 rpm screw speed with a 4 mm nozzle diameter and different moisture contents (14, 17, 20%) on the organoclay intercalation of the nanocomposites were examined. The first (X-ray) diffraction peak (001) *d*-spacing was shifted to lower angles compared to those of pristine Cloisite 10A, indicating that the intercalation of TS/PLA polymer into the organoclay layers occurred, as shown in Fig. 2. The 2θ peak of the pristine Cloisite 10A clay was 4.45º while the 2θ peak for the TS/PLA/Cloisite 10A nanocomposites at 14 and 17% moisture contents was 2.61º. The peak shifted to an even lower value of 2.53º for the TS/PLA/Cloisite 10A

nanocomposites at 20% moisture content. The first diffraction peaks for the intercalated nanocomposites were narrow, indicating a strong intercalated behavior and a high stacking order of the successive clay layers in the nanocomposites. Similar occurrences were observed by Kumar et al. (2003) and Ranade et al. (2004).

The d_{001}-spacings of the TS/PLA/Cloisite 10A nanocomposites at 14 and 17% moisture contents were 34.34Å, a 13.70 Å increase compared to that of the Cloisite 10A (19.64 Å), as shown in Table 1. The d_{001}-spacing increased even further in the case of 20% moisture content (25.28 Å), suggesting an increasing interaction between TS/PLA and Cloisite 10A at the higher moisture content. An increase in moisture content caused the swelling of Cloisite 10A. At higher moisture contents, the degrees of gelatinization of starch were higher, causing more interaction between TS/PLA and the increased interlayer spacings of Cloisite 10A. Similar results were observed by Chiou et al. (2006) using wheat starch and Cloisite Na^+ at 47% moisture content. It is believed that the greater the d_{001}-spacings, the greater the interaction of polymer molecular chains with clay layered silicate (Choi et al., 2003). The interactions between polymer and organoclays depend on the compatibility of the surface polarities of polymer and clay (Park et al., 2003). Polar-type intercalations also are critical for the formation of intercalated or exfoliated nanocomposites via polymer melt intercalation (Vaia and Giannelis, 1997). In addition, the mixing screws enhanced the mixing action and increased the residence time of the material in the barrel. An increase in the residence time at a higher moisture content (20 %) again allowed for more interaction between the TS/PLA and Cloisite 10A, causing a higher intercalation. Park et al. (2006) and Borse

and Kamal (2006) reported that increased residence time assisted in producing extruded nanocomposites with high degrees of exfoliation.

X-ray diffraction results of the nanocomposites made using compression screws at 135 rpm screw speed, a 4 mm nozzle diameter and different moisture contents (14, 17, 20%) are shown in Fig. 3. The 2θ peak shifted to 2.61º for the TS/PLA/Cloisite 10A nanocomposites at 14, 17 and 20% moisture contents indicating that the TS/PLA polymer was intercalated into the organoclay layers. However, the degree of enlargement of the d_{001}-spacing was the same (13.70 Å) for nanocomposites at all moisture contents, as shown in Table 1. Using mixing and compression screws, at 135 rpm screw speed, different moisture contents (14, 17, 20%) but with a 3 mm nozzle diameter produced similar XRD patterns as with a 4 mm nozzle diameter (Table 1). Using mixing and compression screws, a 4 mm nozzle diameter at 17 % moisture content but at different screw speeds (100, 135 and 175 rpm) produced similar XRD patterns again (Table 1). With the same extrusion conditions except for changing the nozzle diameter to 3 mm, similar XRD results were obtained as shown in Table 1.

SEM micrograph of TS/PLA/Cloisite10A nanocomposite foams using mixing screws, a 3 mm nozzle diameter, 17 % moisture content and175 rpm screw speed are shown in Fig 4. The nanocomposite foams had a high cell density and exhibited small and compact cells. Similar cell structures were produced with all other extrusion variables. However, the TS/PLA foam without organoclay filler exhibited very large cell structure (Lee et al., 2008).

3.2 Thermal properties of TS/PLA/Cloisite 10A nanocomposite foams

Glass transition (T_g) and melting temperatures (T_m) of the first and second heatings of the TS/PLA/Cloisite 10A nanocomposite foams were determined by DSC. The first and second heating scans of samples produced with the *compression screws*, a 3 mm diameter nozzle, at 17% moisture content and at different screw speeds (100, 135 and 175 rpm) are presented in Fig. 5 and 6, respectively. In the DSC cooling processes, none of the foams showed crystallization peaks. T_m of the TS/PLA/Cloisite10A nanocomposite foams were 156.1 °C, 162.8 °C and 154.1 °C at 100, 135 and 175 rpm screw speeds, respectively (Table 2). During the second heating, T_m of the TS/PLA/Cloisite10A nanocomposite foams were 163.9 °C, 161.8 °C and 163.1 °C at 100, 135 and 175 rpm screw speeds, respectively (Table 2). The change in endothermic peaks (T_m) was indicative of the effect of screw speed. A smaller endothermic peak was observed at 113.8°C for the nanocomposite foam produced at the 175 rpm screw speed. The presence of this small peak could have been due to the presence of clay and the effect of high speed (175 rpm) which caused the melting of recrystallized crystals during the heating process or due to the formation of an intercalated matrix. Similar results were reported by Phang et al. (2004) who reported multiple peaks caused by heterogeneous nucleation caused by nanofillers. Using compression screws, 135 rpm screw speed, a 3 mm nozzle diameter but at different moisture contents (14, 17, 20 %) produced similar trends of endothermic peaks for the first and second heating scans as above. However, at 17 % moisture content, a T_g of 61.7 °C was observed indicative of a semi-crystalline structure. The T_ms of the TS/PLA/Cloisite10A nanocomposite foams were 161.1 °C, 162.8 °C and 162.1 °C at 14, 17 and 20% moisture contents, respectively (Table 2). During the second heating, the T_ms of the TS/PLA/Cloisite10A nanocomposite foams were 163.5 °C, 161.8 °C and

161.4 °C at 14, 17 and 20% moisture content, respectively (Table 2). Again, these results showed that the 3 mm nozzle diameter and compression screws at three different moisture contents had an effect on the T_m which could have been due to the effect of the intercalated structure caused by the presence of organoclay. Results similar to those explained above were observed for the nanocomposite foams produced using the mixing screws and a die nozzle diameter of 4 mm. These results confirmed that extrusion variables had an influence on the thermal properties of the nanocomposite foams due to intercalation of the organoclay.

3.3 Physical and mechanical properties of TS/PLA/Cloisite 10A nanocomposite foams

Table 3 shows the means of RER, unit density, bulk compressibility and BSI of the nanocomposite foams as affected by extrusion variables. Screw configuration, nozzle diameter and moisture content had significant effects ($p<0.05$) on RER of the nanocomposite foams. *Mixing screws*, a nozzle diameter of 3 mm and moisture content of 17 % produced foams with higher RER. These results were consistent with the XRD results which showed that the extrusion variables caused intercalated nanocomposite foams. Higher RER with the mixing screws could have been due to the enhanced mixing action and the increased residence time of the material in the barrel which increased expansion. A smaller die nozzle diameter (3 mm) produced higher RER as shown in Table 3. A smaller opening restricted the material to flow inside the extruder barrel, increasing the shear rate and residence time, which increased the gelatinization of starch, causing increased expansion. The effect of moisture content on expansion is two fold as explained by Fang et al. (2003). At lower moisture contents, expansion increases as the moisture increases. There is a maximum expansion at optimum moisture content. Above

that, expansion decreases as more moisture is added. At low moisture content (14 %), there was insufficient water to cause the starch to gelatinize fully to produce good expansion since water acted as the blowing agent. At high moisture content (20 %) the expansion was reduced. This could have been due to a higher moisture content resulting in lower viscosity and thereby lower pressure. Similar results were reported by Hagnimana et al. (2006). Moisture content of 17 % produced the highest RER. Fang and Hanna (2000) reported that moisture content significantly affected the mechanical properties.

Screw speed and moisture content had significant effects ($p<0.05$) on the unit density of the nanocomposite foams as shown in Table 3. Low screw speed (100 rpm) produced significantly lower unit density compared to the higher screw speeds. This could have been due to the longer residence time at low screw speed which enhanced the interaction of organoclay and the TS/PLA matrix to form an intercalated structure which promoted expansion and reduced the density of the nanocomposite foams. Ding et al (2005) reported that screw speed had only a slight impact on the density of extrudate in their work. Low moisture content (14 %) produced significantly lower unit density compared to the higher moisture contents. Similar results were observed by Bryant et al. (2001).

BSI and bulk compressibility are interrelated properties. BSI relates to resiliency, and refers to the ability of a material to recover its original shape after it has been deformed. A greater BSI indicates a greater degree of rebound of a material after being compressed. Bulk compressibility describes the cushioning ability of a material, and is related to its relative softness or hardness. High BSI and low compressibility are

desirable for loose-fill packaging material (Bhatnagar and Hanna, 1995). Table 3 shows that screw configuration, nozzle diameter and moisture content had significant effects ($p<0.05$) on bulk compressibility of the nanocomposite foams. Using mixing screws produced foams with significantly lower bulk compressibilities. Again, this could have been due to the enhanced mixing action and also increased residence time of the material in the barrel which increased the expansion. Low bulk compressibility was produced by a smaller die nozzle diameter (3 mm) which restricted the material flow inside the extruder barrel, increasing the shear rate and residence time and increasing expansion. Moisture content of 17 % produced the lowest bulk compressibility. The effect of moisture content on the bulk compressibility was similar to the effect on the RER as explained above. BSI was influenced ($p<0.05$) significantly by the screw configuration as shown in Table 3. The compression screws had a more positive influence on the BSI than the mixing screws.

4 Conclusions

The influences of screw speed, screw configuration, die nozzle diameter and moisture content on the organoclay intercalation and properties of TS/PLA/Cloisite 10A nanocomposite foams were examined. X-ray diffraction indicated the first diffraction peak was shifted to lower angles compared to those of pristine Cloisite 10A. The first diffraction peaks for the intercalated nanocomposites were narrow, indicating a strong intercalated behavior. These results were observed for all extrusion variables using mixing and compression screws; screw speed of 100, 135 and 175 rpm; moisture contents of 14, 17 and 20%; and die nozzle diameters of 3 and 4 mm. These extrusion variables

had significant effects on the structural, thermal, physical and mechanical properties of TS/PLA /Cloisite 10A nanocomposite foams due to the intercalation of organoclay.

References

Artzi, N., et al., "Melt Blending of Ethylene-Vinyl Alcohol Copolymer/Clay Nanocomposites: Effect of the Clay Type and Processing Conditions", J. Polym. Sci.: Part B: Polym. Physics, **40**, 1741-1753 (2002)

Bhatnagar, S., Hanna, M. A., "Effect of Lipids on Physico-Chemical Properties of Extruded Corn Starch", ASAE Paper No. 916541. St. Joseph, Mich.: ASAE (1991)

Bhatnagar, S., Hanna, M. A., "Physical, Mechanical and Thermal Properties of Starch-Based Plastic Foams", Trans. ASAE, **38**, 567-571 (1995)

Borse, N. K., Kamal, M. R., "Melt Processing Effects on the Structure and Mechanical Properties of PA-6/Clay Nanocomposites" Polym. Eng. Sci., **46**, 8, 1094-1103 (2006)

Bryant, R. J., et al., "Functional and Digestive Characteristics of Extruded Rice Flour", Cereal Chem., **78(2)**, 131-137 (2001)

Chang, J-H., et al., "Poly (Vinyl Alcohol) Nanocomposites with Different Clays: Pristine Clays and Clays", J. Appl. Polym. Sci., **90**, 3208-3214 (2003)

Chiou, B-S., et al., "Effects of Processing Conditions on Nanoclay Dispersion in Starch-Clay Nanocomposites", Cereal Chem., **83(3)**, 300-305 (2006)

Choi, W. M., et al., "Preparation and Characterization of Poly (Hydroxybutyrate-Co-Hydroxyvalerate)-Clay Nanocomposite", J. Appl. Polym. Sci., **90**, 525-529 (2003)

Dennis, H. R., et al., "Effect of Melt Processing Conditions on the Extent of Exfoliation in Clay-Based Nanocomposites", Polym., **42**, 9513-9522 (2001)

Di, Y., et al., "Poly(Lactic Acid)/Clay Nanocomposites: Thermal, Rheological Properties and Foam Processing", J. Polym. Sci.: Part B: Polym. Phys., **43**, 689-698 (2005)

Ding, Q-B., et al., "The Effect of Extrusion Conditions on the Physicochemical Properties and Sensory Characteristics of Rice-based Expanded Snacks", J. Food Eng. **66**, 283-289 (2005)

Fang, Q., Hanna, M. A., "Mechanical properties of starch-based foams as affected by ingredient formulation and foam physical properties", Trans. ASAE, **43**, 1715-1723 (2000)

Fang, Q., et al., "Extrusion System Design", in Encyclopedia of Agricultural, Food, and Biological Engineering. Marcel Dekker, Inc.: New York, p. 306-309 (2003)

Hagenimana, A., et al., "Evaluation of rice flour modified by extrusion cooking", J. Cereal Sci., **43**, 38-46 (2006)

Hwang, M. P., Hayakawa, K., "Bulk Densities of Cookies Undergoing Commercial Baking Process", J. Food Sci., **45(5)**, 1400-1402, 1407 (1980)

Kalambur, S., Rizvi, S.S.H., "Biodegradable and Functionally Superior Starch-Polyester Nanocomposites from Reactive Extrusion", J. Appl. Polym. Sci., **96**, 1072-1082 (2005)

Kumar, S., et al., "Preparation and Characterization of Poly(Methyl Methacrylate)-Clay Nanocomposites via Melt Intercalation: The Effects of Organoclay on the Structure and Thermal Properties", J. Appl. Polym. Sci. **89**, 1186-1194 (2003)

Lim, Y. T., Park, O. O., "Rheological Evidence for the Microstructure of Intercalated Polymer/Layered Silicate Nanocomposites", Macromol. Rapid Commun., **21**, 231-235 (2000)

Lee, S. Y., et al., "Tapioca Starch-poly(lactic acid)-based Nanocomposite Foams as Affected by Type of Nanoclay", Intern. Polym. Process., XXII 5, 429-435 (2007)

Lee, S. Y., et al., "Preparation and Characterization of Tapioca Starch-poly(lactic acid) Nanocomposite Foams", Ind. Crops and Prod., **28(1)**, 95-106 (2008)

Morgan, A. B., "Flame Retarded Polymer Layered Silicate Nanocomposites: A Review of Commercial and Open Literature Systems", Polym. Adv. Technol., **17**, 206-217 (2006)

Nam, P.H., et al., "A Hierarchical Structure and Properties of Intercalated Polypropylene/Clay nanocomposites", Polym., **42**, 9633-9640 (2001)

Park, H-M., et al., "Environmentally Friendly Polymer Hybrids: Part 1 Mechanical, Thermal, and Barrier Properties of the Thermoplastic Starch/Clay Nanocomposites", J. Mater. Sci. **38**, 909-915 (2003)

Park, H-M, et al., "Effect of Sequential Mixing and Compounding Conditions on Cellulose Acetate/Layered Silicate Nanocomposites", J. Polym. Environ., **14**, 27-34 (2006)

Phang, I. Y., et al., "Crystallization and melting behavior of Polyester/Clay Nanocomposites", Polym. Int., **53**, 1282-1289 (2004)

Pollet, E., et al., "New Aliphatic Polyester Layered-Silicate Nanocomposites, in Biodegradable Polymers and Plastics, Chiellini, E. and Solaro, R., (Eds.)", Kluwer Academic/Plenum Publishers, New York, p. 327-350 (2002)

Ranade, A., et al., "Effect of Coupling Agent on the Dispersion of PETG Montmorillonite Nanocomposite films", in Mat. Res. Soc. Symp. Proc. – Mechanical Properties of Nanostructured Materials and Nanocomposites, Ovid'ko, I., Pande, C.S., Krishnamoorti, R., Lavernia, E., Skandan, G., (Eds.), Materials Research Society: Warrendale, Pennsylvania, Vol. 791, p. 283-288 (2004)

Ray, S. S., et al., "Structure – Property Relationship in Biodegradable Poly (Butylene Succinate)/Layered Silicate Nanocomposites," Macromol., **36**, 2355-2367 (2003)

Simmons, S., Thomas, E .L., "Structural characteristics of Biodegradable Thermoplastic Starch/Poly (Ethylene-Vinyl Alcohol) Blends," J. Appl. Polym. Sci., **58**, 2259- 2285 (1995)

Stevens, E. S., "Chapter 7 The Reemergence of Bioplastics," in Green Plastics – An Introduction to the New Science of Biodegradable Plastics, Princeton University Press, Princeton, p. 104-134 (2002)

Tanoue, S., et al., "Effect of Screw Rotation Speed on the Properties of Polystyrene/Clay Nanocomposites Prepared by a Twin-Screw Extruder", J. Appl. Polym. Sci., **101**, 1165-1173 (2006)

Vaia, R. A., Giannelis, E. P., "Polymer Melt Intercalation in Organically-Modified Layered Silicates: Model Predictions and Experiment", Macromol., **30**, 8000- 8009 (1997)

Xiao, J., et al., "Effect of Order of Mixing on Morphology and Thermal Properties of the Compatibilized PBT and ABS Alloys/OMT Nanocomposites", J. Appl. Polym. Sci., **104**, 2130-2139 (2007).

Yuen, J-H., et al., "Poly (Vinyl Alcohol) Nanocomposite Films: Thermo Optical Properties, Morphology, and Gas Permeability", J. Appl. Polym. Sci., **101**, 591-596 (2006).

Table 1. Diffraction peaks and d_{001}-spacings and Δ d_{001}-spacings of Cloisite 10A and its nanocomposites with tapioca starch-PLA (TS/PLA)

Materials	Screw configuration	Nozzle diameter mm	Screw speed rpm	Moisture content %	Diffraction peak 2θ, degree	d_{001}-spacings Å	Δ d_{001}-spacings Å
Cloisite 10A					4.45	19.64	
TS/PLA/ Cloisite 10A	Mixing screws	4	135	14	2.61	33.34	13.70
				17	2.61	33.34	13.70
				20	2.53	34.92	25.28
TS/PLA/ Cloisite 10A	Compression screws	4	135	14	2.61	33.34	13.70
				17	2.61	33.34	13.70
				20	2.61	34.34	13.70
TS/PLA/ Cloisite 10A	Mixing screws	3	135	14	2.61	33.34	13.70
				17	2.61	33.34	13.70
				20	2.61	33.34	13.70
TS/PLA/ Cloisite 10A	Compression screws	3	135	14	2.61	33.34	13.70
				17	2.61	33.34	13.70
				20	2.61	33.34	13.70
TS/PLA/ Cloisite 10A	Mixing screws	4	100	17	2.61	33.34	13.70
			135		2.61	33.34	13.70
			175		2.61	33.34	13.70
TS/PLA/ Cloisite 10A	Compression screws	4	100	17	2.61	33.34	13.70
			135		2.61	33.34	13.70
			175		2.61	34.34	13.70
TS/PLA/ Cloisite 10A	Mixing screws	3	100	17	2.61	33.34	13.70
			135		2.61	33.34	13.70
			175		2.61	33.34	13.70
TS/PLA/ Cloisite 10A	Compression screws	3	100	17	2.61	33.34	13.70
			135		2.61	33.34	13.70
			175		2.61	33.34	13.70

Table 2. Thermal properties of TS/PLA/Cloisite 10A nanocomposite foams using compression screws and 3 mm diameter nozzle

Screw speed rpm	Moisture content %	First heating		Second heating	
		T_g ° C	T_m ° C	T_g ° C	T_m ° C
100	17	-	156.1±0.8	-	163.9±0.9
135		-	162.8±1.1	-	161.8±1.0
175		-	154.1±1.2	113.8±1.0	163.1±0.4
135	14	-	161.1±0.7	-	163.5±0.6
	17	61.7±1.1	162.8±0.8	-	161.8±0.8
	20	-	162.1±0.9	-	161.4±0.8

Table 3. Means* of physical and mechanical properties of the TS/PLA/Cloisite 10A nanocomposite foams as affected by extrusion variables

Extrusion variable	Level	Radial expansion ratio	Unit density kg/m^3	Bulk compressibility MPa	Bulk spring index
Screw configuration	Compression	11.47 S	34.73	35.68 S	0.949 S
	Mixing	14.14 S	35.06	13.08 S	0.934 S
Nozzle diameter (mm)	3	15.36 S	35.10	17.41 S	0.940
	4	10.26 S	34.68	31.34 S	0.943
Screw speed (rpm)	100	13.66	27.67 S	27.60	0.942
	135	12.35	34.47 S	23.88	0.941
	175	12.71	42.54 S	21.65	0.942
Moisture content (%)	14	11.25 S	33.98 S	25.59 S	0.943
	17	15.58 S	35.45 S	16.36 S	0.939
	20	11.58 S	35.25 S	31.18 S	0.943

S = Means for the levels of this extrusion variable were significantly different ($p < 0.05$)

* Main effects means of each extrusion level were computed over all the other extrusion variables

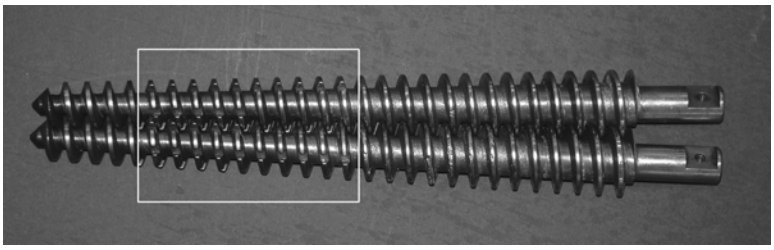

Fig. 1. Picture of mixing screws with small portions of the screw flights cut away (small box)

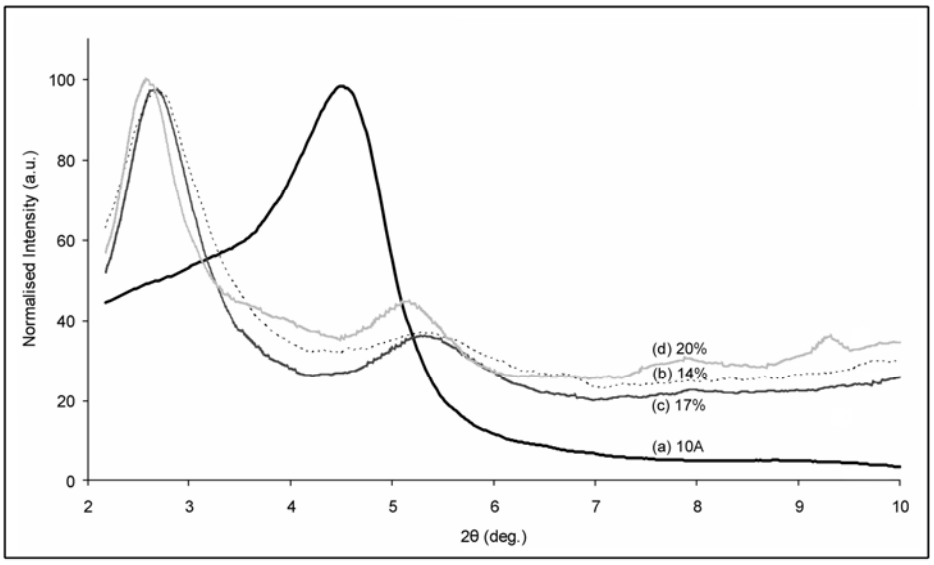

Fig. 2. X-ray patterns of (a) Cloisite 10A, and its nanocomposite foams at different moisture contents (b) 14 %, (c) 17 %, and (d) 20 % using mixing screws, 135 rpm and 4 mm diameter nozzle

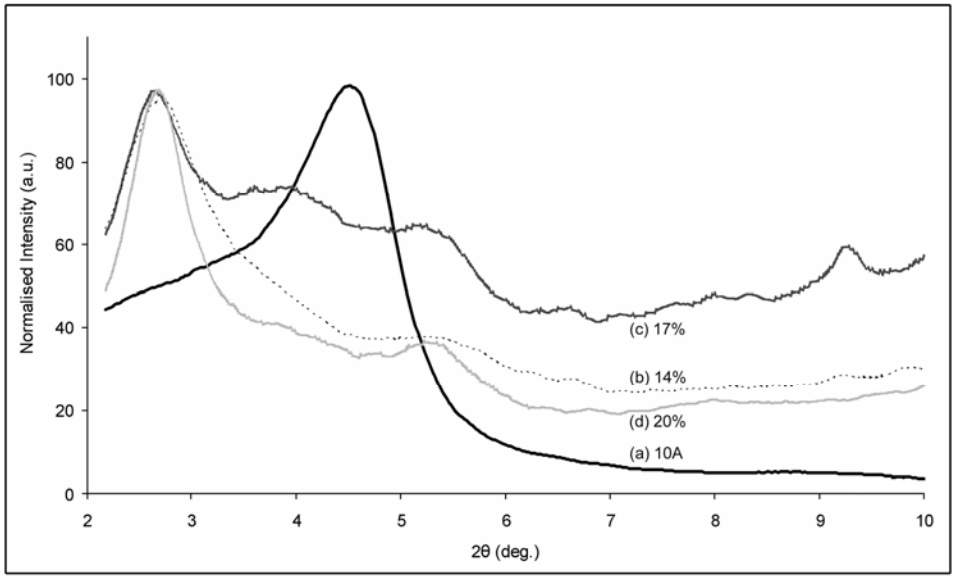

Fig. 3. X-ray patterns of (a) Cloisite 10A, and its nanocomposite foams at different moisture contents (b) 14 %, (c) 17 %, and (d) 20 % using compression screws, 135 rpm and 4 mm diameter nozzle

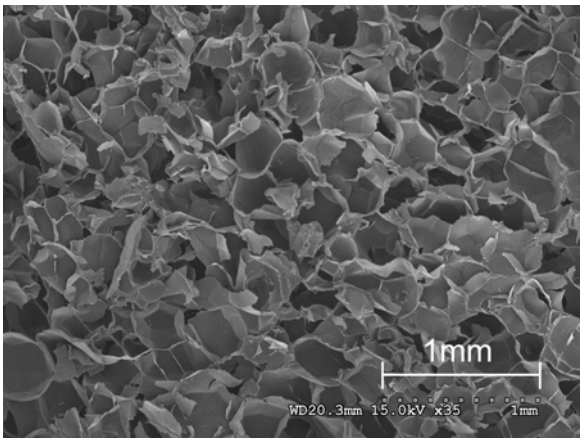

Fig. 4. Scanning electron micrograph of tapioca starch-PLA TS/PLA/Cloisite 10A nanocomposite foams (magnification 35x) using (A) mixing screws at 135 rpm, 17 % moisture content and 3 mm diameter nozzle

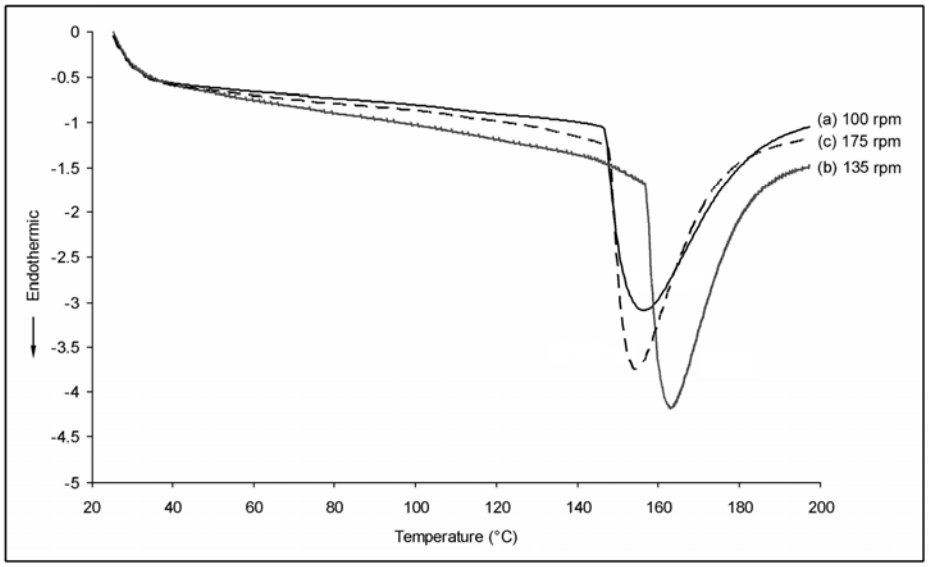

Fig. 5. DSC thermographs (first heating scans) of TS/PLA/Cloisite 10A nanocomposite foams using compression screws, 3 mm diameter nozzle and 17% moisture content, at different screw speeds (a) 100 rpm, (b) 135 rpm, and (c) 175 rpm

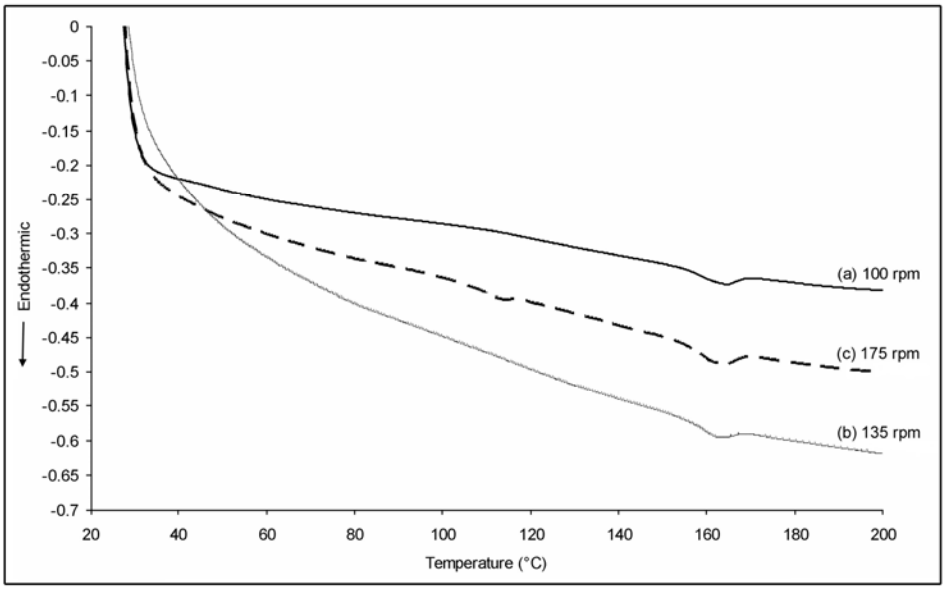

Fig. 6. DSC thermographs (second heating scans) of TS/PLA/Cloisite 10A nanocomposite foams using compression screws, 3 mm diameter nozzle and 17% moisture content, at different screw speeds (a) 100 rpm, (b) 135 rpm, and (c) 175 rpm

CHAPTER V

AN ADAPTIVE NEURO-FUZZY INFERENCE SYSTEM FOR MODELING MECHANICAL PROPERTIES OF TAPIOCA STARCH-POLY(LACTIC ACID) NANOCOMPOSITE FOAMS

This research paper has been published as:

Siew Yoong Lee, Milford A. Hanna, David D. Jones (2008). An Adaptive Neuro-Fuzzy Inference System for Modeling Mechanical Properties of Tapioca Starch-Poly(Lactic Acid) Nanocomposite Foams. *Starch*, 60: 159-164.

An Adaptive Neuro-Fuzzy Inference System for Modeling Mechanical Properties of Tapioca Starch-Poly(Lactic Acid) Nanocomposite Foams

Summary

Tapioca starch, poly(lactic acid), and Cloisite 30B nanocomposites foams, with clay contents of 1, 3, 5 and 7 wt%, were prepared by a melt-intercalation method. Multiple inputs single output models were developed to predict radial expansion ratio, unit density, bulk compressibility and spring index of the nanocomposite foams. An individual ANFIS model was developed for each mechanical property using clay content, temperature, pressure and torque as input parameters. All models preformed well with R^2 values > 0.71. All models had very low root mean squared error values.

Keywords: Modeling; Clay; Temperature; Pressure; Torque

1 Introduction

Poly(lactic acid) (polylactate or polylactide) (PLA) is a polyester, and is synthesized from L- and D-lactic acids, which are produced from the fermentation of sugar and (poly)saccharides such as sugar feedstocks and corn, wheat and other starches. The lactic acid is converted to PLA either by ring-opening polymerization or by condensation polymerization. PLA is insoluble in water and has good moisture and grease resistance. PLA is used widely as a biodegradable and renewable plastic for uses in service ware, grocery, waste-composting bags, mulch films, controlled release matrices for fertilizers, pesticides and herbicides [1].

Starch is an inexpensive and readily available resource, and is often used as a filler for the replacement of petroleum-derived synthetic polymers to decrease environmental pollution. However, starch has severe limitations because of its solubility and poor water-resistance, making starch products very sensitive to the relative humidity at which they are stored and used [2]. Starch-polyester blends are being produced with the objective of maintaining the excellent physical properties of the polyesters while reducing cost. A process was developed at the University of Nebraska-Lincoln to produce starch-based plastic foam with 70% starch combined with a variety of ingredients and plastics [3]. Fang and Hanna [4] found that addition of PLA to regular and waxy corn starches improved the physical and mechanical properties of the foams. More recently, formation of nanocomposites with the aim of improving functional properties has become popular. Polymer nanocomposites are a class of reinforced polymers containing small quantities (1-5 wt%) of nanometric-sized clay particles. The functional properties of the

nanocomposites were improved markedly compared to those of the unfilled polymer or conventional composites. These improvements included high moduli [5,6]; increased tensile strength [7] and thermal stability [8]; decreased gas permeability [9] and flammability [10]; and increased biodegradability of biodegradable polymers [11].

Melt intercalation by extrusion is the most common approach to synthesize nanocomposites because it is an environmentally friendly process that requires no solvent and is suitable for industrial uses [12, 13]. Extrusion processing is considered to be more of an art than science. Numerous studies have reported on the complexities of the extrusion process and modeling of the process. Extrusion cooking can be described as a process whereby moistened materials are cooked and worked into viscous, plastic-like dough. Cooking is accomplished through the application of heat, either directly by steam injection or indirectly through jacketed barrels and by dissipation of mechanical energy through shearing of the dough [14].

Mathematical modeling of the extrusion process began in the field of plastic and polymer engineering. Because of the complexity of the extrusion process, complex mathematical models have been proposed to study the process. In recent years, new modeling tools like fuzzy modeling have been developed. Fuzzy modeling in extrusion is challenging due to the complexity of the process which consists of multiple inputs and multiple outputs which are highly non-linear. Fuzzy modeling makes it possible to utilize experience, knowledge and large amounts of process data. Artificial neutral networks

have been used to model and identify predictive models for a food extrusion process [15], control a food extrusion process [16], and for polymer extrusion [17].

In this study, we present a novel neuro-fuzzy approach, i.e. adaptive network-based fuzzy inference system (ANFIS), to model extrusion of nanocomposite foams. ANFIS is a fuzzy inference system implemented in the framework of an adaptive neural network. By using a hybrid learning procedure, ANFIS can construct input-output mapping based on both human-knowledge as fuzzy If-Then rules and given input-output data pairs for neural networks training [18]. ANFIS is a powerful tool in fuzzy modeling to learn information about the given input and output data set in order to compute the membership functions that describes the associated fuzzy inference system.

The objectives of this study were to prepare tapioca starch/PLA/Cloisite 30B nanocomposite foams of different clay contents via extrusion and to investigate the influence of clay content on the mechanical properties of the foams and to use ANFIS to model the clay content, temperature, pressure and torque on the mechanical properties of the foams.

2 Material and Methods

2.1 Materials

Semicrystalline poly(lactic) acid (PLA) resin of MW_n 85,000 was produced by Cargill, Inc. (Minneapolis, MN). It contained ~93% L-lactide, 2% D-lactide and 5% mesolactide. Commercially available tapioca starch (17% amylose and 83% amylopectin) was purchased from Starch Tech, Inc. (Golden Valley, MN). Tapioca starch was agglomerated into spherical granules of 2-4 mm diameter to facilitate feeding into the extruder. The moisture content of the tapioca starch was adjusted to 18%, dry basis, with distilled water prior to extrusion. Tapioca starch, PLA, sodium bicarbonate, citric acid and clay were blended in a Hobart mixer (Model C-100, Horbart Corp., Troy, OH) and stored in plastic jars prior to extrusion. PLA content of 10% was selected based on preliminary experiments. Fang and Hanna [19] used three levels of polymer content (10, 25 and 40%) in their study of mechanical properties of starch-based foams. They found that, at 10% PLA content, the foams possessed the highest spring index and intermediate compressibility and Young's modulus values. Sodium bicarbonate (0.5%) and citric acid (0.5%) were added to degrade the biodegradable polymer into chains of between 1,000 and 100,000 Daltons or approximately 500 to 50,000 monosaccharide groups to promote expansion [3]. Organically modified montmorillonite under the trade name of Cloisite 30B (methyl-tallow-bis-2-hydroxyethyl ammonium)(MT2EtOH) was purchased from Southern Clay Products Inc. (Gonzalez, TX). The particle size range of the nanoclay was 2-13 ηm. Four different relative contents of Cloisite 30B (1, 3, 5 and 7 wt%) were added to the formulation. The PLA and the nanoclay were dried at 70ºC for at least 24 h before preparing the formulations.

2.2 Extrusion

A twin-screw extruder (Model DR-2027-K13, C. W. Brabender, Inc., S. Hackensack, NJ, USA) with corotating mixing screws (Model CTSE-V, C. W. Brabender, Inc., S. Hackensack, NJ, USA) was used to conduct extrusions. The conical screws had diameters decreasing from 43 mm to 28 mm along their length of 365 mm from the feed end to the exit end. On each screw, there was a mixing section, in which small portions of the screw flights were cut away. The mixing section enhanced mixing and also increased the residence time of the sample in the barrel. A 150-rev/min screw speed was used for all extrusions. The temperature at the feeding section was maintained at 50°C, the second barrel section at 120°C, the third barrel section at 150°C and the die section at 170°C. A 3 mm diameter die nozzle was used to produce continuous cylindrical rope-like extrudates which were cut by a rotary cutter. The extruder was controlled by a Plasti-Corder (Type FE 2000, C. W. Brabender, Inc. S. Hackensack, NJ). Temperature profiles, pressure profiles and torque readings were recorded for fuzzy modeling. Extrusion conditions selected were based on preliminary studies and previous experiments.

2.3 Radial expansion ratio (RER)

RER of the extruded foams were calculated by dividing the mean cross-sectional areas of the extrudates by the cross-sectional area of the die nozzle. Each calculated value was a mean of 20 observations.

2.4 Unit density (UD)

UD of the extrudates were determined using a glass bead displacement method [20]. The glass beads had 0.1 mm diameter. Mean values of UD were obtained by averaging five replicates.

2.5 Bulk spring index (SI)

BSI measurements were made using an Instron universal testing machine (Model 5566, Instron Engineering Corp., Canton, MA). A cylindrical aluminium container with a volume of 365 cm^3 (6.93 cm in diameter and 9.68 cm in depth) was used to confine the bulk samples. The forces required to initially compress the samples to 80% of their original volumes and the forces required to recompress the same samples 1 min after releasing the initial load were recorded. BSI was calculated by dividing the recompression force by the initial compression force and has an ideal value of 1. A mean value was obtained by averaging five replicates.

2.6 Bulk compressibility (BC)

BC was calculated using the same data collected in the BSI test. It was calculated by dividing the peak force required to compress (deform) the sample by 80% [to 20% of their original dimension (diameter)] by the initial axial cross-sectional area of the foams [19]. A mean value was obtained by averaging five replicates.

2.7 ANFIS modeling

Modeling was performed using Matlab 7.2. ANFIS and Sugeno type fuzzy inference systems were used in the modeling of properties of the nanocomposite foams. Multiple Input Single Output (MISO) models consisting of four inputs including clay content, temperature, pressure and torque were developed to predict outputs. Figure 1 shows the ANFIS structure of clay content and process parameters as four input parameters and four mechanical properties as output parameters. The outputs were RER, UD, SI and BC. Sugeno-type fuzzy inference systems were generated by using Genfis2 (Matlab fuzzy logic toolbox) which utilized subtractive clustering to compute the models for the product properties. The purpose of clustering was to identify natural groupings of data to produce a concise representation of the behavior of the system [21].

The fuzzy models generated from the membership functions and rules were data-driven by the process data for each mechanical property. Each set of process data collected from the extrusions consisted of 80 data points from which 70% and 30% were selected randomly for training and testing, respectively. The models were developed and implemented using 300 epochs and a radius of 0.5. The input data were the process data acquired by the computer consisting of temperature, pressure and torque readings from extrusion. The input data also consisted of the clay contents. The output data were the properties consisting of RER, UD, SI and BC.

The input and output data sets contained four inputs [clay content (%), melt temperature (°C), pressure (psi), torque (Nm)] and one output (RER). The same data sets were used for each mechanical property, namely UD, SI and BC. Table 1 gives the experiment

results of clay content and process parameters as four input parameters and four properties as output parameters. Predicted values for each model were produced using the evalfis function of Matlab software. Models developed were evaluated by the R^2 of prediction and root mean squared error (RMSE).

3 Results and Discussion

Multiple Input Single Output (MISO) models were developed to predict each property separately from the input parameters (clay content, temperature, pressure and torque). These models were computed based on the input and output data that were used to train the model. The patterns were tuned using a hybrid system that contained a combination of the back propagation and least-squares-type methods. An error tolerance of 0 was used and the number of epochs was 300. After training and testing, the RMSE became steady, the training and testing were regarded as converged [22]. The predicted output values from the models were obtained for training and testing using the evalfis function of Matlab software. Models developed were evaluated by the R^2 of prediction and RMSE values. Figure 1 shows the ANFIS model structure of RER which had four inputs and one output. Each input was connected to six membership functions, and further networked with six rules. Each rule was connected with one membership function and these membership functions generated the output. Figure 2 shows the rule viewer of RER which is a mapping of inputs and output that describes the fuzzy inference system. Each row in the figure represents one rule and consists of four membership functions corresponding to each of the four inputs (clay, temperature, pressure and torque). The

membership functions are shown in the first four columns which also are known as antecent memberships. The last column is the output (RER) also known as consequent membership, which represents inputs of each of the six rules. The rule viewer shows only one calculation at a time in detail. In this example, the input values for the rule viewer were data driven values of 1.59 for clay, 161ºC for temperature, 1250 psi for pressure and 76.5 Nm for torque. The calculated value for the model RER was 17 kg/m^3.

For each individual membership function, the range of input values was represented by values on the x-axis and membership value represented on the y-axis. The shaded region depicted the visual representation of the resulting membership of input values. In fuzzy modeling, inputs membership functions can be described by different shapes including triangular, sigmoidal, bell-shaped or irregular [23]. In this work, the inputs membership functions were described with Gaussian membership functions. The model used a logical 'AND' relationship to combine the data space into fuzzy clusters. The portion of the bar of the last column represents the weighting factor for that rule, and is determined by the minimum membership value in each rule. For example, in Rule 1, the shaded region of the clay membership function was zero. Therefore, this rule did not contribute to the firing strength. Similarly, Rule 2 did not contribute to the firing strength. Rule 3 and 4 contributed to about 15 and 10% of the contribution, respectively. In Rule 5, the shaded regions of the clay and torque membership functions were about 90%, showing this rule had a strong firing strength. In the Sugeno fuzzy inference system, every rule contributes to predicting the output to a certain degree based on the degree of membership of the input values to the input fuzzy sets. A single output was defussified using the center of

gravity or a weighted average of output from each of the six rules, and is shown in the lower right hand corner. Therefore, for the RER model, clay content and torque had the greatest impacts on RER. Figure 3 shows the surface plot of RER as a function of clay content and torque. This surface plot shows that RER had a complex and nonlinear nature based on the relationships between the inputs [24].

Figures 4 through 7 show the plots of predicted versus actual values for all properties for testing data using the MIMO models. All the plots show relatively good accuracy. Table 1 shows the R^2 and RMSE values for testing and training of ANFIS for all product property models. For RER, comparison of predicted values with the actual values produced R^2 values of 0.9857 and 0.7682 for training and testing data, respectively. As can be observed, the R^2 values for training for all the properties were higher than the R^2 values of testing suggesting that a bigger set of data produced better models.

RMSE values of 0.0641 and 0.8590 were achieved for training and testing, respectively, for RER. All models had very low RMSE values for both training and testing. Models with the highest R^2 and minimum RMSE values were considered the best models. Once trained and tested, the ANFIS models can be used to predict the outputs expected for new levels of input parameters.

4 Conclusions

The results obtained indicate that ANFIS was a promising tool for modeling extrusion of biodegradable nanocomposite foams. ANFIS models were developed for selected mechanical properties of tapioca starch-PLA nanocomposite foams using different clay contents and process parameters. Individual models were developed predicting radial expansion ratio, unit density, spring index and bulk compressibility. The R^2 values for training for all the mechanical properties were higher than the R^2 values of testing suggesting that a bigger set of data produced better prediction of the models. All models preformed well with R^2 values > 0.71 for testing. All models had very low RMSE values for both training and testing. Model with the highest R^2 and minimum RMSE values were considered the best models. These models serve as tools for predicting the input levels needed to generate a desired property.

References

[1] Q. Fang, M. A. Hanna: Rheological Properties of Amorphous and Semicrystalline Poly (Lactic Acid) Polymers. *Ind. Crops and Prod.* **1999**, 10, 47-53.

[2] S. Simmons, E. L. Thomas: Structural Characteristics of Biodegradable Thermoplastic Starch/Poly (Ethylene-Vinyl Alcohol) Blends. *J. Appl. Polym. Sci*. **1995**, 58, 2259-2285.

[3] R. Chinnaswamy, M. A. Hanna: U.S. Pat. 496,895 (1993).

[4] Q. Fang, M. A. Hanna: Mechanical Properties of Starch-Based Foams as Affected by Ingredient Formulations and Foam Physical Characteristics. *Trans. ASAE* **2000,** 43, 1715-1723.

[5] Y. T. Lim, O. O. Park: Rheological Evidence for the Microstructure of Intercalated Polymer/Layered Silicate Nanocomposites. *Macromol. Rapid Commun*. **2000,** 21, 231-235.

[6] P. H. Nam, P. Maiti, M. Okamoto, T. Kotaka, N. Hasegawa, A. Usuki: A Hierarchical Structure and Properties of Intercalated Polypropylene/Clay nanocomposites. *Polymer* **2001**, 42, 9633-9640.

[7] H. R. Dennis, D. L. Hunter, D. Chang, S. Kim, , J. L. White, J. W. Cho, D. R. Paul: Effect of Melt Processing Conditions on the Extent of Exfoliation in Clay-Based Nanocomposites. *Polymer* **2001**, 42, 9513-9522.

[8] J- H. Chang, T- G. Jang, K. J. Ihn, W- K. Lee, G. S. Sur: Poly (Vinyl Alcohol) Nanocomposites with Different Clays: Pristine Clays and Clays. *J. Appl. Polym. Sci.*, **2003**, 90, 3208-3214.

[9] J- H. Yuen, G- S. Bang, B. J. Park, S. K. Ham, J- H. Chang: Poly (Vinyl Alcohol) Nanocomposite Films: Thermo Optical Properties, Morphology, and Gas Permeability. *J. Appl. Polym. Sci*. **2006**, 101, 591-596.

[10] A. B. Morgan: Flame Retarded Polymer Layered Silicate Nanocomposites: A Review of Commercial and Open Literature Systems. *Polym. Adv. Technol*. **2006**, 17, 206-217.

[11] S. S. Ray, K. Yamada, M. Okamoto, K. Ueda: Control of Biodegradability of Polylactide via Nanocomposite Technology. *Macromol. Mater. Eng.* **2003**, 288, 203-208.

[12] W. M. Choi, T. W. Kim, O. O. Park, Y. K. Chang, J. W. Lee: Preparation and Characterization of Poly (Hydroxybutyrate-Co-Hydroxyvalerate)-Clay Nanocomposite. *J. Appl. Polym.* Sci. **2003**, 90, 525-529.

[13] X. C. Li, C- S. Ha: Nanostructure of EVA/Clay Nanocomposites: Effects of Kinds of Clay and Grafting of Maleic Anhydride onto EVA. *J. Appl. Polym. Sci*. **2003**, 87, 1901-1909.

[14] J. M. Harper: Food Extrusion, in Extrusion of Foods. Vol. I CRC Press, Inc. Boca Raton, Fl. **1981**.

[15] G. M. Ganjyal, M. A. Hanna, D. D. Jones: Modeling Selected Properties of Extruded Waxy Maize Cross-Linked Starches with Neural Networks. J. Food Sci. **2005**, 68:1384-1388.

[16] O. Popescu, D. C. Popescu, J. Wilder: A New Approach to Modeling and Control of a Food Extrusion Process Using Artificial Neural Network and an Expert System. J. Food Process Eng. **2001**, 24, 17-36.

[17] H.-X. Huang, S. Lu : Modeling Parison Formation in Extrusion Blow Molding by Neural Networks. J. Appl. Polym. Sci**. 2005**, 96, 2230-2239.

[18] J- S. R. Jang: ANFIS: Adaptive-Network-Based Fuzzy Inference System. IEEE Transactions on Systems, Man and Cybernetics **1993**, 23, 665-685.

[19] Q. Fang, M. A. Hanna: Functional Properties of Poly (Lactic Acid) Starch-Based Loose-Fill Packaging Foams. *Cereal Chem*. **2000**, 77, 779-783.

[20] S. Bhatnagar, M. A. Hanna: Effect of Lipids on Physico-Chemical Properties of Extruded Corn Starch. ASAE Paper No., 916541 St. Joseph, Mich.: ASAE **1991**.

[21] V. S. Sharma, S. K. Sharma, A. K. Sharma: An Approach for Condition Monitoring of a Turning Tool. Proc. IMechE Vol. 221 Part B: J. Eng. Manufacture **2007**, 636-646.

[22] G. Daoming, J. Chen: ANFIS for High-Pressure Waterjet Cleaning Prediction. Surface & Coatings Tech. **2006**, 201, 1629-1634.

[23] E. Cox: The Fuzzy Sytems Handbook: A Practitioner's Guide to Building, Using and Maintaining Fuzzy Systems, Academic Press, San Diego, CA. **1994**.

[24] M. A. Ghoush, M. Samhouri, M. Al-Holy, T. Herald: Formulation and Fuzzy Modeling of Emulsion Stability and Viscosity of a Gum-Protein Emulsifier in a Model Mayonnaise System. J. Food Sci. **2008**, 84, 348-357.

Tab. 1. R^2 and RMSE values for training and testing of ANFIS models for product properties.

Product property	R^2 (Training)	RMSE (Training)	R^2 (Testing)	RMSE (Testing)
Radial expansion ratio	0.9857	0.0641	0.7682	0.8590
Unit density	0.9431	1.1206	0.7128	0.4260
Spring index	0.9953	0.0286	0.9926	0.0317
Bulk compressibility	0.9998	0.0185	0.8821	0.5539

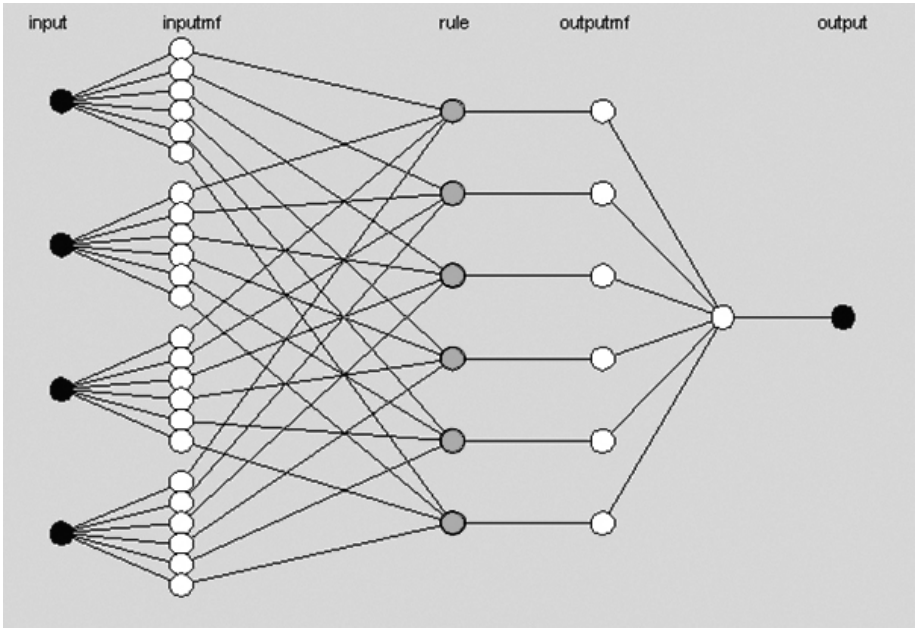

Fig. 1. ANFIS model structure for radial expansion ratio.

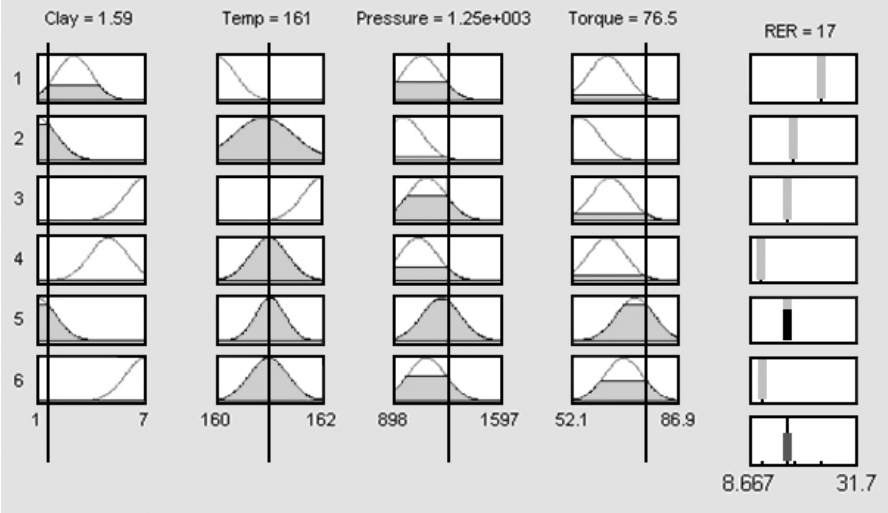

Fig. 2. Rule viewer for radial expansion ratio.

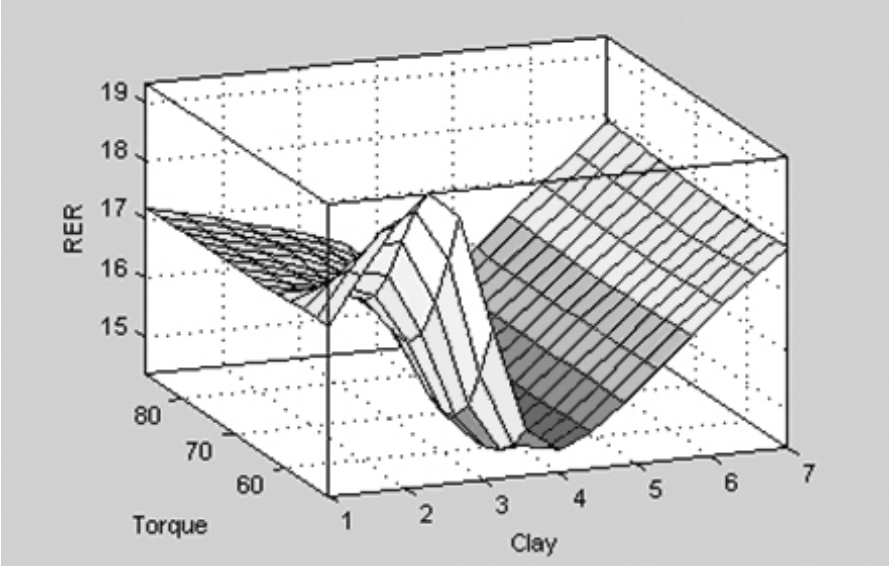

Fig. 3. A surface plot of radial expansion ratio mapping the relationships between clay content and torque.

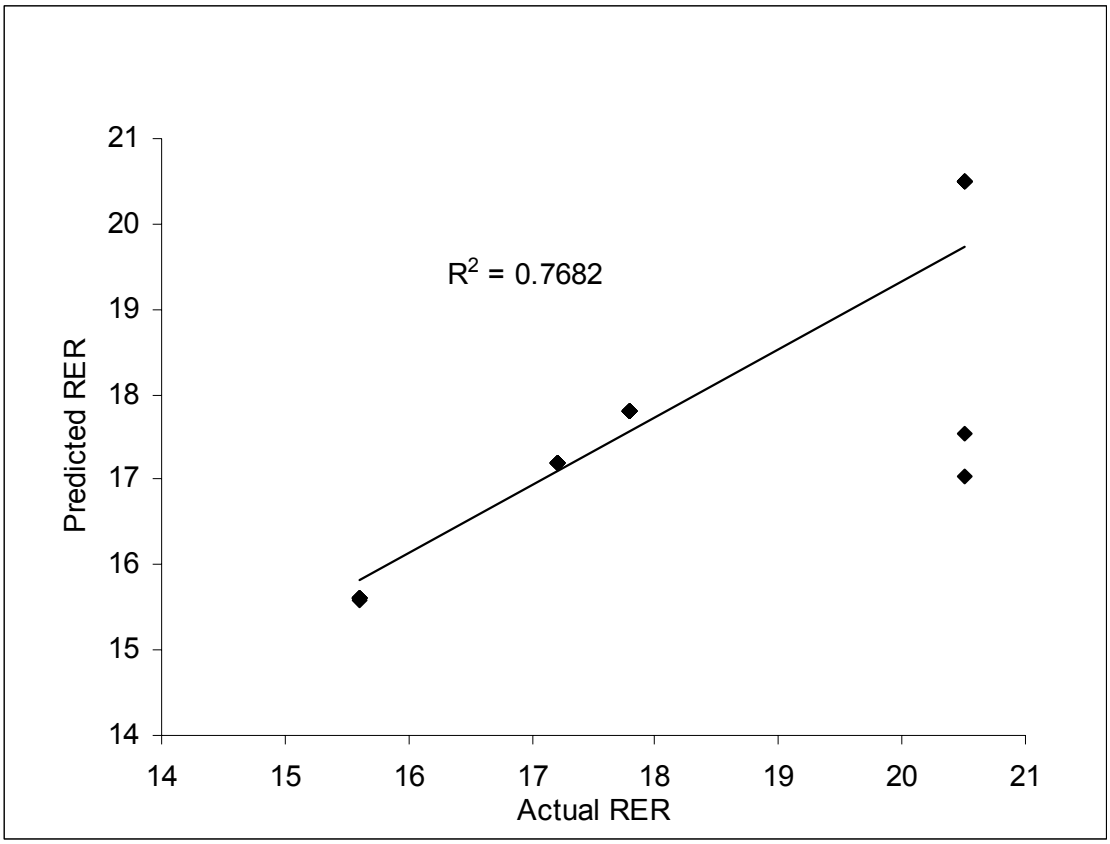

Fig. 4. Relationships between predicted values of radial expansion ratio and actual values.

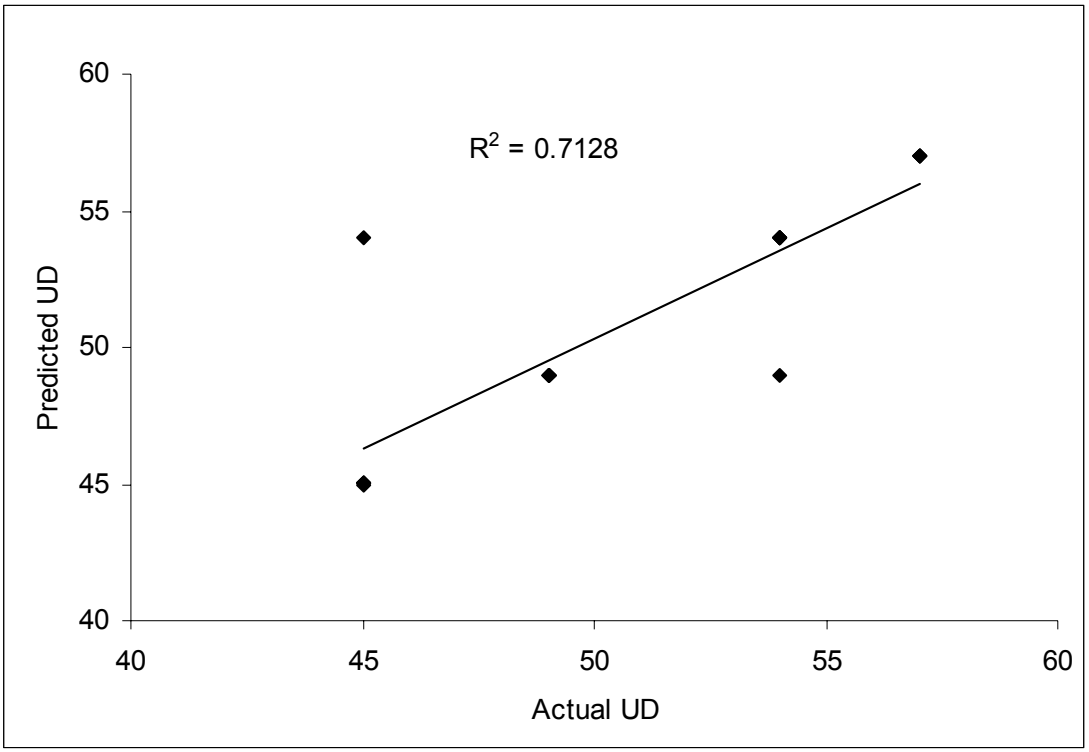

Fig. 5. Relationships between predicted values of unit density and actual values.

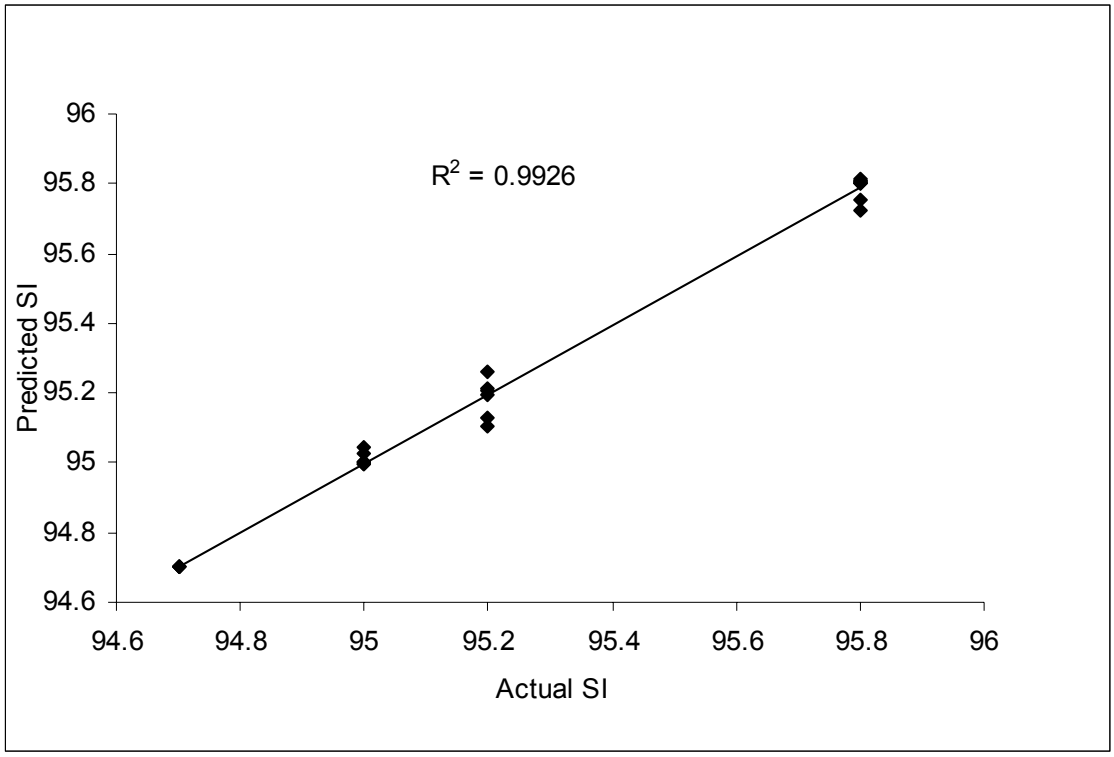

Fig. 6. Relationships between predicted values of spring index and actual values.

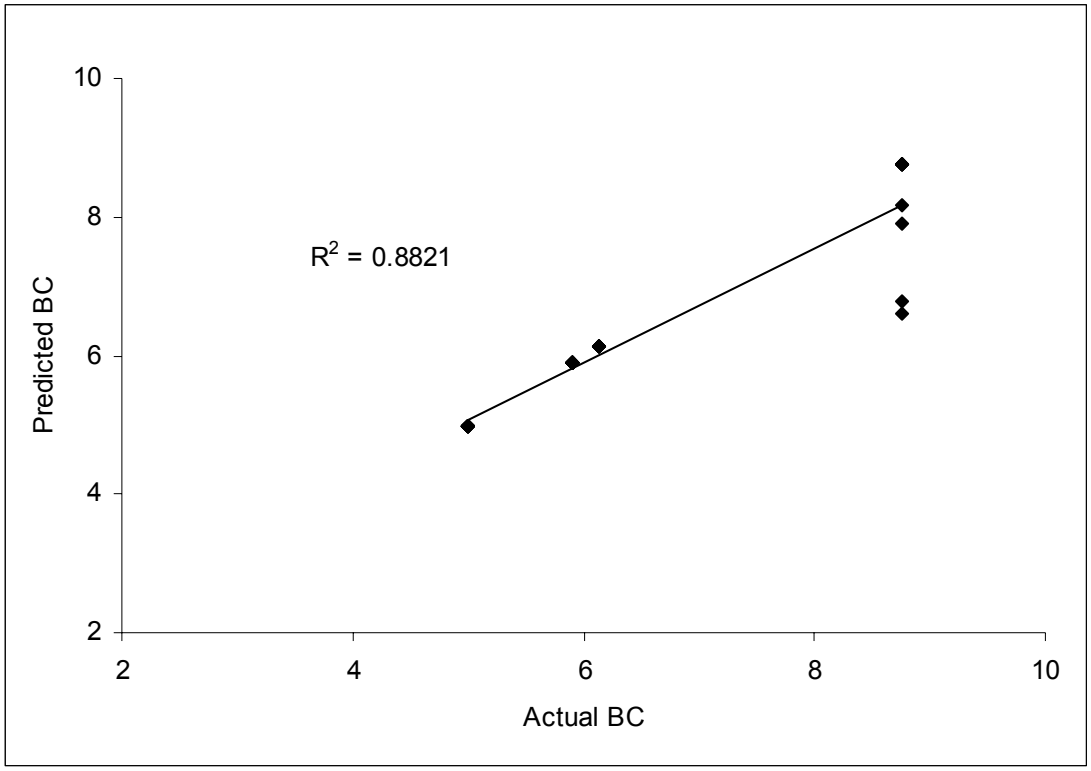

Fig. 7. Relationships between predicted values of bulk compressibility and actual values.

CHAPTER VI

RESIDENCE TIME DISTRIBUTION AND MODELING OF MECHANICAL PROPERTIES OF EXTRUDED NANOCOMPOSITE FOAMS USING ADAPTIVE NEURO-FUZZY INFERENCE SYSTEM

This research paper has been submitted to *Starch*. The co-authors are Siew Yoong Lee, Milford A. Hanna, David D. Jones.

Residence Time Distribution and Modeling of Mechanical Properties of Extruded Nanocomposite Foams Using Adaptive Neuro-Fuzzy Inference System

Summary

Effects of two screw configurations (compression and mixing screws) and two barrel temperatures (150 and 160 ºC) on residence time distribution (RTD) and modeling of mechanical properties of nanocomposite foams were studied. Multiple inputs single output (MISO) models were developed using Adaptive Neuro-Fuzzy Inference System Modeling (ANFIS) to predict radial expansion ratio (RER), unit density (UD), bulk spring index (BSI) and bulk compressibility (BC) of the nanocomposite foams. An individual ANFIS model was developed for each mechanical property using torque (Nm), pressure (psi) and melt temperature (°C) as input parameters. Models were evaluated by the R^2 of prediction and root mean squared error (RMSE) for training and testing. Wide-angle x-ray diffraction (WAXD) results showed the diffraction peaks for the mixing screws at 150 ºC were narrow and had higher intensity indicating a strong intercalation in the nanocomposites. Screw configuration and temperature had significant effects ($P<0.05$) on the mean residence time (MTR) which affected the mechanical properties of the nanocomposites.

Keywords: Models; Mean residence time; System variables; Root mean square error; R-squared

1 Introduction

Polymer-clay nanocomposites are a class of reinforced polymers containing small quantities (1-5 wt%) of nanometric-sized clay particles. The functional properties of these materials are improved markedly compared to those of the unfilled polymers or conventional composites. These improvements included high moduli [1], increased tensile strength [2], thermal stability [3] and biodegradability [4] and decreased gas permeability [5] and flammability [6]. Melt intercalation by extrusion is the most common approach to synthesize nanocomposites because it is an environmentally friendly process that requires no solvent and is suitable for industrial uses [7]. Intercalated nanocomposites occur when a small amount of polymer moves into the gallery spacing between the silicate platelets. However, the formation of intercalation depends on the types of clay and on the processing conditions [8, 9].

RTD in an extruder is a useful means of determining optimal processing conditions for mixing, cooking and shearing reactions during the process. From the RTD functions one can estimate the degree of mixing, the life expectancy of mass flow and the average total strain exerted on the mass during its transition, and thus provide a clear picture of how an extruder behaves as a chemical reactor [10]. These results coupled with the knowledge of the operating variables such as temperature, screw speed and screw configuration provide sufficient information to predict what fraction of material will undergo specific reactions.

Numerous studies have reported the complexities of the extrusion process and the modeling of the process. Because of the complexity of the extrusion process, complex mathematical models have been proposed. In recent years, new modeling tools, like fuzzy modeling, have been used. Fuzzy modeling in extrusion is challenging due to the complexity of the process which consists of multiple inputs and multiple outputs which are highly non-linear. Fuzzy modeling makes it possible to utilize experience, knowledge and large amounts of process data. Artificial neutral networks have been used to model and identify predictive models for a food extrusion process [11], control a food extrusion process [12] and polymer extrusion [13].

In this study, we present a novel neuro-fuzzy approach, i.e. ANFIS to model extrusion of nanocomposite foams. ANFIS is a fuzzy inference system implemented in the framework of an adaptive neural network. By using a hybrid learning procedure, ANFIS can construct input-output mapping based on both process data and human-knowledge as fuzzy if-then rules and given input-output data pairs for neural networks training [14]. ANFIS is a powerful tool in fuzzy modeling to learn about given input and output data sets in order to compute the membership functions that describe the associated fuzzy inference system.

The objectives of this study were to investigate the influence of screw configurations and barrel temperatures on the RTD and to use ANFIS to model the mechanical properties of specific nanocomposite foams.

2 Material and Methods

2.2 Materials

Semicrystalline poly(lactic) acid (PLA) resin of MW_n 85,000 was produced by Cargill, Inc. (Minneapolis, MN). Commercial tapioca starch was purchased from Starch Tech, Inc. (Golden Valley, MN). Tapioca starch was agglomerated into spherical granules of 2-4 mm diameter to facilitate feeding into the extruder. The moisture content of the tapioca starch was adjusted to 20 %, dry basis, with distilled water prior to extrusion. Tapioca starch and PLA (90:10 weight ratio) were blended with 3 % Cloisite 10A in a Hobart mixer (Model C-100, Horbart Corp., Troy, OH) and stored in plastic bottles prior to extrusion. Organoclay under the trade name of Cloisite 10A was purchased from Southern Clay Co. (Gonzales, TX) and used as nanofillers. The organoclay was organically-modified montmorillonite (MMT) also known as organoclay.

2.2 Extrusion

A twin-screw extruder (model DR-2027-K13, C. W. Brabender, Inc., S. Hackensack, NJ, USA) with two types of corotating screws, namely the compression and mixing screws (model CTSE-V, C. W. Brabender, Inc., S. Hackensack, NJ, USA) was used to conduct extrusions. The conical screws had diameters decreasing from 43 mm to 28 mm along their length of 365 mm from the feed end to the exit end. *The compression screws* were universally single flighted corotating intermeshing screws with interrupted flight mixing

zones. The mixing screws had a mixing section, in which small portions of the screw flights were cut away. The mixing section enhanced the mixing action and also increased the residence time of the sample in the barrel. A 90-rev/min screw speed was used for all extrusions. The temperature at the feeding section was maintained at 50 °C; the second barrel section at 120°C and the third barrel section and die section were maintained at 150°C. A 3 mm diameter die nozzle was used to produce extrudates which were cut by a rotating cutter. The extruder was controlled by a Plasti-Corder (Type FE 2000, C. W. Brabender, Inc. S. Hackensack, NJ). Data, including barrel temperature profiles, pressure profiles and torque readings, were recorded for subsequent modeling. The extrusion conditions selected were based on preliminary studies and previous experiments.

2.3 Determination of residence time distribution (RTD)

The RTD study was performed using a dye technique [15]. The tracer used for determining the RTD was prepared by mixing 0.05 g of red dye sodium erythrosine (Sigma Chemical Co., St. Louis, MO) with 5 g of tapioca starch and the amount of water needed to bring the moisture content of the tracer to that of the feed material (20%). The tracer was added as a pulse input through the inlet port of the extruder when steady state conditions were achieved. Foam samples were collected every 5 s for 3 min after adding the tracer. The a^* value (of $L^* a^* b^*$ color space) was used as a measure of concentration of tracer in the extrudate [16]. The samples were ground in a mill to pass through a No. 50 US standard sieve. $L^* a^* b^*$ values were measured three times for each ground sample using a Chroma meter (Model CR-300, Minolta, Japan). The mean

residence time (MRT) which represents the mean time the material spent in the extruder was calculated from the RTD functions [17].

2.4 Extrudate property evaluations

The x-ray patterns of the samples were obtained using a Rigaku D/Max– B X-ray diffractometer (Tokyo, Japan) with Cu-Kα radiation (λ = 1.544 Å) at a voltage of 40 KV and 30 mA. Pelletized ground samples were mounted on a sample holder and scanned in the range of diffraction angle 2θ = 2-10° with a scan speed of 1°/min at room temperature.

Radial expansion ratio (RER) of the extruded foams was calculated by dividing the mean cross-sectional areas of the extrudates by the cross-sectional area of the die nozzle. Each calculated value was a mean of 20 observations.

Unit density (UD) of the extrudates were determined using a glass bead displacement method [18]. The glass beads had 0.1 mm diameter. Mean values of UD were obtained by averaging five replicates.

Bulk spring index (BSI) measurements were made using an Instron universal testing machine (Model 5566, Instron Engineering Corp., Canton, MA). A cylindrical aluminium container with a volume of 365 cm^3 (6.93 cm in diameter and 9.68 cm in depth) was used to confine the bulk samples. The forces required to initially compress

the samples to 80% of their original volumes and the forces required to recompress the same samples 1 min after releasing the initial load were recorded. BSI was calculated by dividing the recompression force by the initial compression force. A mean value was obtained by averaging five replicates [19].

Bulk compressibility (BC) was calculated using the same data collected in the BSI test. It was calculated by dividing the peak force required to compress (deform) the sample by 80% [to 20% of their original dimension (diameter)] by the initial axial cross-sectional area of the foams [19]. A mean value was obtained by averaging five replicates.

2.5 Experimental design and statistical analyses

The experimental design was a 2 x 2 factorial design (with three replications) to analyze the effects of screw configurations (compression and mixing screws) and barrel temperatures (150 and 160 ºC) on the RTD and the mechanical properties of the foams. Results of MRT measurements were analyzed by the general linear models (GLM) in SAS analysis program (SAS Institute Inc., Cary, NC). Duncan's multiple range tests were conducted to check for significant ($p<0.05$) differences between treatment groups.

2.6 ANFIS modeling

Modeling was performed using Matlab 7.2 (The MathWorks Inc., Natick, MA, USA). ANFIS was used in the modeling of mechanical properties of the foams. Multiple Input

Single Output (MISO) models consisting of five inputs including torque, pressure and three melt temperatures were developed to predict outputs. The predicted outputs were RER, UD, BSI and BC. Sugeno-type fuzzy inference systems were generated using Genfis2 which utilized subtractive clustering to compute the models for the properties. The purpose of clustering was to identify natural groupings of data from a large data set to produce a concise representation of the behavior of the system [20]. Subtractive clustering has been used in this study for estimating the number of clusters and the cluster centers in a set of data.

The fuzzy models generated from the membership functions and rules were data-driven by the system variables for each mechanical property. The reason for using data-driven modeling is that the extrusion variables were highly nonlinear and were a strongly interactive multivariable process [21]. In addition the data acquired from the computer was large. For RER, the process data collected from the extrusions consisted of 1200 data points (for each screw configuration) from which 70% and 30% were selected randomly for training and testing, respectively. For UD, BSI and BC, the process data consisted of 300 data points for each screw configuration. The models were developed and implemented using 300 epochs and a radius of 0.5. The data sets contained five inputs [torque (Nm), pressure (psi), three melt temperatures (°C)] and one output (RER). The same approach was used for the other mechanical properties. Predicted values for each model were produced using the evalfis function of Matlab software. Models developed were evaluated by the R^2 of prediction and root mean squared error (RMSE) for training and testing.

3 Results and Discussion

Wide-angle x-ray diffraction (WAXD) is a classical method for determining the gallery height (*d*-spacing distance) in clay particles [22]. The *d*-spacing can be determined from the diffraction peak in the XRD patterns [23]. During melt intercalation, the insertion of polymer into the organoclay galleries forces the platelets apart and increases the *d*-spacing, resulting in a shift of the diffraction peak to lower angles. Our WAXD results showed the first diffraction peaks were observed to shift to lower angles compared to organoclay 10A, indicative of intercalation of polymer into the organoclay layers (Fig. 1). The peak of the organoclay 10A ($2\theta = 4.44^{o}$) shifted to 2.98^{o} for the nanocomposite foams for both screw configurations. However, the diffraction peaks for the mixing screws were narrow and had higher intensities than those for the compression screws, indicating a strong intercalated behavior and a high stacking order of the successive clay layers in the nanocomposites. Similar results were reported by Kumar et al. [24]. Similarly, the diffraction peaks for 150ºC barrel temperature were narrow and had higher intensities than those for 160ºC barrel temperature, indicating strong intercalation at 150ºC.

MISO models were developed to predict each property separately from the input parameters [torque (Nm), pressure (psi) and three melt temperatures (°C)]. These models were computed based on the input and output data that were used to train the models. The patterns were tuned using a hybrid system that contained a combination of the back

propagation and least-squares-type methods. A range of influence of 0.5 was used and the number of epochs was 300. After training and testing, the RMSE became steady and the training and testing results converged [25].

Tab. 1 shows the R^2 and RMSE values for testing and training of ANFIS for all models for both the mixing and compression screws. For both screw configurations, the R^2 values for training for almost all the properties were higher than the R^2 values of testing. The R^2 values for training and testing of ANFIS for the mixing screws were higher than those of the compression screws. This could have been due to greater intercalation of the nanocomposites produced by the mixing screws. Fig. 2 shows the RTD curves for mixing and compression screws at 150 and 160ºC. Tab. 2 shows the MRTs for mixing and compression screws at 150 and 160ºC. The MRTs were significantly different for mixing and the compression screws at 150 and 160ºC. The mixing screws had longer MRTs than did the compression screws. Lower temperature had longer MRTs with both screws. Longer MRT produced more mechanical energy which increased the viscosity of the mass and increased the torque and pressure, hence causing an increase in radial expansion but a reduction in longitudinal expansion. On the other hand, higher temperature produced more heat energy which decreased the viscosity of the mass, decreased the torque and pressure, and hence causing a reduction in radial expansion but an increase in longitudinal expansion. Similarly, screw configuration and temperature had significant effects ($P<0.05$) on the MRTs which affected the mechanical properties of the nanocomposites. Yoon et al. [26] found that a longer residence time and/or broader RTD were more effective for dispersing the organoclay. Similarly, Dennis et al, [2]

concluded that increasing the MRT in the extruder generally improved the delamination and dispersion of organoclay. Therefore, mixing screws at 150ºC had higher MRTs which produced greater intercalation, which affected the mechanical properties of the nanocomposites. The RMSE values for both testing and training of ANFIS for all the models were small, indicating the trained neural network models showed a high degree of prediction precision [13]. Fig. 3 – Fig. 6 show the plots of predicted versus actual values for the mechanical properties of extrudates produced with mixing screws. Models for RER and BC showed relatively good prediction compared to UD and BSI models. In general, the models performed quite satisfactorily and gave good results.

4 Conclusions

The results obtained indicate that ANFIS is a promising tool for modeling the mechanical properties of extruded foams using extrusion processing variables. ANFIS models were developed for the mechanical properties of nanocomposite foams using system variables. Individual models were developed predicting RER, UD, BSI and BC. The R^2 values for the training data set for almost all the mechanical properties were higher than the R^2 values of the testing data set. These models serve as tools for predicting the input variables needed to generate a desired property. Once trained and tested, the ANFIS models can be used to predict the outputs expected for new input variables, thereby reducing the amount of experimental work required to describe a process or characterize a product.

References

[1] Y. T. Lim, O. O. Park: Rheological Evidence for the Microstructure of Intercalated Polymer/Layered Silicate Nanocomposites. *Macromol. Rapid Commun*. **2000,** 21, 231-235.

[2] H. R. Dennis, D. L. Hunter, D. Chang, S. Kim, , J. L. White, J. W. Cho, D. R. Paul: Effect of Melt Processing Conditions on the Extent of Exfoliation in Clay-Based Nanocomposites. *Polym.* **2001**, 42, 9513-9522.

[3] J- H. Chang, T- G. Jang, K. J. Ihn, W- K. Lee, G. S. Sur: Poly (Vinyl Alcohol) Nanocomposites with Different Clays: Pristine Clays and Clays. *J. Appl. Polym. Sci.*, **2003**, 90, 3208-3214.

[4] S. S. Ray, K. Yamada, M. Okamoto, K. Ueda: Control of Biodegradability of Polylactide via Nanocomposite Technology. *Macromol. Mater. Eng.* **2003**, 288, 203-208.

[5] J- H. Yuen, G- S. Bang, B. J. Park, S. K. Ham, J- H. Chang: Poly (Vinyl Alcohol) Nanocomposite Films: Thermo Optical Properties, Morphology, and Gas Permeability. *J. Appl. Polym. Sci*. **2006**, 101, 591-596.

[6] A. B. Morgan: Flame Retarded Polymer Layered Silicate Nanocomposites: A Review of Commercial and Open Literature Systems. *Polym. Adv. Technol*. **2006**, 17, 206-217.

[7] W. M. Choi, T. W. Kim, O. O. Park, Y. K. Chang, J. W. Lee: Preparation and Characterization of Poly (Hydroxybutyrate-Co-Hydroxyvalerate)-Clay Nanocomposite. *J. Appl. Polym.* Sci. **2003**, 90, 525-529.

[8] N. Artzi, Y. Nir, M. Narkis, A. Siegmann: Melt Blending of Ethylene-Vinyl Alcohol Copolymer/Clay Nanocomposites: Effect of the Clay Type and Processing Conditions. *J. Polym. Sci.: Part B: Polym. Physics* **2002**, 40, 1741-1753.

[9] B -S. Chiou, E. Yee, D. Wood, J. Shey, G. Glenn, W. Orts: Effects of Processing Conditions on Nanoclay Dispersion in Starch-Clay Nanocomposites. *Cereal Chem*. **2006**, 83, 300-305.

[10] J. Fichtali, F. R. van de Voort: Fundamental and Practical Aspects of Twin Screw Extrusion. *Cereal Foods Worlds* **1989**, 34, 921-929.

[11] G. M. Ganjyal, M. A. Hanna, D. D. Jones: Modeling Selected Properties of Extruded Waxy Maize Cross-Linked Starches with Neural Networks. *J. Food Sci.* **2005**, 68:1384-1388.

[12] O. Popescu, D. C. Popescu, J. Wilder: A New Approach to Modeling and Control of a Food Extrusion Process Using Artificial Neural Network and an Expert System. *J. Food Process Eng*. **2001**, 24, 17-36.

[13] H.-X. Huang, S. Lu : Modeling Parison Formation in Extrusion Blow Molding by Neural Networks. *J. Appl. Polym. Sci***. 2005**, 96, 2230-2239.

[14] J- S. R. Jang: ANFIS: Adaptive-Network-Based Fuzzy Inference System. *IEEE Trans. Systems, Man and Cybernetics* **1993**, 23, 665-685.

[15] J. K. Lin, D. J. Armstrong: Process Variables Affecting Residence Time Distributions of Cereals in an Intermeshing, Counter Rotating Twin Screw Extruder. *Trans. ASAE* **1990**, 33, 1971-1978.

[16] S. Y. Lee, K. L. McCarthy: Effect of Screw Configuration and Speed on RTD and Expansion of Rice Extrudate. *J. Food Process Eng*. **1996**, 19, 153-170.

[17] O. Levenspiel: *Chemical Reaction Engineering*, 2nd Ed., Wiley, N.Y., **1972**.

[18] Q. Fang, M. A. Hanna: Functional Properties of Poly (Lactic Acid) Starch-Based Loose-Fill Packaging Foams. *Cereal Chem*. **2000**, 77, 779-783.

[19] Q. Fang, M. A. Hanna: Mechanical Properties of Starch-Based Foams as Affected by Ingredient Formulation and Foam Physical Properties. *Trans. ASAE* **2000**, 43, 1715-1723.

[20] V. S. Sharma, S. K. Sharma, A. K. Sharma: An Approach for Condition Monitoring of a Turning Tool. Proc. IMechE Vol. 221 Part B: *J. Eng. Manufacture* **2007**, 636-646.

[21] L. Yliniemi, J. Koskinen, K. Leiviska: Data-driven Fuzzy Modeling of a Rotary Dryer. *Int. J. Syst. Sci*. **2003**, 34, 819-836.

[22] Y. Di, S. Iannace, E. D. Maio, L. Nicolais: Poly(lactic acid)/organoclay nanocomposites: thermal, rheological properties and foam processing. *J. Polym. Sci. Part B: Polym. Phys.* **2005**, 43, 689-698.

[23] W. M. Choi, T. W. Kim, O. O. Park, Y. K. Chang, J. W. Lee: Preparation and characterization of poly(hydroxybutyrate-co-hydroxyvalerate)-organoclay nanocomposite. *J. Appl. Polym.* Sci. **2003,** 90: 525-529.

[24] S. Kumar, J. P. Jog, U. Natarajan: Preparation and Characterization of Poly(methyl methacrylate)-Clay Nanocomposites via Melt Intercalation: The Effects of Organoclay on the Structure and Thermal Properties. *J. Appl. Polym. Sci*. **2003**, 89, 1186-1194.

[25] G. Daoming, J. Chen: ANFIS for High-Pressure Waterjet Cleaning Prediction. *Surface & Coatings Tech*. **2006**, 201, 1629-1634.

[26] P. J. Yoon, D. L. Hunter, D. R. Paul: Polycarbonate Nanocomposites: Part2. Degradation and Color Formation. *Polym*. **2003**, 44, 5341-5354.

Tab. 1. R^2 and RMSE values for training and testing data sets of ANFIS models for mechanical properties for mixing and compression screws.

Mechanical property	Mixing screws				Compression screws			
	R^2	RMSE	R^2	RMSE	R^2	RMSE	R^2	RMSE
	Training		Testing		Training		Testing	
RER	0.9186	1.649	0.9505	1.294	0.8536	0.7783	0.8286	0.7987
UD [kg/m^3]	0.5783	4.770	0.3266	6.482	0.5536	7.807	0.4033	9.677
BSI	0.5952	0.0064	0.1695	0.0117	0.0492	0.0491	0.0117	0.0185
BC [MPa]	0.9553	0.2483	0.9322	1.395	0.7866	2.393	0.8083	2.119

Tab. 2. Mean residence time (MRT) for mixing and compression screws at two temperatures.

Screw type	Temperature [ºC]	MRT [s]
Mixing	150	110.7a
Mixing	160	98.74b
Compression	150	91.74c
Compression	160	83.43d

[a-d] means with same letter within a column indicate no significant (P>0.05) difference by Ducan multiple range test

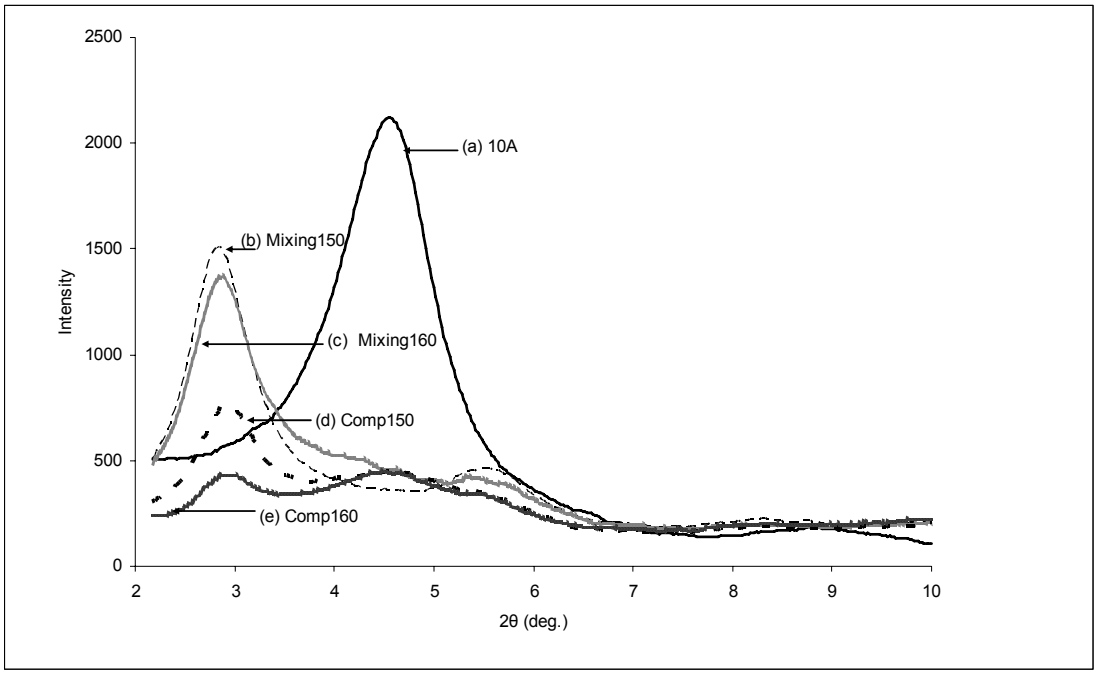

Fig. 1. X-ray patterns of (a) Cloisite 10A and its nanocomposite foams using (b) mixing screws at 150ºC, (c) mixing screws at 160ºC, (d) compression screws at 150ºC, and (e) compression screws at 160ºC.

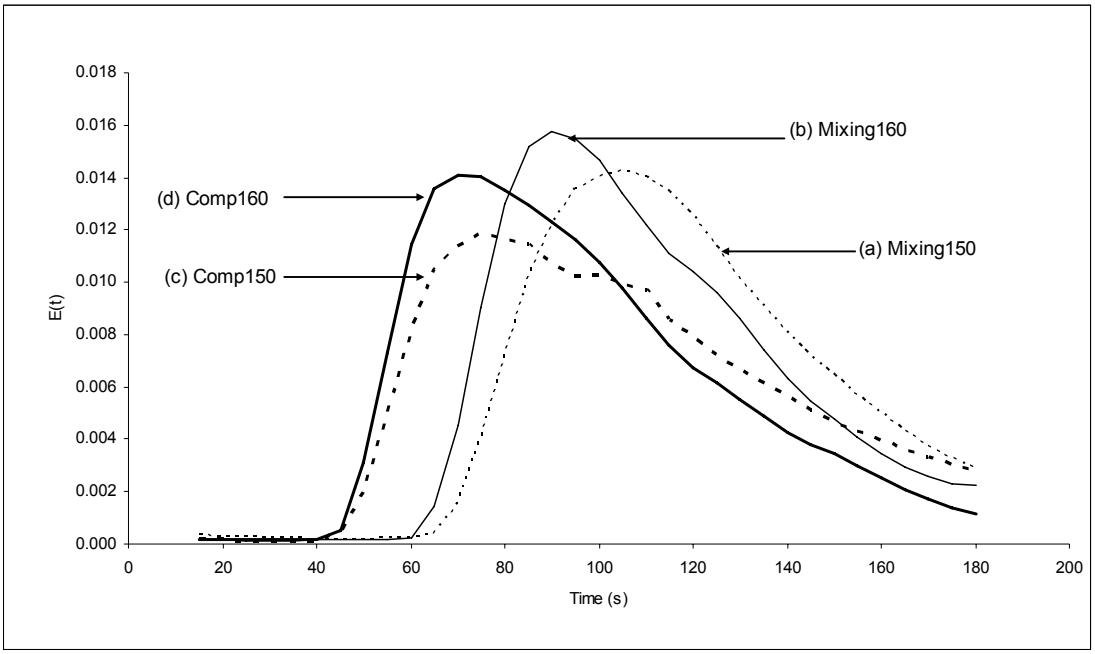

Fig. 2. Residence time distribution of (a) mixing screws at 150ºC, (b) mixing screws at 160ºC, (c) compression screws at 150ºC, and (d) compression screws at 160ºC.

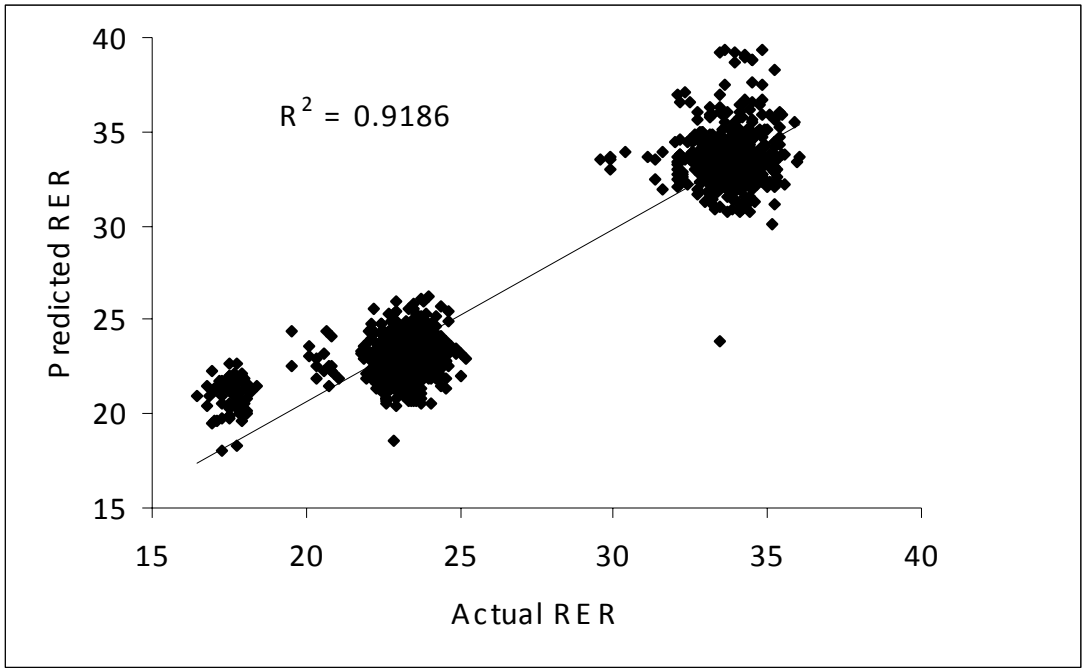

Fig. 3. Relationships between predicted values of RER and actual values for the training data using mixing screws.

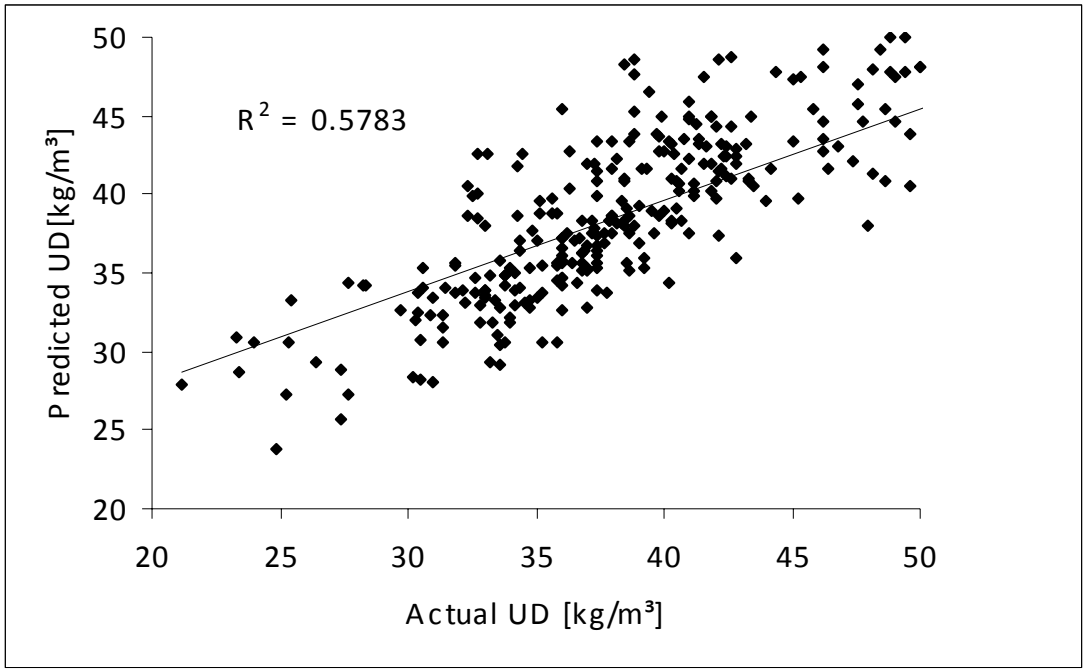

Fig. 4. Relationships between predicted values of UD and actual values for the training data using mixing screws.

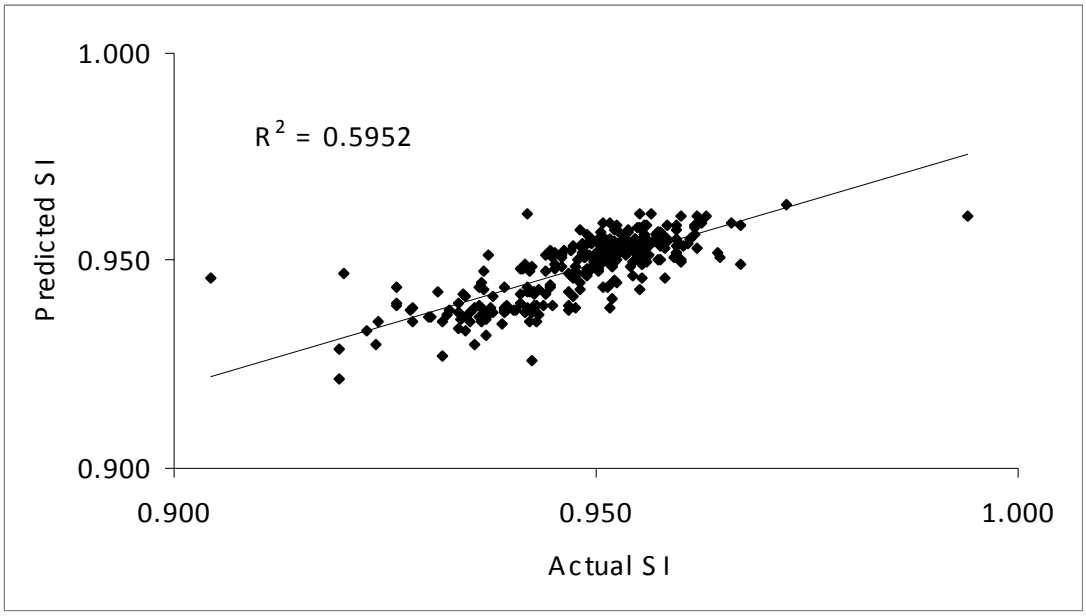

Fig. 5. Relationships between predicted values of BSI and actual values for the training data using mixing screws.

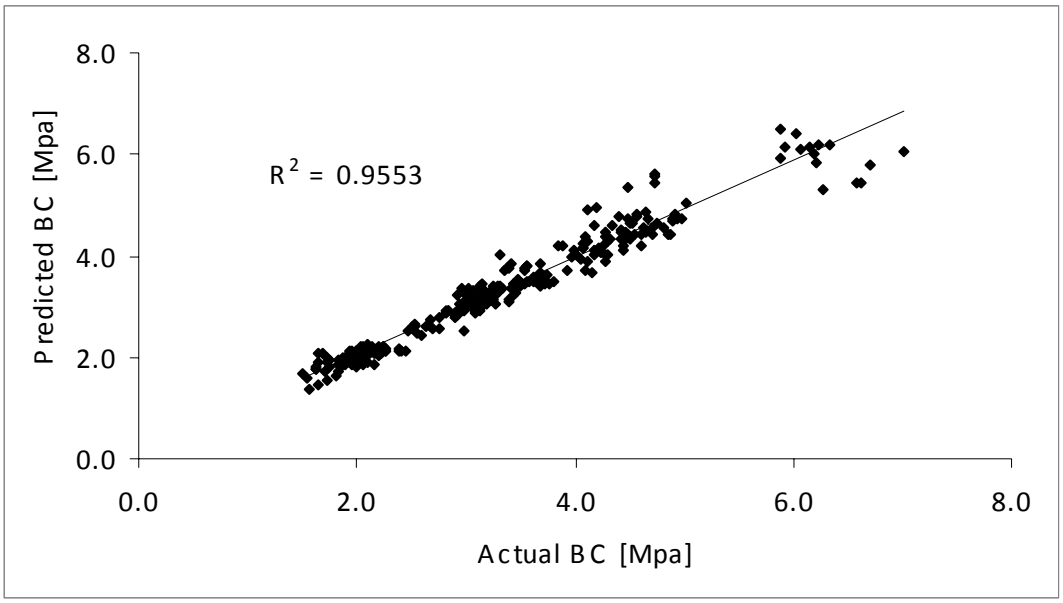

Fig. 6. Relationships between predicted values of BC and actual values for the training data using mixing screws.

CHAPTER VII

RESIDENCE TIME DISTRIBUTION DETERMINATION USING ON-LINE DIGITAL IMAGE PROCESSING

This research paper has been submitted to *Starch*. The co-authors are Siew Yoong Lee, Milford A. Hanna, David D. Jones.

Residence Time Distribution Determination Using On-Line Digital Image Processing

Summary

A less laborious, time-consuming and non-destructive on-line digital image processing (DIP) technique was developed to measure the residence time distribution (RTD) in an extruder. The a* value of L* a* b* color space coordinates was measured using DIP and compared to the colorimeter method. The R^2 values showed a high correlation ($R^2 = 0.88$) of a* values between both methods. The influence of screw configuration (compression and mixing screws) and barrel temperature (150 and 160 ºC) on RTD were analyzed by the mean residence time (MRT) and variance for both methods. Mixing screws and lower temperature resulted in higher MRT and variance for both methods. The DIP method was faster and less subject to human and experimental errors as compared to traditional off-line measurements.

Keywords: Correlation; Mean residence time; Screw configuration; Temperature; Color space

1 Introduction

Numerous studies have reported the complexities of the extrusion process. From the view point of the product, the extrusion process is composed of a series of physical, thermal and chemical changes occurring in a simultaneous or consecutive manner inside the extruder barrel. The quality of the product is related to the time the material is in the extruder. The degree of mixing or the extent of degradation of the material depends on how long it is exposed to the processing conditions. Residence time distribution (RTD) in an extruder is a useful means of determining optimal processing conditions for mixing, cooking and shearing reactions during the process. From the RTD functions one can estimate the degree of mixing, the life expectancy of mass flow and the average total strain exerted on the mass during its transition and thus provide a clear picture of how an extruder behaves as a chemical reactor [1]. These results coupled with the knowledge of the operating variables such as temperature, screw speed and screw configuration can provide sufficient information to predict what fraction of material will undergo specific reactions. RTD data also are used for scale-up and improving equipment design [2]. RTD also can be used to characterize and to predict the extrusion process [3, 4].

RTD can be measured off-line, on-line or in-line. In the off-line method, an inert tracer is injected as a pulse at a chosen location of the extruder, and its concentration at another location downstream (usually at the die exit) is determined by taking samples in a discrete manner [5, 6]. The off-line method is time-consuming and the resulting data points may not be numerous enough to allow for a detailed analysis at the tail region of

the RTD curves. On-line methods differ slightly from the in-line methods, in which no sampling is needed and the analysis is done continuously in real time and analyzed subsequently [7, 8]. This method is much less tedious and time-consuming. The in-line method uses probes and data acquisition systems which continuously analyze the flow material in real time [9, 10].

Image processing techniques are being used increasingly in many different fields of science and industry, where the analysis of images can help in understanding processes. Digital image processing (DIP) involves the manipulation of images by computer in such a way that the retrieval of desired information is extended or improved. Image processing is widely used in the extrusion field to characterize an extruded food product [11], to measure the color of potato chips [12], and to quantify the textural properties of meat analogs [13].

The overall goal of this study was to develop a less laborious and time-consuming, but practical, on-line DIP technique to measure the RTD. The objectives were to (a) establish an imaging process to measure the a* value (red color intensity) of an extrudate, (b) compare the a* values obtained by DIP and by colorimetry methods, (c) investigate the influence of screw configurations and barrel temperatures on the RTD and (d) analyze the influence of extrusion variables on the MRT and variance of RTD.

2 Material and Methods

2.1 Materials

Semicrystalline poly(lactic) acid (PLA) resin of MW_n 85,000 was produced by Cargill, Inc. (Minneapolis, MN). Commercially available tapioca starch was purchased from Starch Tech, Inc. (Golden Valley, MN). Organoclay, under the trade name of Cloisite 10A, was purchased from Southern Clay Co. (Gonzales, TX) and used as nanofillers. The organoclay was organically-modified montmorillonite (MMT). Tapioca starch was agglomerated into spherical granules of 2-4 mm diameter to facilitate feeding into the extruder. The moisture content of the tapioca starch was adjusted to 20 %, dry basis, with distilled water prior to extrusion. Tapioca starch and PLA (90:10 weight ratio) were blended with 3 % Cloisite 10A in a Hobart mixer (Model C-100, Horbart Corp., Troy, OH) and stored in plastic bottles prior to extrusion.

2.2 Extrusion

A twin-screw extruder (model DR-2027-K13, C. W. Brabender, Inc., S. Hackensack, NJ, USA) with two types of corotating screws, namely the compression and mixing *screws* (model CTSE-V, C. W. Brabender, Inc., S. Hackensack, NJ, USA) was used to conduct extrusions. The conical screws had diameters decreasing from 43 mm to 28 mm along their length of 365 mm from the feed end to the exit end. The compression screws were universally single flighted corotating intermeshing screws with interrupted flight mixing zones. The mixing screws had a mixing section, in which small portions of the screw flights were cut away. The mixing section enhanced the mixing action and also increased

the residence time of the sample in the barrel. A 90-rev/min screw speed was used for all extrusions. The temperature at the feeding section was maintained at 50 °C; the second barrel section at 120°C and the third barrel section and die section were maintained at 150°C. Die nozzle of 3 mm diameter was used to produce extrudates which were cut be a rotating cutter. The extruder was controlled by a Plasti-Corder (Type FE 2000, C. W. Brabender, Inc. S. Hackensack, NJ). Data including barrel temperature profiles, pressure profiles and torque reading were recorded by a computer for subsequent analyses. Extrusion conditions selected were based on preliminary studies and previous experiments.

2.3 Determination of RTD

The RTD study was performed using a dye technique [14]. The tracer used for determining the RTD was prepared by mixing 0.05 g of red dye sodium erythrosine (Sigma Chemical Co., St. Louise, MO) with 5 g of tapioca starch and the amount of water needed to bring the moisture content of the tracer to that of the feed material (20%) [15]. The tracer was added as a pulse input through the inlet port of the extruder when steady state conditions were achieved. Foam samples were collected every 5 s for 3 min after adding the tracer.

2.4 Colorimeter

The 5 s samples were ground in a mill to pass through a 50 US standard sieve. $L^* a^* b^*$ values were measured three times for each ground sample using a Chroma meter (Model CR-300, Minolta, Japan). The red color intensity, c was calculated as,

$$c = \sqrt{(a^*)^2 + (b^*)^2}$$

where a* represents the value of redness and b* is the value of blueness. However, the value of b* did not contribute to the red color intensity [16], so c was simplified as,

c = a*

Thus, the value of the redness, a* was used as a measure of red color intensity of the concentration of tracer in the extrudate in the DIP method [17].

2.5 On-line digital image processing

During extrusion when the tracer was dropped into the inlet port of the extruder, the on-line digital image of the extrudate was captured by a color digital video camcorder (model ZR50 MC, Cannon USA., Inc., NY, USA) using the video mode with no flash for 3 min. The on-line images were captured on a black background surrounded by fluorescent light. There were 30 frames of images in 1 s of the tape. The image of each frame had 640 x 480 pixels. The images were encoded into a QuickTime movie using QuickTime 7 Pro (Apple Computer Inc.) which were exported to JPEG images.

2.6 Modeling of on-line digital imaging of RTD

Images were processed using the image processing toolbox of the MATLAB software (version 7.2; The MathWorks Inc., Natick, MA, USA). The RGB color space signal was obtained after reading the digital color image in MATLAB. The background was removed from the image of the extrudates (Fig. 1.) using a common threshold of RGB-value greater than 300 (of RGB color space), which was determined for this setup of lighting and background. RGB color was converted to L* a* b* color space. The conversion was carried out using a MATLAB sub-routine. Average a* values of all pixels for each extrudate in each frame were calculated and used to obtain RTD. There were 5400 JPEG images for each experimental run and every 90^{th} image was selected by the MATLAB sub-routine for the conversion to produce the RTD.

2.7 RTD Functions

RTD generally can be described with two functions which are closely related : the E(t) and F(t) diagrams [18]. The response of the extruder to a pulse at the inlet is given by an E(t) diagram, which represents the age distribution of the material in the extruder. Since it is difficult to ensure that the same amount of tracer is used in all experiments, it is common to normalize the tracer concentrations at each point in time by dividing them by the total amount of tracer passing through the system. Thus, the E(t) diagram can be obtained by dividing the concentration, at any time interval, by the total amount of tracer injected,

$$E(t) = \frac{c_i}{\int_{i=0}^{\infty} c_i dt} \approx \frac{c_i}{\sum_{i=0}^{\infty} c_i \Delta t}$$

where c is the tracer concentration at time t.

The F(t) diagram is related to the E(t) diagram and represents the cumulative distribution function in the exit stream at any time

$$F(t) = \int_{i=0}^{i=t} E(t)dt \cong \frac{\sum_{i=0}^{i=t} c_i \Delta t}{\sum_{i\approx 0}^{i\approx\infty} c_i \Delta t}$$

The mean residence time (MRT) or ($\bar{t}$) which represents the mean time the material spent in the extruder can be described as

$$\bar{t} = \int_{i\approx 0}^{i\approx t} t_i E(t)dt \cong \frac{\sum_{i\approx 0}^{\infty} t_i c_i \Delta t}{\sum_{i\approx 0}^{\infty} c_i \Delta t}$$

While the variance (σ^2) can be described as

$$\sigma^2 \cong \frac{\sum_{i\approx 0}^{\infty} (t_i - \bar{t})^2 c_i \Delta t}{\sum_{i\approx 0}^{\infty} c_i \Delta t}$$

2.8 Experimental design and statistical analyses

A 2 x 2 factorial design (with three replications) was used to analyze the effects of screw configurations (compression and mixing screws) and barrel temperatures (150 and 160

ºC) on the RTD. Results of measurements were analyzed by the general linear models (GLM) in the SAS analysis program (SAS Institute Inc., Cary, NC). Duncan's multiple range tests were conducted to check for significant ($p<0.05$) differences between treatment groups.

3 Results and Discussion

The procedure for the comparison of RTD obtained by colorimeter and DIP method is shown in the block diagram in Fig. 2. The comparison of the average a* values measured with a colorimeter and determined by DIP for compression screws at 150ºC are plotted in Fig. 3. Tab. 1. shows the R^2 of a* values obtained by colorimeter and DIP methods for mixing and compression screws at two temperatures. The R^2 values showed a good correlation ($R^2 = 0.88$) between the two methods. The correlation was high even though the color analysis by the DIP did not reflect the actual concentration of the color since the image digitized only the color from the surface of the extrudate whereas the color from the colorimeter method was from the whole ground extrudate. Kumar et al. [19] used an off-line DIP of still pictures of extrudates taken on black background and reported a difference between a* values obtained by the colorimeter and off-line DIP method. They attributed the error to the sub-routine in MATLAB, which converted the RGB to L* a* b* color space coordinates which could be corrected by a multiplication factor. In our study, the sub-routine in MATLAB did not contribute to any error. Fig. 4. shows the RTD obtained by colorimeter and DIP method for compression screws at 150ºC. Both curves had the same distributions but the peak intensity of the distribution obtained by

colorimeter was higher than by DIP method. This was not an issue since the MRT was derived from the distribution rather than on the peak intensity. Moreover, both curves matched well at the two tails of the RTD indicating that the a* values obtained by both methods correlated well at lower red intensity. This may have been due to the DIP method which measured color of the surface only while the colorimeter measured the color of the total ground sample.

The reproducibility of our experiments was very good as shown in Fig. 5. The figure shows the RTD for two experimental runs, at the same operating conditions, were almost identical using the colorimeter method and the DIP method. The influences of screw configuration and temperature on MRT were analyzed by both methods as shown in Tab. 2. Fig. 6 shows the RTD as affected by the screw configuration and temperature obtained by colorimeter method. The MRTs obtained by the colorimeter method were significantly different ($p < 0.05$) for mixing and compression screws at 150 and 160ºC. As expected the mixing screws had longer MRT than the compression screws. Again, as expected, lower temperature resulted in longer MRT for both screws. Higher temperature produced more heat energy which decreased the viscosity of the mass, resulting in a more flowable material. Similar results were reported by Altomare and Ghossi [20]. Data from mixing screws at 150ºC had significantly higher variance. The MRTs obtained by DIP method were significantly different ($p<0.05$) for mixing and compression screw*s*. The MRTs were significantly different for mixing screws at 150 and 160ºC. However, the MRTs were not significantly different for compression screws at 150 and 160ºC. The variances were not significantly different for both sets of screws at 150 and 160ºC.

Comparing the MRTs from both methods, the error was about 5% which was not significantly large.

4 Conclusions

RTD results obtained by colorimeter were highly correlated to the RTD determined by DIP method ($R^2 = 0.88$). Furthermore, both methods gave reproducible results. In addition, both methods produced curves with the same distribution, which is related to the MRT of the process, even though the peak intensity obtained by colorimeter was higher than by DIP method. This was not an issue since the MRT was derived from the distribution rather than on the peak intensity. The influences of screw configuration and temperature on RTD were predicted well by the process. Mixing screws and lower temperature resulted in higher MRT for both methods. Therefore, a simple, non-labor-intensive and non-destructive on-line DIP method was developed to measure the RTD in an extruder. This method was faster and less subject to human and experimental errors and could replace the traditional off-line measurements.

References

[1] J. Fichtali, F. R. van de Voort: Fundamental and Practical Aspects of Twin Screw Extrusion. *Cereal Foods Worlds* **1989**, 34, 921-929.

[2] D. B. Todd: Residence Time Distribution in Twin-Screw Extruders. *Int. Polym. Process*. **1975**, 6, 143-147.

[3] L. G. Chen, H. Hu, J. T. Lindt: Residence Time Distribution in Non-Intermeshing Counter-Rotating Twin-Screw Extruders. *Polym Eng. Sci*. **1995**, 35, 598-603.

[4] J. Gao, G. C. Walsh, D. Bigio, R. M. Briber, M. D. Wetzel: Residence-Time Distribution Model for Twin-Screw Extruders. *Process Syst. Eng*. **1999**, 45, 2541-2549.

[5] B. K. Gogoi, L. K. Yam: Relationship Between Residence Time and Process Variables in a Corotating Twin-Screw Extruder. *J. Food Eng*. **1994**, 21, 177-196.

[6] D. Wolf, N. Holin, D. H. White: Residence Time Distribution in a Commercial Twin-Screw Extruder. *Polym. Eng. Sci*. **1986**, 26, 640-646.

[7] G. –H. Hu, I. Kadri: On-Line Measurement of the Residence Time Distribution in Screw Extruders. *Polym. Eng. Sci*. **1999**, 39, 930-939.

[8] H. Chen, U. Sundararaj, K. Nandakumar: Investigation of the Melting Mechanism in a Twin-Screw Extruder Using a Pulse Method and Online Measurement. *Ind. Eng. Chem. Res.* **2004**, 43, 6822-6831.

[9] Y. Chalamet, M. Taha: In-line residence Time Distribution of Dicarboxylic Acid Oligomers/Dioxazoline Chain Extension by Reactive Extrusion. *Polym Eng. Sci*. **1999**, 39, 347-355.

[10] T. J. A. Mêlo, S. V. Canevarolo: An Optical Device to Measure In-Line Residence Time Distribution Curves During Extrusion. *Polym Eng. Sci*. **2002**, 42, 170-181.

[11] J. Tan, X. Gao, F. Hsieh: Extrudate Characterization by Image Processing. *J. Food Sci*. **1994**, 59, 1247-1250.

[12] S. Segnini, P. Dejmek, R. Öste: A Low Cost Video Technique for Color Measurement of Potato Chips. *Lebensm.–Wiss. u.-Technol*. **1999**, 32, 216-222.

[13] J. Ranasinghesagara, F. Hsieh, G. Yao: An Image Processing Method for Quantifying Fiber Formation in Meat Analogs Under High Moisture Extrusion. *J. Food Sci*. **2005**, 70, E450-E454.

[14] J. K. Lin, D. J. Armstrong: Process Variables Affecting Residence Time Distributions of Cereals in an Intermeshing, Counter Rotating Twin Screw Extruder. *Trans. ASAE* **1990**, 33, 1971-1978.

[15] S. Y. Lee, K. L. McCarthy: Effect of Screw Configuration and Speed on RTD and Expansion of Rice Extrudate. *J. Food Process Eng*. **1996**, 19, 153-170.

[16] M. Seker: Residence Time Distributions of Starch of High Moisture Content in a Single Screw Extruder. *J. Food Eng*. **2005**, 67, 317-324.

[17] C. Bi, B. Jiang, A. Li: Digital Image Processing Method for Measuring the Residence Time Distribution in a Plasticating Extruder. *Polym Eng. Sci*. **2007**, 47, 1108-1111.

[18] O. Levenspiel: *Chemical Reaction Engineering*, 2nd Ed., Wiley, N.Y., **1972**.

[19] A. Kumar, G. M. Ganjyal, D. J. Jones, M. A. Hanna: Digital Image Processing for Measurement of Residence Time Distribution in a Laboratory Extruder. *J. Food Eng*. **2006**, 75, 237-244.

[20] R. E. Altomare, P. Ghossi: An Analysis of Residence Time Distribution Patterns in a Twin Screw Extruder. *Biotechnol. Progr*. **1986,** 2, 157-163.

Tab. 1. R^2 of a* values obtained by colorimeter and digital imaging methods for mixing and compression screws at two temperatures.

Screw type	Temperature [ºC]	R-squared
Mixing	150	0.8631
Mixing	160	0.8691
Compression	150	0.8718
Compression	160	0.8600

Values were from average of six measurements.

Tab. 2. Mean residence time (MRT) and variance obtained by colorimeter and digital imaging methods for mixing and compression screws at two temperatures.

Screw type	Temperature [ºC]	Colorimeter method		Image processing method	
		MRT [s]	Variance [s^2]	MRT [s]	Variance [s^2]
Mixing	150	110.7a	1008a	116.6a	1258a
Mixing	160	98.74b	750.2b	103.8b	1187ab
Compression	150	91.74c	734.5b	95.99c	993.0bc
Compression	160	83.43d	658.5b	88.58c	883.6c

[a-d] means with same letter within a column indicate no significant (P>0.05) difference by Duncan multiple range test.

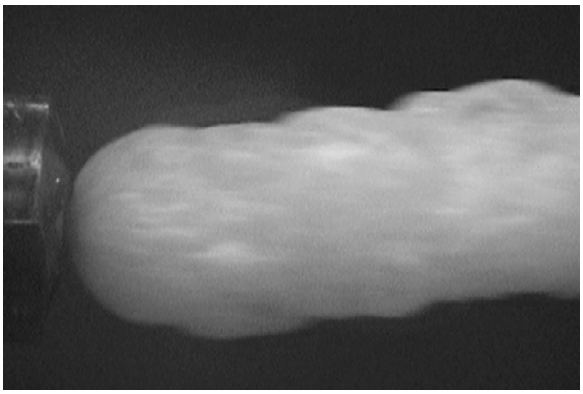

Fig. 1. Picture of extrudate as captured by camcorder.

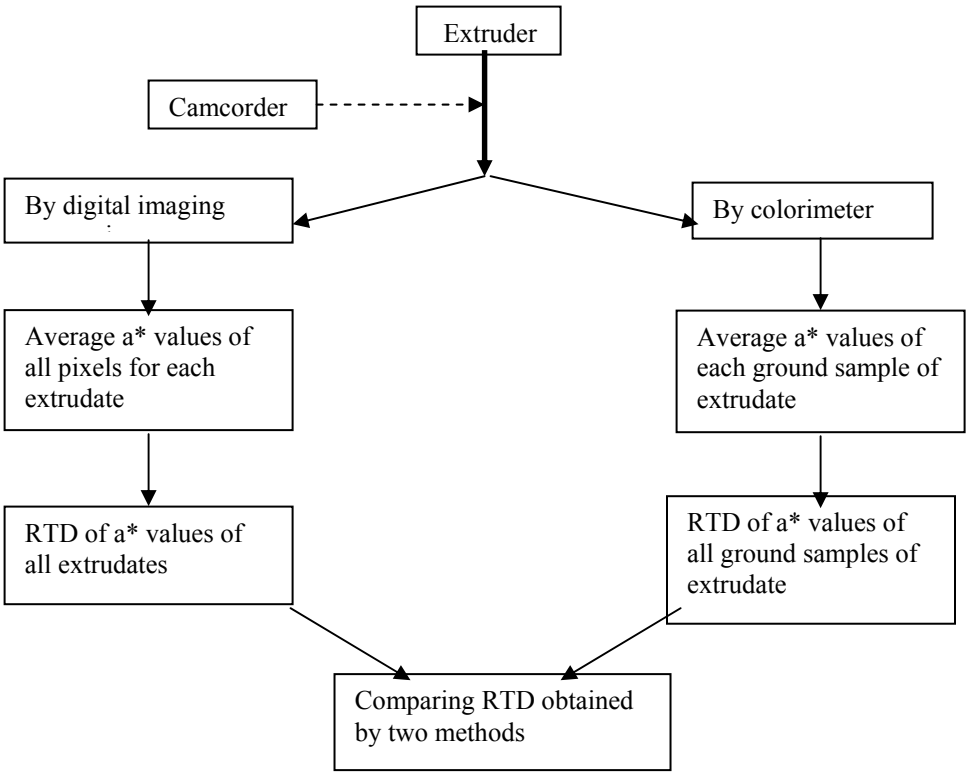

Fig. 2. Procedure for comparison of RTD obtained by colorimeter and by digital image processing methods.

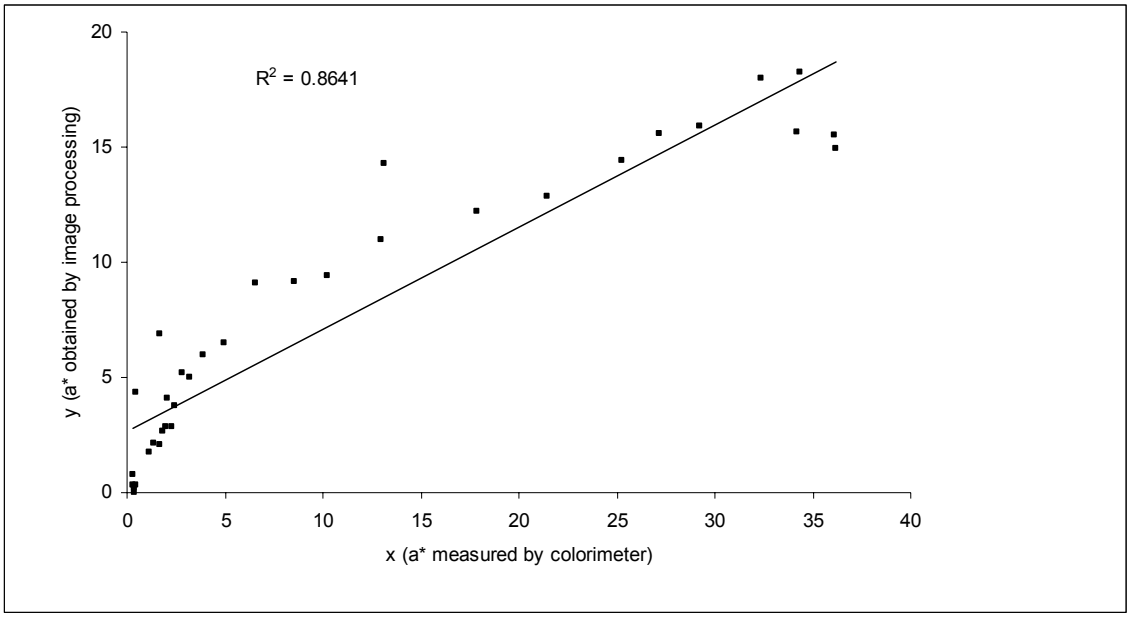

Fig. 3. Comparison of a* values obtained by colorimeter and digital image processing for compression screws at 150ºC.

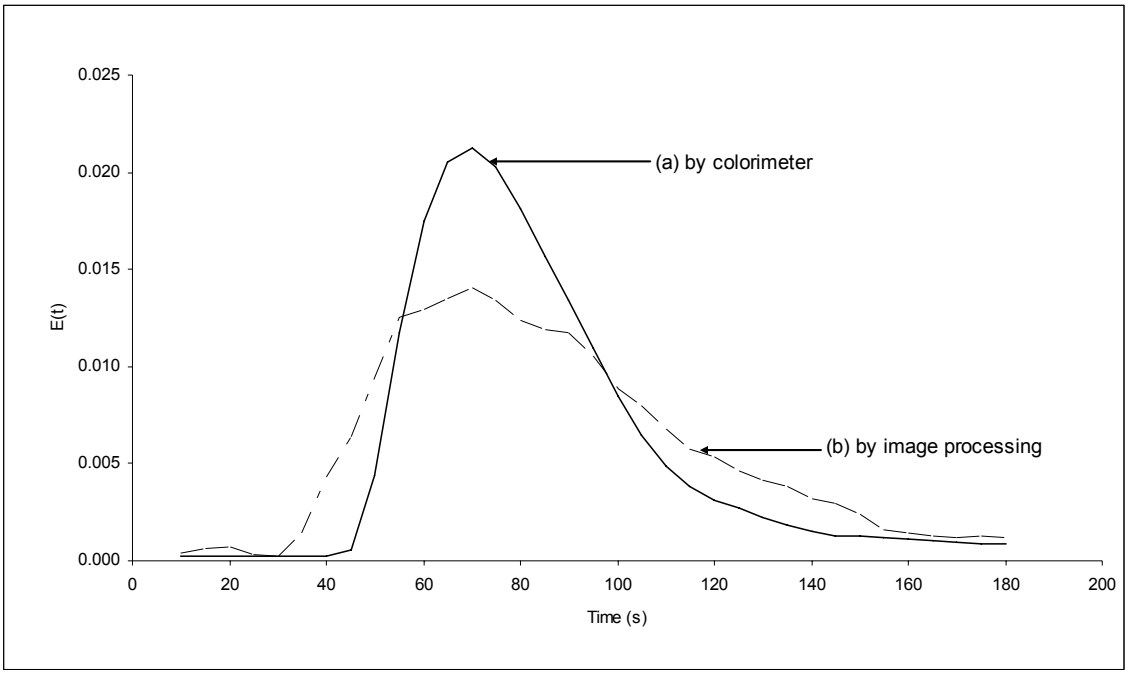

Fig. 4. Residence time distribution obtained (a) by colorimeter and (b) by digital image processing method for compression screws at 150ºC.

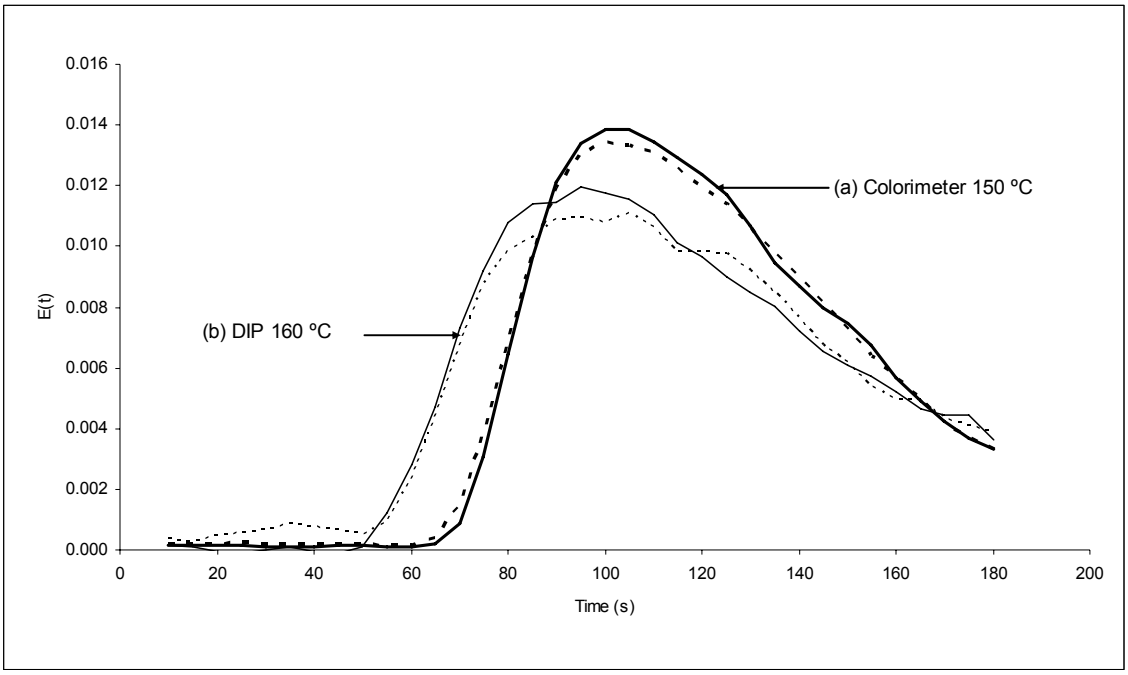

Fig. 5. Residence time distribution of mixing screws obtained at the same operating conditions (a) 150ºC by colorimeter method and (b) 160ºC by digital image processing method, for two experimental runs.

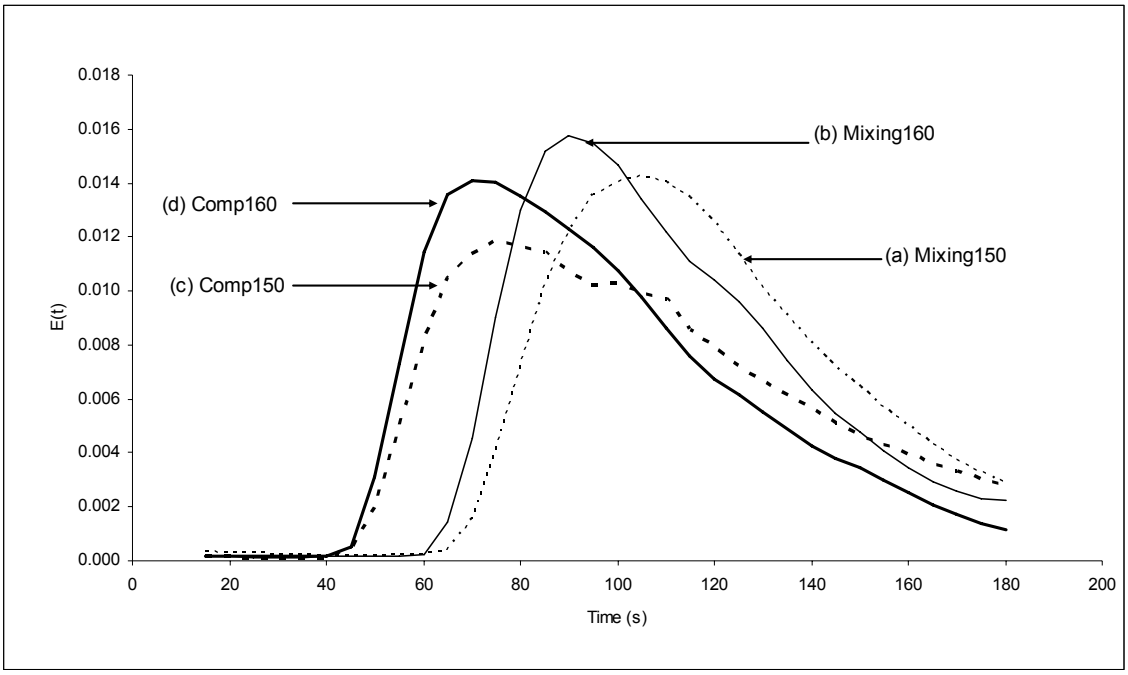

Fig. 6. Residence time distribution of (a) mixing screws at 150ºC, (b) mixing screws at 160ºC, (c) compression screws at 150ºC, and (d) compression screws at 160ºC, obtained by colorimeter method.

CHAPTER VIII

RECOMMENDATIONS FOR FUTURE STUDY

The future research recommendations are to:

1. Use a suitable compatibilizer or coupling agent to improve the interaction between starch/polymer and organoclay blend, therefore improving miscibility.

2. Use an internal mixer which has dispersive and distributive design with heating, cooling and speed control for compounding the blends.

3. Use other characterization techniques:

    - Rheological (dynamic oscillatory shear measurements, storage modulus [G'], loss modulus [G'])
    - Thermodynamics (gas permeability)
    - Mechanical (dynamic mechanical analysis [DMA], stress-deformation, fatigue life, durability)
    - Transmission electron microscopy (TEM).
    - Atomic force microscopy (AFM).

4. Use on-line digital processing of RTD for the measurement of other physical properties, e.g. radial and volume expansion, color and texture of foams.

5. Include L* values in measuring the images to cater for the reflectance effect.